Physics – Uspekhi **46** (8) 789 – 820 (2003)

REVIEWS OF TOPICAL PROBLEMS PACS numbers: 61.72.Cc, 61.72.Tt, 61.72.Yx

Defect-impurity engineering in implanted silicon

A R Chelyadinskiĭ, F F Komarov

DOI: 10.1070/PU2003v046n08ABEH001371

Contents

Abstract. The basic results of the studies of defect – impurity interaction in implanted silicon are presented. Factors affecting the way in which quasichemical reactions proceed — namely, temperature, level of ionization, and internal electric and elastic-stress fields — are analyzed. Methods for suppressing residual damage effects (rodlike defects, dislocation loops), and schemes for reducing the impurity diffusivity and for gettering metallic impurities in implanted silicon are considered. Examples of the practical realization of defect-impurity engineering are presented and discussed.

1. Introduction

Ion implantation is now one of the main methods of fabricating doped semiconductor layers. It has a number of indisputable advantages over the common method of thermal diffusion of doping impurities from an external source and the epitaxy method. Here are the factors that make this method so special: high purity of the process, reproducibility in the concentration of the injected impurity and the impurity depth, and the possibility of forming thin doped layers directly at the surface of the wafer or in its bulk.

The injection of ions into single crystals leads to the formation of a large number of radiation-induced defects, which are stable at room temperature. Removing these defects and moving the injected impurity to the lattice sites requires applying high-temperature annealing treatment to the implanted structures. However, thermal treatment does not totally anneal the defects — some of the radiation-induced defects transform into what is known as residual damage — dislocation loops. These defects substantially reduce the parameters of the devices and the device yield.

In the process of high-temperature annealing, the radiation-induced defects participate in the diffusion redistribution of the injected impurities. Here the effective diffusivity may exceed the values observed in the absence of excess point defects by several orders of magnitude. This limits the possibility of forming an abrupt depth distribution of electrically active impurities, which is required in some cases. Accelerated lateral diffusion is one of the main obstacles in the transition to submicron technology in semiconductor electronics.

The most important problem in the fabrication of semiconductor devices and integrated circuits is the chemical purity of the semiconductor. Estimates of the prospects of the development of microelectronics [1, 2] have shown that by 2007 the industry will need crystals in which the metallic impurity concentration is no higher than 2.5×10^9 cm^{-3}.

A R Chelyadinskiĭ Physics Department, Belarussian State University, prosp. F. Skoriny 4, 220050 Minsk, Belarus
Tel./Fax (375-17) 209 54 45. Tel. (375-17) 209 50 84
E-mail: yavid@bsu.by
F F Komarov A N Sevchenko Research Insitute of Applied Physics Problems, Belarussian State University,
prosp. Kurchatova 7, 220064 Minsk, Belarus
Tel. (375-17) 277 48 33
E-mail: KomarovF@bsu.by

Received 27 November 2002, revised 29 April 2003
Uspekhi Fizicheskikh Nauk **173** (8) 813 – 846 (2003)
Translated by E Yankovsky; edited by S N Gorin

Since the very process by which microelectronic devices are fabricated is a source of contamination of crystals by impurities, the introduction into the technological process of operations of purification of the critical zones of devices sometimes becomes more effective than using crystals that are initially ultrapure.

The present review focuses on the main ways of solving these problems through purposefully controlling the defect – impurity interaction. Such control ensures the proper parameters of the implanted structures and devices based on such structures. This is the topic of defect-impurity engineering.

2. Main data on radiation-induced defect formation in implanted silicon

When ions accelerated to high energies (tens and hundreds of kiloelectronvolts and megaelectronvolts) are injected into a crystal, they lose their energy in collisions with lattice atoms. There are two channels through which the ions lose their energy: in elastic collisions and in inelastic collisions. The energy that the lattice absorbs in inelastic collisions transforms into the energy of excited electrons of the target atoms and is lost to ionization of atoms and to the generation of plasma oscillations. The elastic component of the ion energy loss is spent on the displacement of atoms from the lattice sites. A characteristic feature of the motion of ions in the crystal is the large cross sections for elastic and inelastic interactions. Hence the ranges of ions with such energies vary from a fraction of a micron to several microns. This sets ion implantation apart from the irradiation of crystals with electrically neutral nuclear particles or photons. When a crystal is irradiated with reactor neutrons or gamma-ray photons, the primary displacements of atoms emerge equiprobably over the entire bulk of the crystal.

The modern concepts of the processes of energy loss by charged particles that interact with condensed media are discussed in detail in Kumakhov and Komarov's book [3] and in the tables on the ranges of various ions in various substances [4] that they published in cooperation with Burenkov and Temkin.

A crystal atom will be displaced from its site if it acquires from an incident particle an energy E that is higher than the binding energy of this atom in the lattice, i.e., if this energy is higher than the threshold energy E_d. Because of this displacement, an interstitial atom and a vacancy form in the lattice. The energy transferred from the ion in an elastic (T_n) and inelastic (T_e) collision depends on the distance at which this ion passes the target atom, i.e., on the impact parameter p. To illustrate, Table 1 lists the values of T_n and T_e in the silicon lattice for different values of p [5]. For large impact parameters p, ion energy is lost primarily in inelastic interactions, while for small values of p it is lost mostly in elastic collisions. The impact parameter p is a probabilistic parameter; it varies from zero to a value determined by the interatomic distances in the target. The amount of energy transferred in elastic and inelastic interactions depends on the ion mass and energy. Allowing for the fact that the result is integrated over all values of the impact parameter, we find that, at equal energies, in elastic collisions heavy ions lose more energy than light ions. There exists a critical energy E_c at which the total elastic and inelastic losses are equal for a given ion [3, 5]. Table 2 lists the values of E_c for ions of different mass implanted into silicon.

Table 1. Dependence of T_n and T_e on the impact parameter p for a 50-keV silicon ion Si^+ in the silicon lattice.

p, Å	1	0.1	0.001
T_n, keV	0.002	8	49
T_e, eV	22.6	396	592

Table 2. Critical energy E_c for ions of different mass.

Ion	B	P	Sb
E_c, keV [5]	20	120	10^3
E_c, keV [3]	17	140	2×10^3

A characteristic feature of ion implantation is that an atom displaced from its site (a recoil atom) receives from an incident ion an energy that is much larger than the threshold value ($E > E_d$). In this case, this atom can generate similar displacements of other atoms, i.e., a single high-energy particle may produce a cascade of displacements. The formation of a defect structure as a result of irradiation of the crystal by reactor neutrons or ions, i.e., the onset of a cascade process, has been examined by several researchers [6, 7]. Computer simulation shows that vacancies and interstitial atoms become separated in space directly in the process of development of a displacement cascade. Inside a cluster there are mainly vacancies, while interstitial atoms are mainly located in the cluster shell. This is especially evident in heavy crystals (Ge and GaAs) and to a lesser extent in silicon. If the knocked-out atoms receive an energy of about 5–10 keV, they can leave the main cluster, thus creating a number of subclusters.

What is the fate of a displacement cascade? Primary defects, i.e., vacancies and interstitials, are mobile even at low temperatures. The mobility of vacancies depends on their charge state. In the neutral charge state the vacancies in silicon begin to move at 140 K, while in the negative charge state they begin to move at 60 K. When vacancies leave a displacement cascade and migrate within the crystal, they can form stable complexes with doping and residual impurities [8, 9]. A complex consisting of a vacancy and a phosphorus atom at the lattice site is known as an E center, and a vacancy and an oxygen atom is known as an A center. The role of impurities in complex formation in irradiated silicon was considered in detail by Watkins [10].

In silicon irradiated with heavy particles, complexes with impurities are formed, but the prevailing defects here are intrinsic defects, which are concentrated primarily in cluster regions. Among the intrinsic vacancy defects, a divacancy is the principal stable defect at room temperature. It is formed in silicon irradiated by any type of high-energy particles, such as electrons, gamma-ray photons from Co^{60}, protons, reactor neutrons, and ions. When silicon is irradiated by light particles, divacancies are formed as isolated defects, are primary defects, and are annealed at about 300 °C. In silicon irradiated at low temperatures by heavy particles (neutrons and ions), for which the formation of cascades is a characteristic feature, the observed divacancies have low concentrations. But if the sample temperature increases after irradiation, then, beginning at a vacancy-mobility temperature, the divacancy concentration increases and attains the same value as in the case of silicon irradiated at room temperature [11, 12]. These experiments have been interpreted as proof that divacancies are formed not as primary defects but primarily

as a result of a combination of vacancies. However, analyzing the entire set of data on vacancy introduction and accumulation, the authors of Ref. [13] concluded that divacancies are primary defects in the case of irradiation of silicon by heavy particles as well. The increase in divacancy concentration with the crystal's temperature from liquid-helium temperatures to room temperature is related not to additional formation of divacancies but to the properties of such divacancies that become pronounced as a result of vacancy annealing. In a primary ('frozen') displacement cascade, the defect concentration is extremely high: the number of vacancies is 20 times greater than that of divacancies [14]. As a result of defect interaction, the defects lose their individual properties. When vacancies leave displacement cascades, divacancies manifest themselves as specific centers.

Silicon atoms knocked out from lattice sites have never been observed in interstitial positions. Their high mobility was estimated on the basis of the results of Watkins's experiments on the irradiation of silicon by electrons at low temperatures. Watkins [15–17] registered signals in the electron paramagnetic resonance (EPR) spectra of silicon doped with Al, Ga, or B after irradiation at 4.2 K that corresponded to the interstitial atoms of these impurities. The probability of direct electron knock-out of impurities from lattice sites is so low that the appearance of impurities in interstitial positions can be explained only by their displacement from lattice sites by interstitial silicon atoms migrating within the crystal. Later Gwozdz, Koehler, and McKeighen [18, 19] observed the displacement of Group III impurities from silicon lattice sites in the process of irradiation of the silicon lattice at lower temperatures, namely, at 1.6 and 0.5 K. Then the idea about athermal migration of an interstitial silicon atom within the silicon lattice emerged in radiation physics. For a long time the widely accepted model of athermal migration of an interstitial silicon atom within silicon was that of Bourgoin and Corbett [20], although the basics of this model were formulated 10 years earlier by Weiser [21]. According to this model, an interstitial silicon atom may be in a hexagonal or tetrahedral interstice in a well-defined charge state. If the charge state changes, such an atom passes from one interstice to another. Nonequilibrium charge carriers generated in the irradiation process can, in principle, ensure consecutive charge exchange of the silicon atom and, hence, nonactivation motion of such an atom within the crystal.

According to another model, proposed by Berezhnov et al. [22], the cause of athermal migration lies not in silicon atoms but in substitutional impurities. This model suggests that all substitutional impurities whose covalent radii differ from the radius of a lattice atom are displaced from the lattice sites. An interstitial silicon atom moves in the field of elastic strains generated by the impurity atoms. The researchers found the radii of the spheres around the substitutional atoms defined by the condition that, when an interstitial silicon atom is within such a sphere, it moves toward the center of distortion even at helium temperatures. In the absence of impurity atoms distorting the lattice, interstitial silicon atoms may be immobile, so that such atoms may accumulate in silicon irradiated with high-energy particles at low temperatures. Berezhnov et al. [22] assumed that interstitial silicon atoms in silicon become mobile at 140 K. At this temperature Watkins [23] observed partial annealing of divacancies, which can be explained by their annihilation with interstitial silicon atoms. He assumed that among the interstitial silicon atoms that are formed as a result of irradiation only those that landed into the regions of elastic strains generated by defect clusters remain immobile up to 140 K. In other words, silicon atoms become mobile at 140 K only because of elastic stresses acting on them. It is still unclear, however, what is the true temperature of migration of intrinsic interstitial atoms. The results of X-ray diffraction studies [24] of silicon irradiated with electrons at 4 K and with light ions [25] question the high mobility of silicon interstitials in silicon. In fact, Mukashev et al. [25] concluded that interstitial silicon atoms may be stable up to temperatures close to room temperature. We see that there is more than one opinion about the mobility of self-interstitials in silicon and that this problem requires further investigation.

Numerous studies that used the EPR [12, 26, 27], IR absorption [28, 29], and photoconductivity [11] methods and combined investigations in IR absorption and ions backscattering suggest that in heavy-particle irradiated silicon the main defects that are stable at room temperature are divacancies concentrated primarily in cluster regions. Tetravacancies exist at somewhat lower concentrations [30]. Finally, it was found that the concentrations of stable self-interstitial–impurity complexes of the Si–P6 [31], Si–B3 [32], Si–A5 [33], or Si–O2 [34] type are lower than the divacancy concentration by a factor of 100 to 1000. This led to a prolonged 'vacancy' period in the development of radiation physics. However, the number of paramagnetic centers in crystals with a highly nonuniform distribution of structural imperfections (which is the case in silicon irradiated with heavy particles) can hardly reflect the true number of defects.

When studying self-interstitial defects in implanted silicon, Berezhnov et al. [35] and Jadan et al. [36] used the Watkins effect, i.e., the displacement of Group III impurities from lattice sites by interstitial silicon atoms. The researchers assumed that if there are stable interstitial complexes at sizable concentrations in irradiated silicon and that if interstitial silicon atoms are freed during annealing, the latter will displace substitutional impurities from lattice sites. This phenomenon was registered by the changes in the crystal lattice parameter, which is sensitive to the arrangement of boron impurities at the sites and, hence, to the displacement of such impurities into interstitial positions. It was found that there are two types of intrinsic (interstitial-related) complexes in implanted silicon: in the positive charge state, these are the Si–P6 and Si–B3 centers, which are annealed at 120 and 480 °C, respectively; in the neutral charge state, the same defects manifest themselves as the paramagnetic centers Si–A5 and Si–O2, with annealing temperatures of 160 and 560 °C, respectively. The concentrations of interstitial complexes were found to be comparable to those of divacancies.

Thus, in the process of implantation of light and medium-weight ions into silicon, stable radiation-induced defects of the vacancy type, primarily divacancies, and two types of interstitial complexes appear in the crystal. These defects and also larger vacancy complexes (tetravacancies) [30] may accumulate in the crystal up to a critical concentration corresponding to the transition of silicon into an amorphous state. When heavy ions with energies up to tens and hundreds of kiloelectronvolts are injected into silicon crystals, the primary tracks (at least their central parts) of the ions are amorphous, since in a primary track there is already an overlap of the displacement cascades that are created by recoil atoms generated by the heavy ions over distances

smaller than the size of a displacement cascade, in view of the large cross sections for the elastic interactions. On the other hand, primary defect clusters are never amorphous in silicon, no matter how high the recoil-atom energy is. When the energies of the heavy ions are high (megaelectronvolts), amorphous tracks may not even appear, in view of the decrease in the cross sections for elastic interactions and the increase in inelastic losses. Even for the heavy ion of krypton with an energy of 210 MeV, the ion tracks are not amorphous, and on the whole the efficiency of injection of stable defects (the ratio of the number of stable radiation-induced defects to the number of displaced atoms) is lower than in the case of medium-weight ions (Si) with an energy of about 100 keV [37].

3. Annealing radiation-induced defects. Residual damage in implanted silicon

3.1 The nature of residual damage

Removing radiation-induced defects and moving the injected impurity to the lattice sites requires high-temperature treatment of the implanted silicon structures. Studies of isochronal annealing of irradiated samples have shown that, in the process of thermal treatment, point defects (including those in cluster regions) are partially annealed, annihilating with each other or moving toward sinks (e.g., on the surface) or partially rearranging into more complicated complexes (e.g., pentavacancy complexes) [38, 39]. Injected or doping impurities may also enter into complicated complexes. For instance, in silicon heavily doped with Group V elements and implanted with Si^+ ions complexes containing P, As, or Sb atoms are formed. The annealing temperature (500–700 °C) of these complexes exceed the annealing temperature of intrinsic polyvacancy complexes by 100 °C [40]. Complicated complexes containing boron atoms are annealed at 700–900 °C [41]. Together with the structure of radiation-induced defects becoming more complicated, more complicated structural imperfections can be formed upon heat treatment; e.g., vacancies that have emerged from complexes may form flat disks. After such a vacancy disk reaches a critical size, the planes adjacent to the disk collapse, and if the packing of the crystal is more complicated than A–A–A, a stacking fault bounded by a dislocation loop is formed. In a similar way, interstitial silicon atoms that emerge as a result of decay of interstitial complexes can form flat disks of the interstitial type, which are also bounded by dislocation loops. These defects are sufficiently stable and may endure the high temperatures of thermal treatment; they are called residual defects. Usually, however, the formation of {311} rodlike defects precedes the formation of dislocation loops.

Transmission electron microscopy (TEM) makes it possible to directly observe residual defects. Both types of such defects, of both vacancy and interstitial nature, have been observed in irradiated silicon [42]. Combined clusterization of vacancies and interstitial atoms in irradiated silicon complicates the formation of extended defects because of the interaction of point defects with each other and with clusters of such defects [43, 44].

Residual defects begin to form even during rapid thermal annealing (RTA). Figure 1 shows TEM micrographs of silicon after implantation with 1-MeV In^+ ions with doses amounting to 1.5 and 2×10^{13} cm^{-2} and annealing at 900 °C of various duration [45]. After annealing for 5 s, the defects that emerge are chiefly rodlike; they are 10-nm long and have

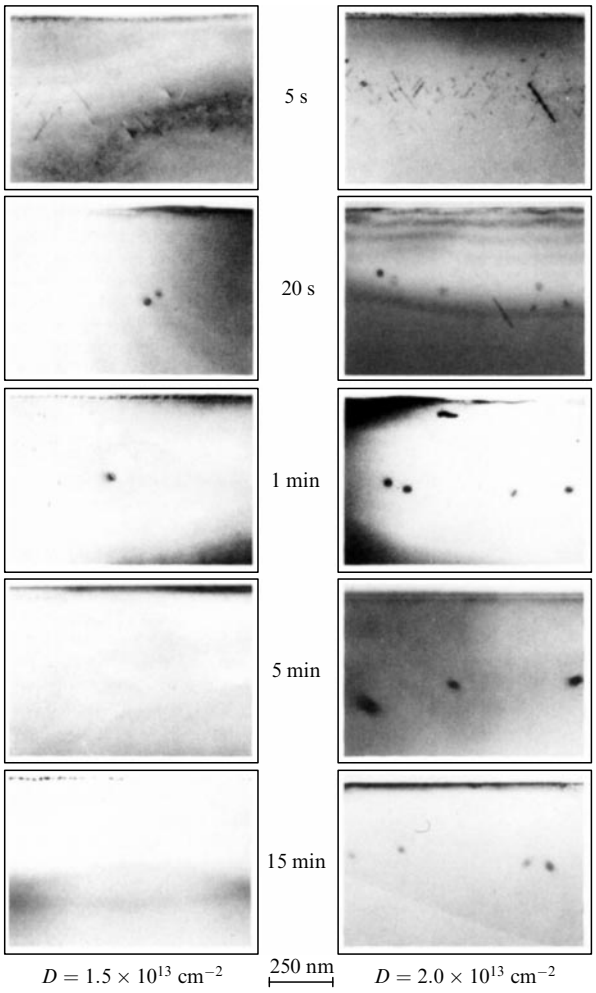

Figure 1. TEM micrographs of silicon after In^+ implantation and annealing (according to Ref. [45]).

a density of 10^{11} cm^{-2}. As the annealing time increases, the rodlike defects transform into circular dislocation loops. Here, as the annealing time grows, the loops increase in diameter by absorbing the point defects of small loops. Only loops of an interstitial nature increase in diameter, while loops of the vacancy type shrink and disappear [42]. Thus, one actually has to deal with residual defects of an interstitial nature. Li and Jones [46] studied secondary-defect formation in silicon implanted with 100-keV Si^+ ions to a dose of 2×10^{14} cm^{-2}. The main defects that form after annealing at 800 °C for less than 5 min are rodlike defects {311} with a concentration of 3×10^{11} cm^{-2}. When the annealing continues for more than 5 min, 50% of the residual defects are circular dislocation loops {111}.

It is still unclear how point defects begin to accumulate and condense into large aggregates and then form dislocations, although this problem has been actively discussed in the literature [44, 47–49]. The main difficulty in describing the nucleation of residual defects is the absence of experimental data on these processes, which is due to the insufficient development of experimental techniques that enable the observation of intermediate defect states between point defects, which are identified by the EPR method, and dislocations, which are visualized directly by the TEM method. It can be expected that ultrahigh-resolution electron microscopy will make it possible to observe these intermedi-

ate defects. Recently, a complex consisting of six vacancies has been visualized. The researchers believe [44] that this complex may serve as a nucleus for the growth of a stacking fault of the vacancy type. It is still unclear what the center of condensation of point defects is and what role the impurities play in this process. It has been suggested that the residual technological impurities in the silicon crystals serve as centers of nucleation and growth of residual defects [50]. An important residual impurity in silicon is oxygen, whose atoms actively participate in the formation of radiation-induced defects. There is no single opinion concerning the role of oxygen in the formation of residual defects. According to Schreutelkamp et al. [51], oxygen has no effect on the formation of residual defects. However, Brown et al. [52] suggest that in Czochralski-grown silicon crystals, after irradiation with 2.3-MeV Si^+ ions to a dose of $2 \times 10^{13} - 10^{15}$ cm^{-2} and annealing at 900 °C, the dislocation-loop concentration is 10 times higher than in crystals grown by the floating-zone method. According to these researchers, oxygen also affects the spatial distribution of the dislocation loops.

Some researchers attribute the formation of residual defects to the presence of implanted impurities [53, 54]. According to Jones et al. [55], residual defects begin to form during annealing if the impurity concentration in the impurity layer reaches a critical value of 1.6×10^{19} cm^{-3}. Bicknell [56] even assumed that dislocation loops are formed because of segregation of boron atoms into flat inclusions. Sechan and Washburn [53, 57] concluded that the boron atoms serve as seeds for the formation of rodlike defects. On the other hand, Tamura et al. [58] concluded that, irrespective of the type of implanted ions, a certain critical dose, which they found to lie between 2×10^{13} cm^{-2} and 1×10^{14} cm^{-2}, must be exceeded. Simpson and Mitchell studied silicon implanted with 540-keV Si^+ ions under various conditions. The researchers varied the target temperature and the ion-current density, which must have an effect on the concentration of the radiation-induced defects, but found no difference in the formation of secondary defects. For doses smaller than 1×10^{14} cm^{-2}, no secondary defects were detected, while at larger doses they detected formation of rodlike defects. The conclusion was that only the dose of ions determines whether residual-defect formation is possible.

However, the nucleation and growth of residual defects are similar in silicon implanted with B^+ [45], Si^+ [46], Ne^+ [61], P^+ [57, 62–64], In^+ [45, 51], or Ga^+ [51, 60] or irradiated with electrons [43, 50], neutrons [65], protons [66], or H_2^+ [67]. The results of these experiments suggest that intrinsic radiation-induced defects are the building blocks for secondary defects.

Benton et al. [68] made an attempt to study the evolution from point defects to extended defects in Si^+-implanted silicon by deep-level transient spectroscopy. They annealed the samples at temperatures ranging from 100 to 680 °C. Point defects disappeared when annealing was carried out up to 600 °C. At an annealing temperature of 600 °C, the dominant clusters were those with levels located in the energy gap at $E_v + 0.29$ eV and $E_v + 0.48$ eV. These are still small clusters, which cannot be observed in a transmission electron microscope. After annealing at 680 °C is completed, there form defects with a level $E_v + 0.50$ eV, and the kinetics of trapping of carriers by these defects suggests that they are large. In the same experiments, the TEM method also reveals the presence of {311} rodlike defects. However, it is still unclear what the intermediate clusters are, although, obviously, such clusters exist [44, 47–49, 69, 70].

There are also papers that present the results of modeling the process of coalescence of interstitial silicon atoms in irradiated silicon [71–75]. Kim et al. [73] calculated the stability of model defect configurations from the viewpoint of the energy minimum as a function of the defect's structure, its size, and the concentration of interstitial atoms in the layer. The researchers found that the formation of chains of interstitial silicon atoms along ⟨011⟩ directions is energy-preferable. Extended {311} defects are formed as a result of the combination of such chains. Pairs of interstitial silicon atoms with a low-energy barrier for incorporation into a cluster play an important role in the process of combining interstitial atoms into chains and then into rodlike defects. Cowern et al. [76] determined the stability of a cluster by calculating the energy of cluster formation as a function of cluster size. When the number of interstitial atoms exceeds 15, the cluster formation energy is approximately 0.18 eV, which is close to the energy of formation of {311} defects. Stable clusters are those that have four or eight atoms. This agrees with the results of Arai et al. [74].

The evolution of residual damage in silicon has been studied by Tamura and Suzuki [60] and Pan et al. [77]. Tamura and Suzuki [60] studied the formation of residual defects in situ, directly in the column of an electron microscope. Heat treatment at 800 °C for no more than 5 min leads mainly to the formation of {311} rodlike defects; when annealing is continued for a longer time, the {311} defects disappear and dislocation loops are formed. Pan et al. [77] distinguish three stages in the evolution of rodlike defects: the nucleation of interstitial clusters, their growth along ⟨110⟩ directions in {311} planes, and their dissolution. Eaglesham et al. [78] used the TEM method to study the evolution of {311} rodlike defects quantitatively. At the beginning of the annealing process, under conditions of strong supersaturation by interstitial silicon atoms, a large number of small precipitates are formed. As the supersaturation diminishes, the small {311} defects begin to dissolve, i.e., they become sources of silicon self-interstitials. This is accompanied by the growth of large precipitates. The driving force of the entire process is the dependence of the binding energy of a silicon atom in an extended defect on the size of this defect. The formation of {111} dislocation loops lags behind the formation of {311} defects, and the material for their formation and growth is the interstitial atoms freed in the decay of rodlike defects. According to Pan et al. [77], at an annealing temperature of 900 °C, 120 s are needed for the decay of {311} defects, while only 60 s are needed for the decay of small {111} loops at 1100 °C. The transformation of point interstitial defects into rodlike defects and then into perfect dislocation loops has been analyzed in Ref. [79]. There, it was assumed that rodlike defects are formed from interstitial complexes in the shape of split dumbbell configurations.

Bonafos et al. [72] theoretically examined the kinetics of coarsening of dislocation loops when such loops are formed in the matrix–amorphous-layer interface, where the loops are both the source of interstitial atoms and, at the same time, sinks for them. With such behavior of interstitial atoms, Ostwald-ripening theory [80] can be used to describe the coarsening of loops. This theory is applied to spherical clusters; Burton and Speight [81] were the first to adopt it to the specific geometry of dislocation loops. The theoretical

description of the evolution of dislocation loops in Ref. [72] consists of two parts. First, the loop growth rate (dr/dt) is calculated on the basis of the theoretical ideas on the growth of stacking faults developed by Hu [82] and Dunham [83]. In these two works the researchers assumed that their growth is determined either by the energy barrier when an atom is trapped by a cluster or by the activation energy of diffusion of an interstitial atom. The second part examines the evolution of the size distribution of loops and the evolution of the loop density. Here the model of Burton and Speight [81] is used.

As a sink, the dislocation encompassing a stacking fault can be represented by a torus of radius r_c (which is usually assumed to be equal to the Burgers vector b) with the loop radius being r [82, 83]. To increase the volume of the loop, an interstitial silicon atom must diffuse to the surface of the torus, overcome the energy barrier, and become a part of the stacking fault. The growth rate is proportional to the concentration gradient in the supersaturated solution of interstitial atoms near the loop and in its vicinity and to the diffusion coefficient D_i of the interstitial silicon atoms. It depends on the height ΔH of the energy barrier on the cluster for a Si atom. The growth rate can be written as follows [83]:

$$\frac{dr}{dt} = \frac{\prod v_m}{b} \frac{r_c^2}{r_a^2} (1 + B)^{-1} \exp\left(-\frac{\Delta H}{kT}\right) D_i (C_i' - C'), \quad (1)$$

where v_m is the atomic volume, r_a is the atomic spacing, kT is the thermal energy, C_i' is the mean concentration of interstitial silicon atoms between loops, C' is the concentration of interstitial silicon atoms in equilibrium with a loop of radius r, and $B = 0.5 \ln(8r/r_c)(r_c/r_a)^2 \exp(-\Delta H/kT)$, which to the first approximation is a constant, since it changes little with r.

The expression for C' corresponding to the minimum value of the total stacking-fault energy can be written as follows [84–86]:

$$C' = C_i^* \exp\left(\frac{\gamma v_m}{bkT}\right) \exp\left(\frac{\sigma v_m}{bkTr}\right), \quad (2)$$

where C_i^* is the thermodynamic equilibrium concentration of interstitial Si atoms in silicon. The first exponential factor is related to the stacking-fault energy (γ is the fault energy per unit area), while the second exponential factor is related to the elastic energy of the loop;

$$\sigma = \frac{\mu b^2 \ln(8r/r_c)}{4\pi(1 - \nu)}$$

is assumed constant since it changes little with r; μ and ν are the shear modulus and Poisson's ratio for silicon, respectively. For sufficiently large values of the loop radius ($r \gg 20$ nm), C' can be written as

$$C' \cong C_i^* \exp\left(\frac{v_m \gamma}{bkT}\right)\left(1 + \frac{\sigma v_m}{bkTr}\right). \quad (3)$$

Equation (3) implies that the concentration of interstitial silicon atoms around the loop increases as the loop decreases. Hence, there is a concentration gradient and a flow of interstitial atoms from small loops to larger loops, i.e., the small loops diminish and the large loops grow in size.

Under conditions where, as the nucleation of loops ceases, no sources and sinks other than the loops themselves exist, the expression for C_i' as the mean concentration of atoms between the loops for $r \gg 20$ nm can be written as

$$C_i' \cong C_i^* \exp\left(\frac{v_m \gamma}{bkT}\right)\left(1 + \frac{\sigma v_m}{bkT\bar{r}}\right) = \overline{C}. \quad (4)$$

Substituting C_i' and C' into the main equation of growth (1), we can find the loop growth rate [81]:

$$\frac{dr}{dt} = \frac{\prod v_m r_c^2}{b r_a^2} (1 + B)^{-1} \exp\left(-\frac{\Delta H}{kT}\right) D_i C_i^* \exp\left(\frac{v_m \gamma}{bkT}\right) \times \left[\frac{\sigma v_m}{bkT}\left(\frac{1}{\bar{r}} - \frac{1}{r}\right)\right]. \quad (5)$$

Equation (5) suggests that loops with $r < \bar{r}$ tend to contract, while loops with $r > \bar{r}$ will grow. Loops with $r = \bar{r}$ neither contract nor grow, but after all small loops disappear the value of $\bar{r}$ increases.

Integrating (5), we arrive at an expression for the evolution of the square of the mean loop radius in time. This growth can be written as follows [81]:

$$\bar{r}^2 = \frac{Kt}{2} + \bar{r}_0^2, \quad (6)$$

where $\bar{r}_0$ is the initial mean loop radius after nucleation. If the coarsening process is determined by the activation energy for diffusion, the coarsening rate $K = K_d$ is given by the expression

$$K_d = \frac{v_m^2 \mu}{2kT(1 - \nu)} D_i C_i^* \exp\left(\frac{v_m \gamma}{bkT}\right). \quad (7)$$

When the loop growth process is determined by the height of the barrier on the cluster, the coarsening rate $K = K_r$ is given by the expression

$$K_r = \frac{v_m^2 \mu}{4kT(1 - \nu)} D_i C_i^* \exp\left(\frac{v_m \gamma}{bkT}\right) \frac{r_c^2}{r_a^2} \ln\left(\frac{8r}{r_c}\right) \exp\left(-\frac{\Delta H}{kT}\right). \quad (8)$$

Equation (6) holds for the case where $\sigma v_m/bkTr \ll 1$, i.e., for loop radii exceeding 20 nm. In a more rigorous approach, Eqn (6) assumes the form

$$\bar{r}^2 \exp\left(-\frac{a}{\bar{r}}\right) = \frac{Kt}{2} + \bar{r}_0^2 \exp\left(-\frac{a}{\bar{r}_0}\right), \quad (9)$$

where $a = \sigma v_m/bkT$.

The solution to the equation of the evolution for the loop-size distribution yields the following distribution as a function of time:

$$N(\rho, t) = A \frac{\rho}{(2 - \rho)^4} \exp\left(-\frac{4}{2 - \rho}\right)\left(\bar{r}_0^2 + \frac{Kt}{2}\right)^{-1}. \quad (10)$$

This distribution holds for $0 < \rho < 2$; at $\rho > 2$, we have $N(\rho, t) = 0$; $\rho = 2$ is the cutoff value. The above suggests that there cannot be a loop whose radius exceeds twice the mean value. Integrating (10) over all possible values of ρ, i.e., from 0 to $\rho = 2$, we arrive at an expression for the following time dependence of loop density [81]:

$$N_t = \frac{N_0}{1 + Kt/2\bar{r}_0^2}. \quad (11)$$

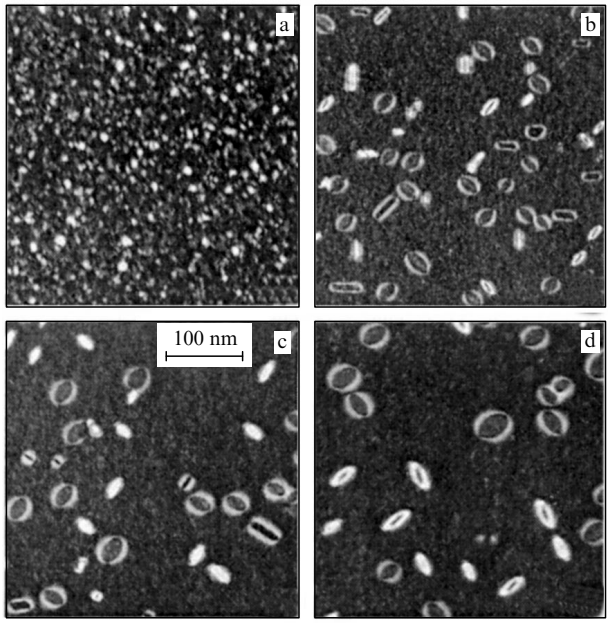

Figure 2. Evolution of secondary defects upon annealing (at 900 °C) of silicon implanted with 150-keV Ge^+ ions to a dose of 2×10^{15} cm^{-2}; the annealing times t were (a) 1, (b) 10, (c) 100, and (d) 1000 s [81].

The results of the experimental work done by Burton and Speight [81] suggest that the temporal variation of the loop-size distribution in silicon implanted with 150-keV Ge^+ ions to a dose of 2×10^{15} cm^{-2} is described fairly well by the theoretical distribution (10). Figure 2 shows the evolution of secondary defects in implanted silicon annealed at 900 °C. Good agreement between the experimental and theoretical results was observed at different annealing temperatures from 900 to 1100 °C. These experiments also determine the activation energy E_{act} for loop growth. The expression for loop growth within a broad range of radii as a function of the annealing temperature was written in Ref. [72] as follows:

$$T\left[\bar{r}^2 \exp\left(-\frac{a}{\bar{r}}\right) - \bar{r}_0^2 \exp\left(-\frac{a}{\bar{r}_0}\right)\right] = C \exp\left(-\frac{E_{act}}{kT}\right), \quad (12)$$

where C is assumed constant. Since $\bar{r}_0 < \bar{r}$, we have

$$\bar{r}_0^2 \exp\left(-\frac{a}{\bar{r}_0}\right) \ll \bar{r}^2 \exp\left(-\frac{a}{\bar{r}}\right),$$

with the result that Eqn (12) becomes

$$T\bar{r}^2 \exp\left(-\frac{a}{\bar{r}}\right) = C \exp\left(-\frac{E_{act}}{kT}\right). \quad (13)$$

This expression shows that it is possible to determine the activation energy of this process from the temperature dependence of loop growth.

In the experiment, the sample was first annealed for a short period (1 s) at 900 °C so that the loops could nucleate. Then the sample was cut into several parts, the temperature curves of loop growth were built, and the activation energy of the process was determined. For short annealing times (10 s), the activation energy was about 1 eV; for long annealing times (longer than 100 s), the activation energy for loop growth was found to be 4.4 eV. Bonafos et al. [72] assume that for annealing times of up to 10 s there is still no equilibrium between the point defects and the clusters; the loops continue growing at the expense of interstitial atoms from the highly supersaturated solution, and the magnitude of the activation energy is still related to the activation energy of diffusion of interstitial silicon atoms. When equilibrium is established, the loops grow only due to the decay of smaller loops. The activation energy for loop growth in this case (4.4 eV) becomes related to the self-diffusion activation energy [87]. We believe that under strong supersaturation the interstitial silicon atoms form Si–Si pairs, each of which is created when two Si atoms not linked by a covalent chemical bond land at random in a single interstitial position. They are held at this site only by the potential field of the crystal and exist as a pair as long as there is strong supersaturation with point defects. We may expect that the activation energy for migration of such a pair is lower than that for an isolated self-interstitial. Such a model was proposed in Ref. [88] for a diffusion pair consisting of an interstitial phosphorus atom and an interstitial silicon atom. The activation energy of diffusion of interstitial Si atoms in silicon for moderate supersaturation, 4 eV, is also typical of experiments concerning both the formation of extended defects and diffusion of impurities in the presence of self-interstitials. At the same time, for the known di-interstitial centers Si–P6 [31] and Si–B3 [32], the activation energies for annealing amount to 0.8 eV and about 2 eV, respectively. These values determine the energies of breakup of these complexes rather than diffusion accompanied by the formation of extended defects. These facts suggest that we are not dealing here with the formation of extended defects directly from split di-interstitial defects. Rather, when irradiated samples are heated, the split interstitial defects disintegrate and form free (i.e., not linked by covalent bonds in split configurations) interstitial silicon atoms, and it is these atoms that form rodlike defects and dislocation loops.

Bonafos et al. [72] theoretically investigated the coarsening of dislocation loops when such loops already existed, while Lampin and Senez [71] theoretically studied the nucleation process. The nucleation of precipitates occurs because of the difference between the free energy of the state with a strong supersaturation in isolated interstitial atoms and that of the state with interstitial atoms localized in dislocation loops. This difference in free energy depends on the precipitate's size and is shown schematically in Fig. 3. The nucleation activation energy Δg^* is related to the critical size of the precipitate. This critical size depends on the deformation parameters of the crystal, temperature, and the degree of supersaturation in interstitial atoms. In examining the

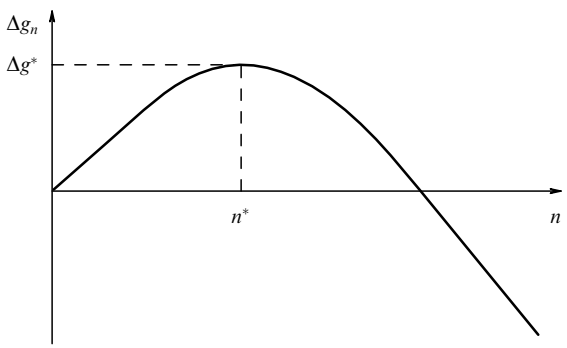

Figure 3. Free energy of dislocation loops as a function of the number n of interstitial atoms [71].

process of cluster formation it is assumed that the process is limited by the diffusion of interstitial atoms rather than by the barrier on the cluster [72].

Following Russell's approach [89], we can write the nucleation rate $J(t)$ as

$$\frac{\partial C_{\mathrm{DL}}}{\partial t} = J(t) = J_{\mathrm{S}} \exp\left(-\frac{\tau}{t}\right), \tag{14}$$

where C_{DL} is the dislocation loop concentration, J_{S} is the equilibrium nucleation rate given by the formula

$$J_{\mathrm{S}} = C_{\mathrm{I}} h^* Z \exp\left(-\frac{\Delta g^*}{kT}\right), \tag{15}$$

and

$$\tau = \frac{1}{2Z^2 h^*} \tag{16}$$

is the incubation period. Here C_{I} is the concentration of free interstitial atoms, h^* is the rate of growth of a critical precipitate, and Z is the Zel'dovich factor, which reflects the curvature of the free-energy curve in the vicinity of the critical point (see Fig. 3). There are three stages in the change of the nucleation rate. The first stage corresponds to the incubation period, during which the nucleation rate increases. At this stage the interstitial Si atoms leave the radiation-induced defects. Then the nucleation rate reaches an equilibrium value J_{S}. The concentration of interstitial atoms, which may form precipitates, decrease in time, and at the third stage the nucleation rate decreases.

The fact that implanted layers are close to the crystal's surface, which is a possible sink for point defects, has aroused interest in studying the effect of the surface on the formation of residual defects. Chason et al. [90] and Moller et al. [91] discovered no such effect, at least when the layer lies deeper than 2000 Å. Raman et al. [92] reduced the distance from the sample's surface to the layer with residual defects that have already formed from 2600 to 1800 Å and even to 1000 Å by polishing the surface. Then the samples were again annealed in a nitrogen atmosphere at 900 and 1000 °C. TEM studies revealed that near the surface the density of small dislocation loops and the loop size diminished. It has also been found that the flux of interstitial atoms to the surface varied in inverse proportion to the depth at which the loops resided. This means that the dissolution of loops is determined by the diffusion of point defects. Assuming that around the loops there is supersaturation in silicon self-interstitials and integrating the flux of Si atoms from the loops to the surface, the researchers estimated the degree of supersaturation at different depths and different annealing temperatures.

3.2 Threshold dose for residual-defect formation

Do residual defects always form in ion-implanted silicon layers upon annealing? Figure 1 shows that in silicon layers created by implantation of 1-MeV In^+ ions with doses of 1.5×10^{13} and 2×10^{13} cm^{-2} and short annealing times (5 s), residual defects emerge primarily in the form of rodlike defects. At the larger dose, as the annealing time increases, the defects transform into dislocation loops, whose concentration stabilizes with the passage of time. At a somewhat smaller dose (1.5×10^{13} cm^{-2}), the residual defects completely disappear as the annealing time is increased. The extent to which these two doses introduce defects into In^+-implanted silicon layers can be estimated if we turn to Fig. 4, which shows the defect profiles registered by the ion Rutherford backscattering (RBS) method. Clearly, the difference in the concentrations of radiation-induced defects in silicon layers for these two doses is moderate, but the formation of residual defects differs dramatically (see Fig. 1). Similar results have been obtained for light and medium-weight ions implanted in silicon at energies of about 100 keV and several MeV [93]. No dislocations were detected in silicon layers created by B^+ implantation with doses of 7×10^{13} cm^{-2}, but they were detected for a dose of 1×10^{14} cm^{-2}. After implantation the samples were annealed at 900 °C for 15 min. No residual defects were detected after annealing for the case of implantation with 200-keV Si^+ and P^+ ions to a dose of 5×10^{13} cm^{-2}, but they were detected at a dose of 1×10^{14} cm^{-2} [51]. These examples show that there is a threshold value of the concentration of radiation-induced defects in the layer for the formation of residual defects upon annealing. The physical meaning of the critical concentration of defects becomes clear after we examine the conditions influencing residual defect formation.

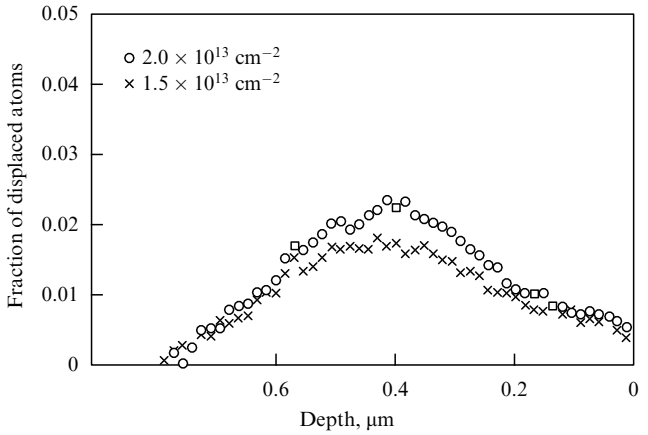

Figure 4. Damage profiles in silicon implanted with 1-MeV In^+ ions to two different doses [45].

3.3 Effect of implantation conditions on residual-defect formation

3.3.1 Ion mass. Investigations have shown that the concentration of radiation-induced defects in a damage layer is not an absolute criterion for dislocation formation. The critical value of concentration depends on the type of ion. Most unexpected were the results of residual-defect formation in silicon implanted with light B^+ ions as compared to silicon implanted with medium-weight ions (Si^+ and P^+) [51]. In these experiments the ion energy was about 100 keV. It turned out that the critical concentration of defects in the damage layer for the case of medium-weight ions was much higher than for case of the light B^+ ions. Schreutelkamp et al. [51], basing their reasoning on Crowder and Title's work [94], relate these differences to the type of radiation-induced defects. In the case of light ions, point defects with a moderate density in the cluster regions are formed. But in the case of Si^+ and P^+, the radiation-induced defects are concentrated in cluster regions with a high local density. Schreutelkamp et al. [51] believe that the central parts of these regions are amorphous. Upon heat treatment, the amorphous inclusions recrystallize, but, naturally, in this process they do not supply point defects for the formation

Table 3. Parameters of DCRs created by Si^+ and B^+ ions.

Ion	D_{cr}, cm^{-2}	C_{cr}, cm^{-3}	V, %	C_{DCR}, cm^{-3}
B^+	9×10^{13}	4×10^{18}	4	1×10^{20}
Si^+	8×10^{13}	4×10^{19}	10	4×10^{20}

of dislocations. The researchers assume that this explains the higher critical concentration of defects in the case of medium-weight ions compared to that of light ions. However, at present it is clear that defect-cluster regions (DCRs) created in silicon implanted with medium-weight ions are not amorphous. For amorphous inclusions to be created by implanting 200-keV Si^+ or P^+ ions in silicon, a threefold overlap of DCRs is required [95]. Studies of the accumulation of radiation-induced defects have made it possible to determine the parameters of the DCRs that arise in silicon implanted with various ions [41, 95, 96]. Table 3 lists the critical doses D_{cr} needed for the beginning of the formation of residual defects, the corresponding concentrations C_{cr} of defects in the layer, the relative volume V occupied by the DCRs at a critical dose, and the defect concentrations C_{DCR} in the DCRs. It is seen that the critical concentration of defects in a silicon layer implanted with Si^+ ions corresponding to the beginning of dislocation formation is 10 times greater than the threshold value for B^+-implanted silicon. What is also important is that in the case of B^+ ions the residual defects are formed if the DCRs occupy 4% of the implanted layer; in the case of Si^+ ions this figure is 10%. The concentration of radiation-induced defects in an average DCR in B^+-implanted silicon amounts to 10^{20} cm^{-3}, while in the case of Si^+ ions this concentration amounts to 4×10^{20} cm^{-3}. In both cases, B^+ and Si^+, at critical doses, the relative volumes occupied by DCRs are still not large, 4% and 10%, respectively. Therefore, it is natural to assume that residual defects are mainly formed in DCRs independently from each other. But if this is so, the meaning of the critical defect concentration becomes unclear. It is also unclear why in the case of DCRs with a higher local defect density (Si^+ ions) a larger number of such regions is needed for residual-defect formation to begin than in the case of DCRs with a lower local defect density (B^+ ions).

As is well-known, the presence of radiation-induced defects increases the lattice parameter of the silicon crystal. In a DCR the lattice parameter must be larger than the average value over the layer, but since this region is surrounded by a more perfect matrix, elastic stresses build up at the interface and diminish as we move away from the DCR. These elastic stresses can serve as an additional driving force for migration of point defects away from the DCR upon heat treatment. The escape of defects from DCRs and the formation of residual defects are competing processes: when there are only a few DCRs, defect escape is predominant and no residual defects are formed; as the number of DCRs increases, the elastic-stress fields generated by them in the layer overlap and thus the total field becomes smoother. As a result, the rate of migration of defects from the DCRs decreases upon heating and hence the efficiency of residual-defect formation increases.

For Si^+ ions, as compared to B^+ ions, the concentration of radiation-induced defects in a DCR is higher than in the matrix. Hence, the elastic stresses around DCRs are higher in this case, so that the smoothing of them requires a greater density of DCRs. In the case of light ions the concentration of defects in DCRs is lower and, what is important, defects are also formed outside the DCRs, so that the smoothing out of the elastic stresses requires lower DCR concentrations. Here, the higher the energy of the ions, the more uniformly the defects are distributed in the layer, which should lower the threshold for the residual-defect formation. This conclusion is corroborated by the data on the critical ion dose, which for 200-keV B^+ ions amounts to 1×10^{14} cm^{-2}, while for 725-keV ions the critical dose is 6×10^{13} cm^{-2} [51]. For Si^+ implantation the threshold dose amounts to about 1×10^{13} cm^{-2} at an ion energy of 1.2 MeV [97] and 7×10^{13} cm^{-2} at 200 keV. The data of Coffa et al. [98] are also an argument in favor of the above ideas concerning the effect of elastic stresses on the formation of secondary defects. The researchers detected an anisotropy in the residual-defect distribution related to elastic stresses at the edges of windows in the SiO_2 or Si_3N_4 masks through which the ions were implanted. Gerasimenko and Mordkovich, together with their colleagues, studied in detail the role of fields (electric and mechanical) in the behavior of radiation-induced defects (e.g., see Ref. [99]).

We have qualitatively examined the effect of elastic stresses on the formation of dislocation loops from the viewpoint of the possibility of uniting interstitial atoms into planar inclusions. On the other hand, Legotin et al. [100] have theoretically studied the effect of elastic stresses on the stability of dislocation loops if such loops exist. They found that the stability of a loop with a critical radius depended on the sign of the elastic stresses acting on this loop.

In addition to the above reasoning for the existence of anomalies in the threshold of residual-defect formation when electrically active impurities are implanted, one must take into consideration factors related to the charge states of the radiation-induced defects. In the process of implantation of boron at room temperature, a considerable fraction (60% [101] or 70% [102]) of this element resides at lattice sites. Hence, we can expect that the two types of interstitial defects that form in the crystal are in the positive charge state, i.e., we have Si–P6 [31] and Si–B3 [32] with annealing temperatures 120 and 480 °C, respectively. In the case of Si^+ implantation, these defects are in the neutral charge state, Si–A5 [33] and Si–O2 [34]. There are no data on the presence of these defects in the negative charge state. Brower [32] and Jadan et al. [36] found that during heat treatment the Si–P6 defects in the positive charge state at 120 °C transformed into the more stable configuration Si–B3. In the neutral charge state, the Si–A5 defects at 160 °C disintegrate and release mobile interstitial Si atoms [36]. These atoms are consumed in annihilation with divacancies. It is the annihilation with interstitial defects that explains the beginning of divacancy annealing at much lower temperatures in silicon irradiated by heavy particles (neutrons and ions) as compared to crystals irradiated with electrons with energies of about 1 MeV or gamma-ray photons, when intrinsic interstitial complexes are not formed in appreciable concentrations. Thus, even before the temperature reaches the annealing temperature, in boron-implanted silicon crystals the low-temperature Si–P6 defects transform into high-temperature Si–B3 defects and add to the concentration of the latter. The data of Lilak et al. [103], who studied the formation (during annealing) of residual defects in silicon heavily doped with boron and irradiated by Ge^+ ions, also serve as an argument in favor of the above ideas. The density of the dislocation loops increases with increasing boron concentration up to 2×10^{18} cm^{-3}. At higher levels of doping of the initial crystals with boron, a reverse effect is observed. This effect is discussed below.

In silicon implanted with Si^+ or P^+ ions, no such additional formation of 'high-temperature' interstitial defects occurs with increasing temperature.

It has been found that ion mass has an effect not only on the residual-defect formation threshold but also on the type of forming residual defects. In the case of the light B^+ ions, at doses of $(1-4) \times 10^{14}$ cm^{-2}, energies of about 100 keV, and annealings for 15 min at 900 °C, the main arising defects are rodlike [104]. But if medium-weight ions are employed, for the same annealing conditions and energies, circular dislocation loops are formed in addition to rodlike defects. However, if the boron ion dose is high (1×10^{15} cm^{-2}), only dislocation loops are formed during annealing. These results suggest that the larger the number of point defects in the impurity layer, the higher the probability that only circular dislocation loops will be formed in the annealing process. Kalinin et al. [67] studied in detail the transformation of residual defects for different H_2^+ ion implantation doses. The researchers found that when the concentration of point defects was high, the emerging rodlike defects interacted with one another and dislocation loops and dipoles were formed. The interaction between dipoles and vacancies also led to the formation of dislocation loops.

The formation of residual defects caused by implantation of heavy ions depends on the ion energy. In silicon implanted with heavy ions Sb^+ [55] or Ga^+ [51] with energies of about 100 keV, no residual defects are formed up to doses that lead to total amorphization. In the annealing and recrystallization of the amorphous layer, point defects are not supplied to the process of residual-defect formation. But when the energies of the ions used in the implantation process are high (mega-electronvolts), more energy is lost in inelastic interactions and the ion tracks are not completely amorphous. In this case there are enough point defects for dislocation loops to form. For 50-keV Ge^+ ions, no residual defects are formed after implantation to a dose of 8×10^{15} cm^{-2} and rapid thermal annealing [105]. But if the energy of these ions is 100 keV, dislocation loops arise at the amorphous-layer – matrix interface; in this case the depth distribution of defects is less slanted, and on the 'tails' of the distribution there are enough point defects for the formation of dislocations.

3.3.2 Implantation temperature. The efficiency of the formation of stable radiation-induced defects is known to depend on the implantation temperature, so it is only natural to expect a certain temperature dependence of residual-defect formation. Figure 5 shows the RBS spectra for silicon samples implanted with 1-MeV B^+ ions to a dose of 5×10^{14} cm^{-2} for different substrate temperatures [106]. The spectra for unimplanted silicon are also shown for the sake of comparison. As expected, the extent of crystal imperfection decreases as the implantation temperature grows. Figure 6 shows TEM micrographs of silicon after implantation at 25, 200, and 400 °C followed by annealing at 900 °C for 15 min. In all implantation regimes, bands of elongated dislocation loops with lengths up to 1 μm were observed at a depth of 1.6 μm. When silicon was implanted with B^+ ions to a dose of 5×10^{14} cm^{-2} at room temperature, the concentration of defects in the layer was eight times higher than the threshold value needed for the formation of residual defects. The concentration of defects at the implantation temperature of 400 °C is much smaller than the critical one. Nevertheless, the residual defects are detected in virtually equal concentrations. The results of these experiments suggest that already in the

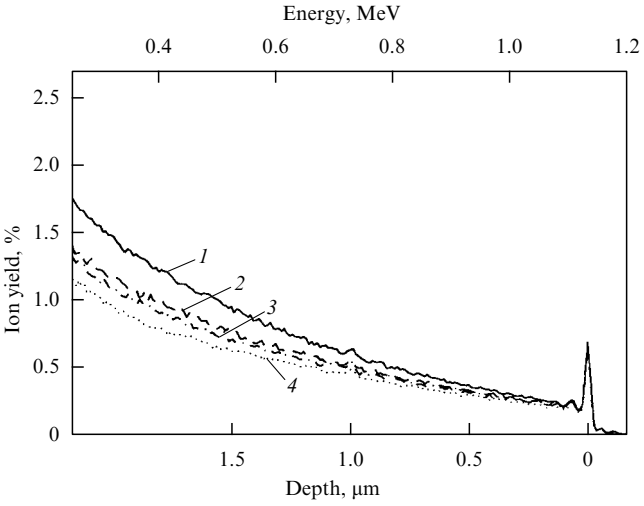

Figure 5. RBS spectra in the channeling regime for silicon implanted with 1-MeV B^+ ions in a dose of 5×10^{14} cm^{-2} at the following substrate temperatures: (*1*) 25, (*2*) 200, and (*3*) 400 °C; (*4*) unimplanted silicon [106].

implantation processes at 200 and 400 °C the formation of residual defects occurs in such a way that in the end, after final annealing at 900 °C, the concentrations of residual defects are roughly the same.

Acco et al. [107] obtained interesting results for heavy ions concerning the dependence of the residual-defect formation on the implantation temperature. Implantation of heavy ions at room temperature leads to the formation of an amorphous layer and, as noted earlier, no residual defects form in the recrystallization process. Residual defects can form only at the interface between the amorphous layer and the crystal, and these are defects of type II. But if implantation is carried out at low temperatures, the layer is amorphous and resides in the transition region. Schreutelkamp et al. [51] found that as the implantation energy decreases, the distribution of the defects in the layer becomes more pronounced, and the transition layer becomes so thin that the number of radiation-induced defects in it is smaller than the critical number, and no residual defects are formed. On the other hand, as the temperature at which heavy ions are implanted grows, amorphization of the layer does not occur, but the number of radiation-induced defects is still large enough for residual defects to form. For instance, when In^+ ions are implanted at −85 °C, the number of displaced atoms estimated by the RBS method is 1.9×10^{17} cm^{-2}, but in view of the amorphization of the layer, no dislocations are formed [106]. On the other hand, if implantation is carried out at 500 °C, the number of displaced atoms (stable defects) is smaller than 10^{16} cm^{-2}, i.e., 40 times smaller, but after annealing at 900 °C residual defects are detected. As noted earlier, at an elevated substrate temperature residual defects can form directly in the amorphization process.

3.3.3 High-intensity ion implantation. Merli and Zignani [108] were, apparently, the first to notice that the amount of energy released in the sample in ion implantation is equal to the amount of energy usually spent on annealing thermally isolated semiconductor wafers by incoherent light or an electron beam in millisecond or second duration intervals. Increasing the ion-current density in implantation can increase the sample temperature up to the surface-melting

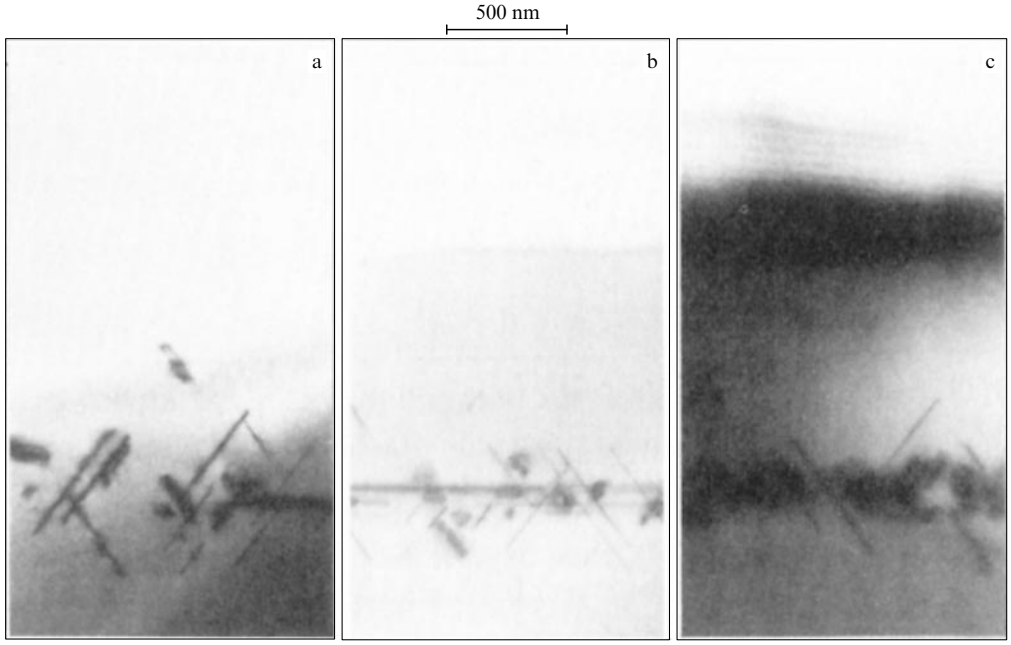

Figure 6. TEM micrographs of silicon implanted with 1-MeV B^+ ions to a dose of 5×10^{14} cm^{-2} at the following substrate temperatures: (a) 25, (b) 200, and (c) 400 °C. Annealing at 900 °C for 15 min [106].

temperature. Implantation regimes that combine in a single operation the dosing of the implanted impurity atoms, the restoration of the crystal structure, and the electric activation of the impurity (when Groups III or V elements are implanted) have become known as self-annealing implantation. The use of self-annealing implantation regimes saves one the trouble of subjecting the samples to postimplantation annealing. The high rate of ion dose buildup and the change in the target temperature in self-annealing implantation lead to a number of special features in defect formation and the behavior of the implanted atoms. All these aspects have been thoroughly studied in experiments and there is an abundance of experimental material on the subject [109 – 114]. It has been established that in the interaction of high-intensity ion beams and semiconductor crystals the nature of the structural changes in the crystals depends on a number of parameters, such as the mass and energy of the implanted ion, the current density of the ion beam, thermal conditions in the implantation process, and the chemical nature of the implanted atoms. In the most general case, a characteristic feature of the self-annealing regime is the presence of four stages in the changes of the crystal structure [115].

The first stage is that of the accumulation of radiation-induced defects. It has been found that, at a constant temperature, the damage inflicted on the crystal increases with ion-current density. For high-intensity implantation the picture is somewhat more complicated, since the target temperature changes during implantation. Defect formation competes with defect annealing. The formation of defects at the initial stage of high-intensity irradiation of silicon has been studied most fully for the case of Si^+ ions [116]. In these experiments the ion energy was 120 keV and ion doses varied from 5×10^{13} to 10^{16} cm^{-2}. The current density in the ion beam varied from 0.14 to 100 μA cm^{-2}. RBS and TEM were used to study the structure of the defects and their distribution in space. It was found that, along with radiation-induced defect accumulation, dislocation loops of the interstitial type with sizes varying from 1 to 10 nm were formed. The number of loops and their size increase with the ion-current density. The first stage ends when a continuous amorphous layer is formed.

In the second stage, stabilization of the amorphous layer occurs. Further irradiation broadens this amorphous layer, but at the same time the temperature of the crystal grows and defect accumulation competes with defect annealing. At a certain critical temperature depending on the ion-current density and the mass and energy of the particles, the thickness of the amorphous layer stabilizes [116 – 121]. In the case of light ions, amorphization of the layer may not even take place. In this case, at a certain critical temperature the concentration of the radiation-induced defects and the width of the damage layer stabilize.

In the third stage, crystallization of the amorphous layer occurs. Studies of the crystallization rates in the self-annealing regimes of the implantation of P^+ ions [122] and As^+ ions [123] have shown that at 550 °C this rate is 45 nm s^{-1}. At the same time, it is known [124] that in ordinary thermal crystallization at 600 °C this rate does not exceed 10 nm s^{-1}. In ordinary thermal crystallization the activation energy is 2.7 eV. The activation energy of crystallization of the amorphous layer upon high-intensity ion implantation does not exceed 1 eV [119, 125]. Apparently, this is due to the presence of excess point defects of both types, vacancy and interstitial. The third stage of structural changes in the process of self-annealing implantation ends by the crystallization of the amorphous layer at a temperature higher than the critical.

The fourth stage ends by the formation of residual defects. Holland and Narayan [126] used the RBS and TEM methods to study the structure of defects and their spatial distribution in silicon after the high-intensity implantation of 120-keV Si^+ ions with a current density of 100 μA cm^{-2} and a dose of 7.5×10^{15} cm^{-2}. They found that the single-crystal structure of the implanted layer was completely restored. However, in

the crystal they detected two layers containing residual defects, primarily in the form of loops of the interstitial type and dislocation tangles. One layer was at a depth of 290 nm at the interface between the crystal and amorphous phases, and the other at a depth of 170 nm. It is assumed that the latter is formed at the place where crystallization fronts travelling from the surface and from the bulk of the crystal meet. Electrical measurements have shown that implantation of Group III or V elements in the self-annealing regime at high ion-current densities guarantees an almost total activation of the impurities [127 – 129]. For instance, at a current density of P^+ ions equal to 230 μA cm^{-2} it takes five seconds for the temperature to rise to 1450 K, and at an ion current density of 500 μA cm^{-2} it takes only two seconds for the temperature to rise to 1630 K. The impurity profiles broaden substantially, and impurity diffusion cannot be described by the common thermal-diffusion model.

Thus, despite the restoration of the crystal structure and complete activation of the injected impurities in self-annealing implantation, layers free of residual defects cannot be produced.

3.3.4 Implantation in the channeling regime. In the channeling regime the ions lose their energy mainly in inelastic collisions, with the result that fewer radiation-induced defects form in this regime than when the implantation is performed in a 'random' direction. However, in practice it has proved difficult to obtain profiles that are uniform over the entire wafer [130], but implantation machines with a combined system of scanning (electrostatic and mechanical) support channeled implantation over wafers up to 200 mm in diameter [131]. Channeled implantation has already found practical application in the industrial fabrication of very large-scale integration (VLSI) circuits [132, 133]. However, in using this method there are certain limitations in the ion dose.

RBS research [51] has shown that when the doses of B^+ ions are moderate (1×10^{14} cm^{-2}), the defect concentration obtained in the channeling regime is much lower than for the nonchanneling regime; the difference in the extent of crystal imperfection rapidly decreases as the implantation dose grows. The reason is that random dechanneled ions produce radiation-induced defects, which in turn promote the dechanneling of other ions and a further increase in the number of defects. Accordingly, after annealing these structures at 900 °C for 15 min, in the case of channeled implantation to a dose of boron ions of 1×10^{14} cm^{-2} no residual defects are produced, while as a result of dechanneled implantation such defects are produced. With a higher boron ion dose (5×10^{14} cm^{-2}), residual defects are formed as a result of both implantation regimes.

4. Suppression of residual-defect formation in implanted silicon

4.1 Multistep ion implantation with intermediate annealing of radiation-induced defects

As noted in Section 3, for residual defects in the form of dislocations to arise in implanted silicon in the course of heat treatment, the concentration of radiation-induced defects must be higher than a certain critical concentration. This experimental fact has made it possible to develop a method for fabricating doped silicon layers without residual defects [134 – 136]. Figure 7 shows the RBS spectra for silicon

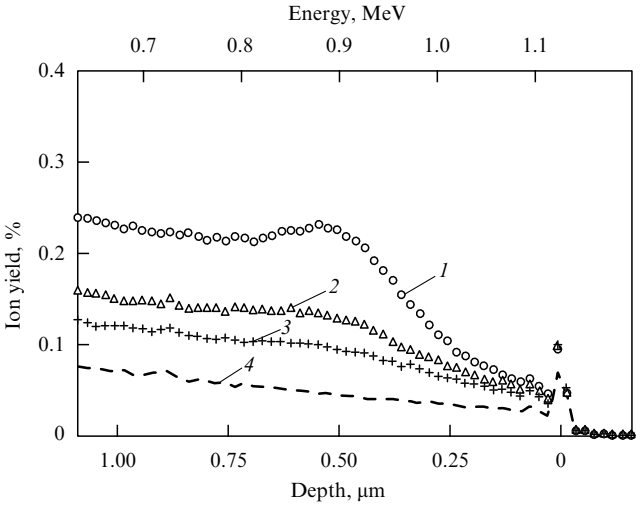

Figure 7. RBS spectra in the channeling regime for silicon implanted by the step-by-step method with As^+ ions (according to Liefting et al. [135]): (*1*) one step, (*2*) two steps, (*3*) four steps, and (*4*) unimplanted silicon.

implanted with 1-MeV As^+ ions to a dose of 8×10^{13} cm^{-2}. This total dose was attained in one, two (4×10^{13} cm^{-2} each), or four (2×10^{13} cm^{-2} each) steps, and after each step the samples were annealed at 900 °C for 15 min. In a single-step implantation, as Figs 8a and 8d show, the high concentration of radiation-induced defects at a depth of 0.5 μm ensures subsequent formation of a high density of dislocation loops. If implantation is carried out in two steps (Figs 8b and 8e) with intermediate annealing, the concentration of dislocation loops is much lower than in the previous case. Four-step implantation (Figs 8c and 8f) results in the formation of doped layers without dislocation loops. Similar results were obtained for P^+ ions. If it took four steps to attain the total dose of 1.1×10^{14} cm^{-2} of 1-MeV P^+ ions (2.8×10^{13} cm^{-2} in each step), no residual defects were formed. For 80-keV boron ions, no residual defects are produced if the dose in one step is lower than 8×10^{13} cm^{-2} [135]. A good illustration of the possibilities that the multistep method opens in fabricating silicon layers implanted with boron ions is Fig. 9, which was taken from Ref. [136]. Clearly, for a total ion dose of 9×10^{14} cm^{-2}, six steps are needed to fabricate silicon layers that are practically free of defects.

4.2 Effect of impurities on the residual-defect formation

Studies of defect formation in silicon implanted with B^+ and C^+ ions, whose masses are close, produced unexpected results [42, 137, 138]. According to RBS data, the concentrations of radiation-induced defects in the implanted layers are practically the same after irradiation, but after annealing in the silicon layer implanted with B^+ ions the residual damage was found to be high; in [135], it is associated with the formation of dislocation loops. In the case of C^+ ions, the RBS spectra after annealing were found to be almost the same as those for unirradiated silicon. Wong et al. [137] and Liefting et al. [138] explain this positive effect by the fact that a carbon atom in the silicon lattice occupies a small volume and that this atom may be surrounded by interstitial silicon atoms that do not participate in the formation of dislocation loops. We believe, however, that this interpretation is unconvincing: usually almost all the interstitial silicon atoms are taken up by residual defects in short-duration annealing and no less than

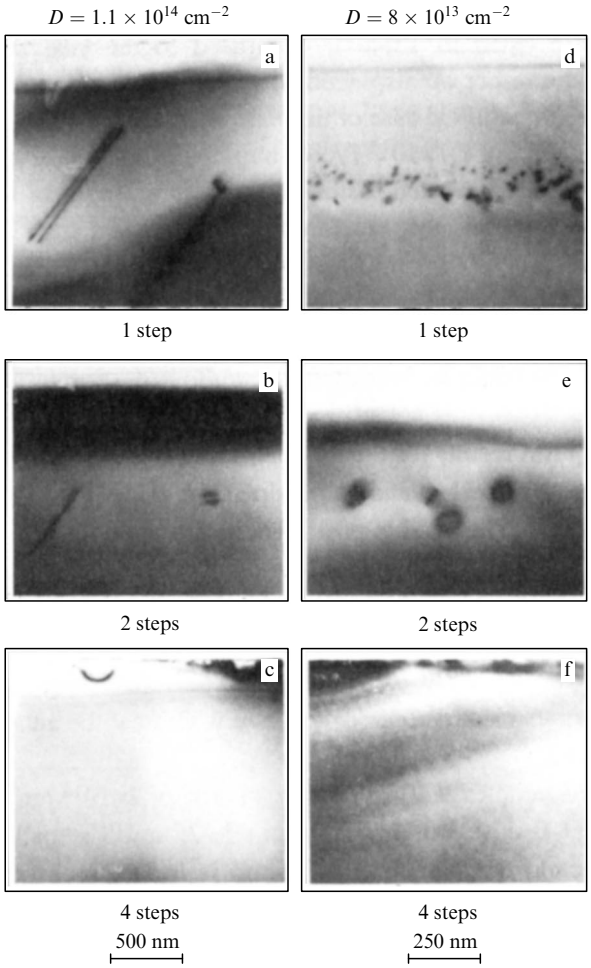

Figure 8. TEM micrographs of silicon implanted using the multistep method with 1-MeV (a–c) P^+ and (d–f) As^+ ions to doses of 1.1×10^{14} and 8×10^{13} cm^{-2}, respectively. Annealing at 900 °C for 15 min [135].

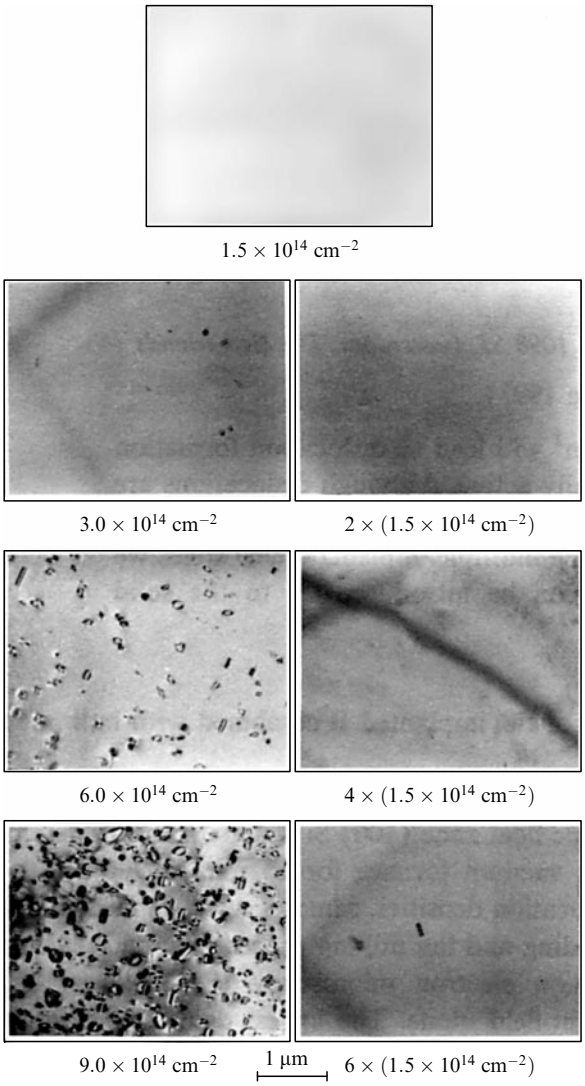

Figure 9. TEM micrographs of silicon implanted with 30-keV B^+ ions in single- and multistep regimes. Annealing at 900 °C for 15 min [136].

10% in prolonged annealing [139, 140]. If these atoms surrounded carbon atoms, their presence should reveal itself in RBS spectra, but so far there is no experimental evidence of this [137].

In our opinion, the mechanism of suppression of residual-defect formation by carbon atoms operates somewhat differently. According to the ideas developed in Ref. [22], all substitutional atoms whose covalent radii differ from the lattice-atom radius are displaced, via the Watkins mechanism, from lattice sites by interstitial Si atoms; this displacement was discovered by Watkins for Group III impurities B, Al, and Ga [15–17]. According to Ref. [22], interstitial silicon atoms move toward substitutional impurity atoms in the elastic strain field generated by these impurities (Fig. 10). The displacement of carbon atoms from lattice sites into interstitial positions by interstitial Si atoms was observed directly by Watkins and Brower [141]. A carbon atom displaced from a lattice site to an interstitial position can then be trapped by a vacancy, etc. Thus, the Watkins effect and subsequent trapping of a substitutional impurity by a vacancy is an additional channel by which point defects are annihilated. This process can be written in terms of the following reactions:

$$C_s + I \rightarrow C_i\,, \qquad C_i + V \rightarrow C_s\,,$$

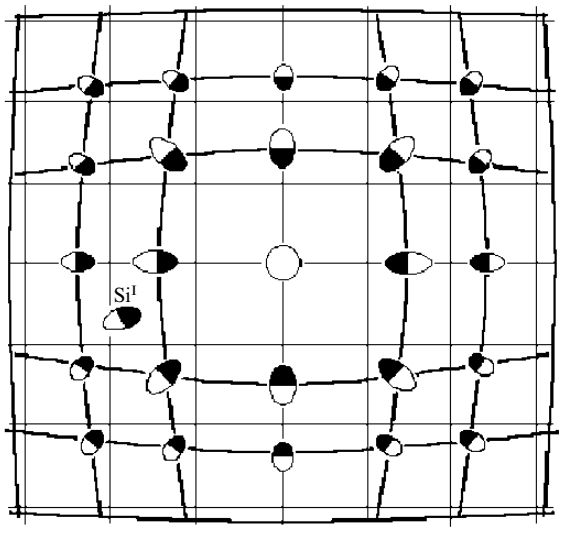

Figure 10. Motion of an interstitial Si atom in the silicon-lattice elastic strain field generated by a substitutional atom whose covalent radius exceeds the radius of a lattice atom [22].

where C_s is a substitutional impurity at a lattice site, I and V are a silicon self-interstitial atom and a vacancy, respectively, and C_i is an impurity in an interstitial position.

The suppression of dislocation formation by using carbon in silicon implanted with phosphorus was described by Tamura et al. [142]. The dose of phosphorus was fairly large, 1×10^{15} cm^{-2}. Additional injection of C^+ ions in a dose of 4×10^{15} cm^{-2} made it possible to suppress dislocation formation almost totally. The equilibrium solubility of carbon in the lattice sites is moderate (2×10^{18} cm^{-2}), but if there is a large concentration of excess vacancies, the carbon solubility increases by several orders of magnitude [143, 144].

Tamura et al. [142] established the need to match the profile of injected C^+ ions to that of the radiation-induced defects generated by the principal impurity. If the carbon profiles are shifted with respect to the profile of radiation-induced defects by 0.2 μm, the positive effect disappears. According to Tsukamoto et al. [145], for small ion doses such a strict match of profiles is unnecessary. The researchers suppressed the formation of residual defects upon annealing of silicon implanted with 700-keV Si^+ ions by additionally implanting 1.6-MeV C^+ ions. In this case the mismatch of the profiles of carbon and radiation-induced defects created by the injection of Si^+ ions amounted to 1.5 μm.

Liefting et al. [138] demonstrated the possibility of suppressing dislocation formation in silicon implanted with B^+ ions within a broad range of doses: from 6×10^{13} to 4×10^{15} cm^{-2}. The doses of 800-keV C^+ ions were within the range from 2×10^{14} to 10^{16} cm^{-2}. On the whole, the results were positive, but it was found that if the dose of C^+ ions exceeds 4×10^{15} cm^{-2}, certain inclusions, apparently related to the supersaturated carbon solution, appear in the layer. There are a number of works devoted to the study of the structure of these inclusions [146 – 148].

If the above mechanism of defect annihilation as a result of consecutive substitution of site carbon by interstitial silicon atoms and its subsequent trapping by vacancies is indeed true, then it is obvious that the carbon atoms in this case are unsaturable traps for point defects and that carbon can eliminate interstitial Si atoms in the amount exceeding that of carbon atoms. Indeed, Claverie et al. [149] found that the efficiency of absorption of interstitial silicon atoms by a carbon atom is greater than unity. But, as the data of Simpson et al. [150] reveal, this absorption is even more effective if carbon atoms are located from the very beginning in lattice sites. This is understandable, since the trapping of interstitial carbon by lattice sites requires some time. Note that the interaction of point defects with carbon and the formation of residual defects are competing processes.

The position of carbon (or another substitutional impurity) at silicon lattice sites is only one of the conditions that ensure the suppression of residual-defect formation. One also needs to know how to control the Watkins reaction and ensure the condition in which carbon will not be displaced from lattice sites by interstitial Si atoms already in the process of implantation of electrically active impurities (boron or phosphorus). During implantation the number of displacements exceeds that of the forming stable interstitial complexes by a factor of roughly 20. It is important to keep the substitutional impurity atoms (e.g., carbon) at sites, so that later they could operate as traps for silicon atoms during heat treatment. Studies of the processes of boron displacement from silicon lattice sites have shown [151] that the Watkins effect can be suppressed by increasing the level of ionization in the implanted layer. In practice this is achieved by increasing the current density in the ion beam. It has also been established that the displacement of boron from lattice sites can be suppressed by heat treatment of the implanted silicon [22]. A characteristic feature of the curves of electrical activation of boron implanted in silicon (these curves reflect the dependence of the charge-carrier concentration on the temperature of isochronal annealing) is the presence of a 'reverse-annealing' stage at 500 – 600 °C. The reason for such a stage is the displacement of boron atoms from lattice sites to interstitial sites by silicon atoms produced as a result of the decay of Si – B3 complexes. If during annealing the implanted layer is irradiated by low-energy (10-keV) electrons with a 5-μA cm^{-2} current density in the electron beam, there is practically no reverse-annealing stage. When the level of ionization is high, the nonequilibrium electrons and holes screen the electric dipoles in the deformed sphere (see Fig. 10), with the result that the motion of silicon atoms in the elastic strain field generated by the substitutional atom is suppressed.

Boron atoms are effectively displaced from lattice sites by interstitial Si atoms [16]. However, as we have noted earlier, in boron-implanted silicon, in contrast to C^+-implanted silicon, residual defects do form. This is probably due to the fact that boron participates in the formation of thermally stable complexes (stage of isochronal annealing at 700 – 900 °C), presumably with divacancies [41]. Both boron and divacancies are used to form these complexes. This hinders consecutive interaction between boron atoms and interstitial Si atoms and vacancies needed for the annihilation of point defects. But if boron atoms are located at the lattice sites, they can serve as traps for interstitial Si atoms [151].

Lilak et al. [103] studied residual-defect formation in silicon heavily doped with boron and irradiated with Si ions. When the concentration of boron in silicon is higher than 2×10^{18} cm^{-3}, the concentration of residual defects decreases with increasing concentration of the substitutional boron in the initial crystals, and at boron concentrations higher than 10^{19} cm^{-3} no dislocation loops are formed during annealing.

4.3 Implantation synchronized with microwave-assisted annealing

Along with traditional methods of annealing of implanted semiconductor structures (furnace annealing and RTA), new methods of annealing are being developed, e.g., microwave-assisted annealing [152]. Most promising among these methods is implantation-synchronized microwave-assisted annealing (ISMAA) [153, 154]. The intensity of absorption of microwave radiation (2.45 GHz) by, and, accordingly, the heating of, a silicon wafer increase with the concentration of free charge carriers. During implantation, a large concentration of nonequilibrium electrons and holes is created due to inelastic losses within the area where the scanning ion beam operates. It is at this moment that there occurs strong absorption of microwave radiation, and local heating follows the scanning ion beam. In this method, the radiation-induced defects created by the ion beam are immediately annealed, and thus there is no accumulation of these defects to a concentration needed for dislocation formation.

The research done by Gay et al. [154] on implanted silicon in the synchronized annealing regime has shown that the doped layers have good electrophysical properties. Electron microscope studies revealed no formation of residual defects.

4.4 Suppression of residual-defect formation in implanted silicon by creating an additional damage layer

Zhao and Wang [155] examined the formation of dislocations in a silicon layer fabricated by implanting 50-keV P^+ ions to two doses, 2×10^{14} and 2×10^{15} cm^{-2}, with complementary irradiation of the crystals by 1-MeV Si^+ ions with doses ranging from 5×10^{14} to 4×10^{15} cm^{-2}. After double implantation had been completed, the samples were subjected to RTA at 950 °C for 20 s in a nitrogen atmosphere. The researchers concluded that the effect of suppression of secondary-defect formation in layers created by P^+ implantation increases with increasing dose of Si^+ ions. Here, as they note, the effect is more pronounced at higher phosphorus doses. The buried damage layer created by the implantation of Si^+ ions serves as a getter for the point defects that form in the surface layer as a result of the decay of radiation-induced defects. On the other hand, Lu et al. [156] studied, by the electron microscopy method, the buried layers of silicon produced by implantation of 2-MeV B^+ ions to a dose of 2.2×10^{14} cm^{-2}, with additional formation of a surface defect layer through the implantation of 140-keV Si^+ ions in three different doses: 1×10^{12}, 1×10^{13}, and 1×10^{15} cm^{-2}. In silicon implanted only with high-energy B^+ ions, a band of defects, mainly in the form of elongated dislocation loops and rodlike defects, appeared at a depth of about 3 μm after annealing at 900 °C for 15 min. If an additional defect layer is created by implanting Si^+ ions in a small dose (1×10^{12} cm^{-2}), then perfect dislocation loops with sizes ranging from 40 to 100 nm arise instead of rodlike defects and elongated dislocation loops. If the dose of Si^+ ions amounts to 1×10^{13} cm^{-2} or greater, then only separate dislocations form in the boron-implanted layer.

Thus, if the number of radiation-induced defects in the additionally created damage layer is smaller than in the main layer, residual defects in the latter form even more effectively than in the absence of an additional layer. Defects leave the main layer for the additional one if the extent of imperfection of the latter is higher than that of the former. This fact can be related to the elastic stresses generated in the implanted crystal [157]. Point defects move in the elastic strain field generated by the defect layers. When there are two defect layers, the resultant field is determined by the layer with the higher concentration of radiation-induced defects.

The use of this method leads to a substantial, but not complete, reduction in the number of residual defects [156]. One more advantage of the method is that the additionally fabricated defect layers are at the same time getters for metallic impurities, which is especially important for the production of semiconductor devices.

5. Examples of implementation of the results of defect-impurity engineering

The use of ion implantation in the fabrication of semiconductor devices and integrated circuits has revealed not only the advantages but also the drawbacks of this method. The obvious advantages are (a) that the doping is uniform over the entire area of the semiconductor wafer and over the depth at which the impurity is located, and (b) that the process is reproducible. At first, the electrophysical parameters of the semiconductor structures fabricated by ion implantation and the device yield were lower than for structures fabricated by the common thermal diffusion method [158]. Electron microscope studies revealed the presence of large numbers of dislocations in the ion-doped layers. With the dislocations in the electrically active regions in devices were associated the elevated leakage currents across junctions, electric short-circuiting, and low gains of transistors. The effect of dislocations becomes stronger if they are decorated by impurities (both doping and residual, metallic). Studies of the temperature dependence of the reverse current–voltage characteristics of p–n junctions have established the values of the activation energy, which were found to be close to half the energy gap. This suggested the presence of deep generation–recombination centers, which were associated with residual defects.

Initially, the efforts of researchers and engineers were directed toward perfecting the regimes of annealing of implanted structures. For instance, it was found that RTA yields somewhat better results compared to ordinary furnace thermal annealing [159]. According to Takahashi et al. [160], an increase in the implantation current density drives the temperature of samples up, and this leads to somewhat better results in residual defects and device parameters. The researchers found that to reduce the dislocation density it is better to carry out postimplantation high-temperature annealing in an inert atmosphere rather than in an oxidizing atmosphere. Subsequent drive-in of the impurity can be done together with oxidation of the wafer surface [161]. The reason is that interstitial Si atoms are produced in the oxidation process, and these atoms add to the interstitial defects of the implantation origin [162–164]. However, the researchers were unable to solve the problem of residual damage solely through thermal treatment.

The next step in eliminating residual structural defects in devices was to carry out implantation through oxide layers. Since in the implanted layers the profiles of the radiation-induced defects and the implanted impurity are spatially separated and the defect profiles are closer to the surface, implantation through an oxide layer of an appropriate thickness created beforehand made it possible to transfer, at least partially, the elastic ion-energy losses into the oxide layer [165]. Figure 11 shows the temperature dependence of the leakage currents across the collector–base junction for different thicknesses of the oxide film. When the film is 0.08-μm thick, the elastic ion-energy losses occur mainly in the crystal. The activation energy determined from the slope of the respective curve amounts to 0.63 eV. This suggests that within the collector–base junction there are generation–recombination centers with energy levels in the middle of the energy gap. If the oxide film is 0.17-μm thick, the dislocation density in the active region of the device is lower by a factor of 1000, according to the data of Ashburn et al. [165], and the activation energy is equal to the energy gap width, thus suggesting that in this case band-to-band generation is predominant. Although, because of the overlap of the defect profile and the implanted-impurity profile, this method does not make it possible to fabricate totally defectless ion-doped silicon layers, it may be considered as the first step in defect engineering in implanted silicon.

The next step in perfecting ion-doping technology followed from the fact that there is a critical concentration of radiation-induced defects at which residual-defect formation begins upon annealing. Liefting et al. [106, 166] demonstrated the potential of defect-impurity engineering by fabricating a vertical bipolar transistor. The schematic of this transistor is shown in Fig. 12. The buried collector in this

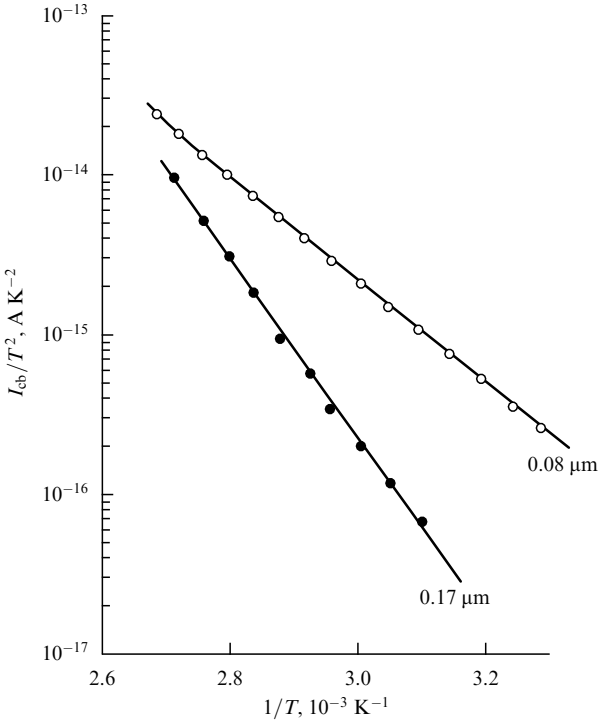

Figure 11. Temperature dependences of the leakage currents across the collector – base junction for 0.17- and 0.08-μm-thick oxide films on the active surface of silicon [165].

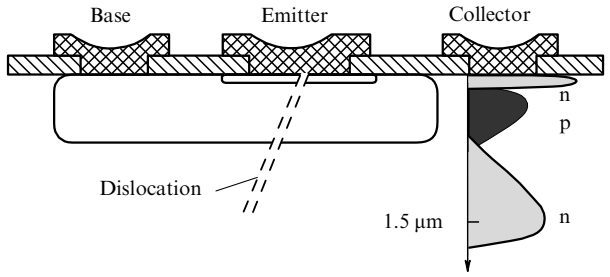

Figure 12. Schematic of a vertical bipolar transistor with a collector formed by implantation of high-energy P^+ ions [166].

transistor is formed by implantation of high-energy (1.5 MeV) P^+ ions. To create a collector with a required low resistance, Bohm et al. [159] and Wijburg et al. [167] used fairly large ion doses, which usually should be no smaller than 4×10^{13} cm^{-2}. At such an energy (1.5 MeV) this dose is much larger than the critical one, and, as a result of annealing of the implanted structures, dislocations must form in the collector region. Studies of the electrophysical parameters of such devices have shown that there are often excess collector currents in them when voltages across the base – emitter junction are low. Figure 13a shows the base current I_b and the collector current I_c as functions of the base voltage V_b. The large values of the collector current I_c are usually related to the electrical short-circuiting of collector and emitter (the c – e short-circuits). These short-circuits determine the device yield. Some dislocations that form in the collector may pass toward the surface, thus short-circuiting the collector – base and base – emitter junctions. Figure 14 shows the device yield as a function of the emitter area. When the emitter area is 10^4 μm^2, 65% of all devices are shorted, while when this area

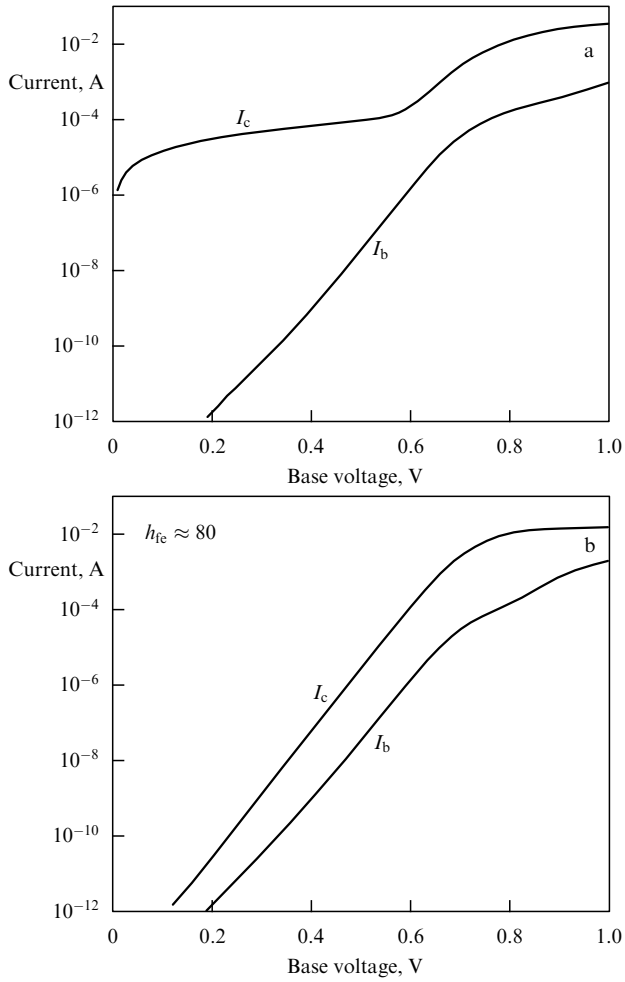

Figure 13. Typical dependence of the collector current I_c and the base current I_b on the potential V_b on the base for (a) a vertical transistor fabricated by the standard technology and (b) a transistor with a collector formed by multistep implantation of P^+ ions or by double implantation of P^+ and C^+ ions; h_{fe} is the current gain of the transistor [166].

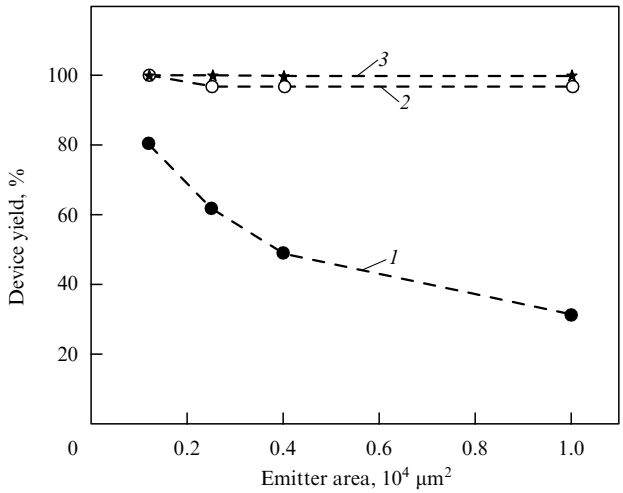

Figure 14. Device yield for transistors with a collector formed by standard implantation of P^+ ions (curve *1*), multistep implantation (*2*), and double implantation with P^+ and C^+ ions (*3*) [166].

is 1200 μm^2, 20% are shorted. This result is expectable, since the greater the emitter area, the higher the probability that a

dislocation will pass through it. To the first approximation, the yield is an exponential function of the emitter area with a 'fatal' dislocation density of 1.25×10^4 cm^{-2} [168]. This value correlates with the results obtained by Bohm et al. [159] and Takahashi et al. [160] for a bipolar transistor with an implanted collector, where the dislocation density was determined from the etch pits on the frontal surface. This means that the dislocation from the collector emerged onto the surface, passing through the entire device. In the collector itself, the dislocation density is on the order of 10^8 cm^{-2} when the dose of 1.5-MeV phosphorus atoms amounts to 4×10^{13} cm^{-2}. Hence only one out of 10^4 dislocations is fatal, i.e., passes through the entire device. Similar results were obtained for a bipolar transistor with a base created by implanting 50-keV B^+ ions to a dose of 6×10^{14} cm^{-2} [165]. Here, the researchers studied the dislocations using data on the etch pits and by the TEM method.

If the collector is formed by two-step implantation, i.e., the dose of 4×10^{13} cm^{-2} is built up in two steps with intermediate annealing at 900 °C for 15 min, the device yield amounts to 97% for an emitter area of 10^4 μm^2 and 100% for small emitter areas (see Fig. 14). For these transistors, the collector currents at low base – emitter voltages correspond to dislocation-free devices (Fig. 13b). Similar results on the device yield have been obtained for transistors fabricated by implanting phosphorus ions and, additionally, carbon ions with doses amounting to 2×10^{14} and 5×10^{14} cm^{-2} (the C^+ ions had an energy of 1.15 MeV).

In Fig. 15 we compare the data on the leakage currents for standard devices and devices with collectors fabricated by two-step implantation of phosphorus or double implantation of P^+ and C^+. For an ideal defectless diode the reverse current – voltage characteristics can be represented in the form $I \sim V^n$, with $n = 0.5$ [165, 168]. Figure 15 shows that for a standard diode (only the collector – base junction is formed; no emitter is present) $n \approx 2$ at low voltages and 4.2 at higher voltages; these are typical characteristics of diodes with dislocations in the junction region [161, 165]. In diodes fabricated by two-step implantation of P^+ or double implantation of P^+ and C^+, the leakage currents under a reverse bias of 5 V are 10 times lower than in diodes fabricated by standard techniques. But under reverse biases from 1 to 5 V, the exponent n is 0.7 rather than 0.5, as it should be for an ideal diode. In the case of additional implantation of C^+, this effect can be related to the existence of carbon precipitates, which, according to Wong et al. [169], lead to an increase in the leakage currents. However, a similar situation is observed in the case of two-step implantation, too; the nature of this effect remains unclear.

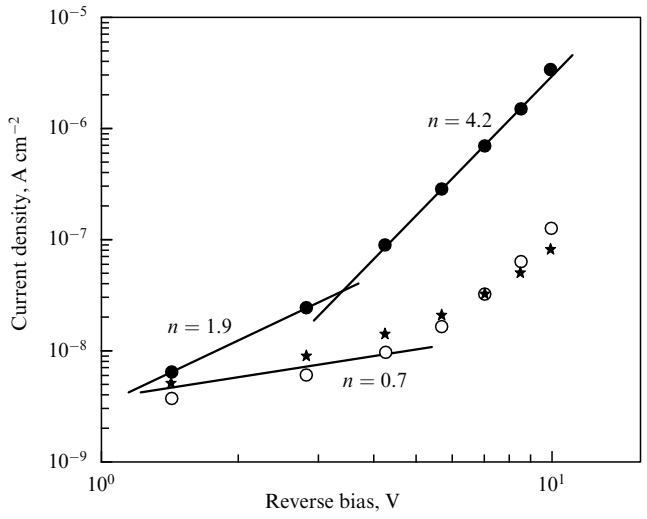

Figure 15. Current – voltage characteristics of the collector – base junction under reverse bias [166]: (●) standard implantation technology, (○) two-step implantation, and (∗) double implantation with phosphorus and carbon.

6. Effect of radiation-induced defects on the diffusion of impurities implanted in silicon. Methods of suppressing anomalously enhanced diffusion

Studies of implanted silicon have revealed that the values of diffusivities of implanted impurities differ substantially from their intrinsic values, i.e., values inherent in ordinary thermal diffusion from an external source. Initially, the enhanced diffusion of implanted boron and phosphorus in RTA was associated with the presence of excess vacancies [170, 171], since it was common practice to assume that in implanted silicon divacancies are the main radiation-induced defects. Interestingly, the retarded diffusion of boron implanted in silicon in thermal annealing in a furnace is also was explained by the effect of excess vacancies as traps for the impurity [172]. According to Werner et al. [173] and Gorban' and Gorodokhin [174], radiation-induced defects have no significant effect on the diffusion of boron and phosphorus. These researchers believe that enhanced diffusion occurs because many implanted atoms are in interstitial positions. It is assumed that the rate of diffusion via the interstitial channel is higher than via the site channel. Enhanced diffusion is present before an equilibrium distribution of the injected impurities over sites and interstices sets in.

To establish the role played by radiation-induced defects in the diffusion of impurities, one group of researchers studied the diffusion of boron [175 – 178] and another group studied the diffusion of phosphorus [179] in silicon layers with different defect concentrations, which were varied by additionally irradiating the layers with Si^+ ions. To exclude the effect of displacement of boron and phosphorus atoms from sites into interstices by interstitial Si atoms in the implantation process (the Watkins effect), silicon was first implanted with Si^+ ions, and only after that was it implanted with boron or phosphorus.

6.1 Diffusion of implanted boron

Table 4 lists the values of the effective diffusion coefficients of boron for different doses of boron ions (Φ_B) and silicon ions (Φ_{Si}) [177]. Also listed are the values of the defect concentration C_d in the implanted layer. Diffusion took place under lamp annealing at 1050 °C for 10 s. In silicon irradiated by small doses of B^+ ions (6×10^{13} cm^{-2}), the diffusivity of boron (7×10^{-13} cm^2 s^{-1}) exceeds the intrinsic value (1×10^{-13} cm^2 s^{-1}) and rapidly increases with the defect concentration in the impurity layer. When boron ion doses are high (3.7×10^{15} cm^{-2}), additional irradiation by Si^+ ions does not lead to a substantial increase in the boron diffusivity; enhanced diffusion is driven by its own internal source. The very process of diffusion at high impurity concentrations creates an excess of interstitial Si atoms, which are responsible for the enhancement of impurity diffusion. This is true not only of the diffusion of an implanted impurity but also of ordinary thermal diffusion from an external source.

Table 4. Boron diffusivities D upon lamp defect annealing vs. concentration C_d of radiation-induced defects in the implanted silicon layer.

Φ_B, cm^{-2}		Φ_{Si}, cm^{-2}			
		0	6×10^{13}	1×10^{14}	6×10^{14}
6×10^{13}	C_d, cm^{-3}	7×10^{18}	4.2×10^{19}	7×10^{19}	Onset of amorphization
	D, cm^2 s^{-1}	7×10^{-13}	4.2×10^{-12}	7×10^{-12}	7×10^{-12}
6×10^{14}	C_d, cm^{-3}	3.6×10^{19}	7.1×10^{19}	1×10^{20}	Onset of amorphization
	D, cm^2 s^{-1}	2×10^{-12}	2.5×10^{-12}	3.2×10^{-12}	3.5×10^{-12}
3.7×10^{15}	C_d, cm^{-3}	1.2×10^{20}	1.6×10^{20}	2×10^{20}	Onset of amorphization
	D, cm^2 s^{-1}	3.5×10^{-12}	4×10^{-12}	4×10^{-12}	4×10^{-12}

Enhanced boron diffusion caused by radiation-induced defects lasts for a short time [180]. At 1050 °C the curve representing the dependence of the boron diffusivity on the annealing time passes through the intrinsic value D_0 on the seventeenth second of annealing, and the diffusivity decreases under further annealing in a furnace (more than 30 s); as the annealing time becomes longer than one hour, the boron diffusivity tends to its intrinsic value.

Table 5 lists the values of the effective diffusivity of boron in thermal annealing in a furnace for different boron doses and different concentrations of the radiation-induced defects in the implanted layer [175]. The annealing temperature was 1050 °C, and the annealing time was 15 min. In the case of thermal annealing in a furnace, for small boron doses (6×10^{13} cm^{-2}), the boron diffusivity D (1.5×10^{-14} cm^2 s^{-1}) is much lower than the intrinsic value (1×10^{-13} cm^2 s^{-1}). With the concentration of radiation-induced defects increasing under additional irradiation with Si^+ ions, the diffusivity increases from 1.5×10^{-14} to 8×10^{-14} cm^2 s^{-1}, but even by the onset of amorphization it does not reach its intrinsic value. For large boron-ion doses (3.7×10^{15} cm^{-2}), as in the RTA case, the appearance of additional radiation-induced defects does not change the diffusivity.

The observed behavior of the diffusion of boron implanted in silicon can be explained by the double-flux diffusion model [181]. Under ordinary conditions, in the absence of excess point defects, boron diffuses partially via the site channel and partially via the interstitial channel. The impurity is mostly situated at lattice sites, but the rate of diffusion over sites is much smaller than interstitial diffusion. And boron atoms continually pass from sites to interstitial positions and vice versa.

The large values of the boron diffusivity in ion-implanted silicon and the increase of this diffusivity with defect concentration is explained by the fact that preferable diffusion via the 'fast' interstitial channel is stimulated by the consecutive displacement of boron atoms from lattice sites to interstitial positions by silicon self-interstitials (the Watkins substitution). Interstitial Si atoms arise as a result of the annealing of interstitial complexes Si – P6 and Si – B3. In view of the large cross section for the displacement of boron atoms from sites by silicon self-interstitials, enhanced diffusion lasts a limited time. Then, interstitial boron atoms are trapped by excess vacancies and the diffusivity drops. The diffusion coefficient is minimum when the impurity concentration is comparable to the vacancy concentration. The state with a preferable distribution of boron over the excess vacancies lives for a fairly long time; at an annealing temperature of 1050 °C approximately one hour is needed for an equilibrium distribution of boron over sites and interstices to set in. As the dose of additional implantation of silicon ions increases, the concentration of vacancy defects becomes much higher than the impurity concentration. The substantial gradient of the defect concentration leads to their diffusion into the bulk of the crystal and, as a result, to the enhancement of boron diffusion over excess vacancies. But since in this case the 'fast' interstitial diffusion channel is excluded, in the limit the boron diffusivity remains smaller than its intrinsic value.

Some researchers (see Refs [182 – 185]) have attributed the observed anomalously low values of the diffusivity of implanted boron during thermal annealing in a furnace to the trapping of boron atoms by dislocation loops that arise as a result of transformation of the radiation-induced defects. However, the observed increase in the diffusivity of boron with the concentration of radiation-induced defects does not support this assumption. Because of an additional implantation of silicon layers with Si ions, the concentration of dislocation loops increases. In accordance with this fact, the diffusivity of boron in these structures must decrease still further if the mechanism of this decrease is the trapping of impurities by residual defects. When suggesting this mechanism of reducing the diffusivity of boron, the researchers probably had in mind a kind of 'dynamic' trapping of boron by residual defects with subsequent freeing of such atoms, since as a result of annealing there is a 100% electric activation of the impurity.

Table 5. Boron diffusivities D in silicon upon thermal annealing in a furnace vs. concentration C_d of radiation-induced defects in the implanted layer.

Φ_B, cm^{-2}		Φ_{Si}, cm^{-2}			
		0	6×10^{13}	1×10^{14}	6×10^{14}
6×10^{13}	C_d, cm^{-3}	7×10^{18}	4.2×10^{19}	7×10^{19}	Onset of amorphization
	D, cm^2 s^{-1}	1.5×10^{-14}	2.5×10^{-14}	6.8×10^{-14}	8×10^{-14}
3×10^{14}	C_d, cm^{-3}	1.8×10^{19}	2×10^{20}	2.5×10^{20}	Onset of amorphization
	D, cm^2 s^{-1}	9×10^{-14}	1.7×10^{-13}	2.5×10^{-13}	3.5×10^{-13}
6×10^{14}	C_d, cm^{-3}	3.6×10^{19}	7.1×10^{19}	1×10^{20}	Onset of amorphization
	D, cm^2 s^{-1}	3×10^{-13}	2×10^{-13}	1×10^{-13}	7×10^{-14}
3.7×10^{15}	C_d, cm^{-3}	1.2×10^{20}	1.5×10^{20}	2×10^{20}	Onset of amorphization
	D, cm^2 s^{-1}	5.5×10^{-13}	5×10^{-13}	5×10^{-13}	5×10^{-13}

Table 5 shows that there is a substantial difference in the boron diffusivity when additional irradiation with Si^+ ions is performed into crystals implanted with small (6×10^{13} cm^{-2}) and moderate (6×10^{14} cm^{-2}) boron doses. In the first case, diffusivity is at its minimum without additional irradiation with Si^+ ions, and this is attributed to the trapping of impurities by excess vacancies. In the second case, additional irradiation by Si^+ ions is needed to reduce the diffusivity. This effect can be explained by the nature of accumulation of radiation-induced ions upon boron implantation. For boron ion doses up to 1×10^{14} cm^{-2}, the number of defects increases linearly with the irradiation dose [41], with the efficiency of the buildup of stable defects being on the order of unity per boron ion. At higher doses there is a sublinear accumulation of defects ($C_d \sim \Phi^{0.5}$), i.e., the volume impurity concentration becomes higher than the volume concentration of stable defects. Hence, only the additional creation of defects by implanting Si^+ ions leads to the trapping of boron atoms by excess vacancies and a decrease in the boron diffusivity upon annealing in a furnace.

The fact that it is silicon self-interstitials that are responsible for the enhanced boron diffusion is supported by the data on the diffusion of boron, including implanted boron, under conditions of oxidation of the silicon surface [186, 187], i.e., the generation of excess interstitial Si atoms. On the other hand, Stel'makh et al. [177, 178] observed a substantial decrease (by a factor of 10) in the boron diffusivity in germanium-predoped silicon layers. Germanium was introduced by implanting it into silicon with subsequent annealing in order to recrystallize the amorphous layer and place Ge atoms at lattice sites. Then boron was implanted and its diffusion was studied. Initially, the reduction in the diffusivity was attributed to the elastic stresses in ion-doped silicon layers [177, 178]. Germanium doping of silicon increases the silicon lattice parameter, while the presence of substitutional boron leads to a compression of the lattice. Since the germanium diffusivity is small, it was assumed that boron remains in the implanted layer to balance the elastic stresses in silicon structures. But it was found later (see Ref. [188]) that a decrease in the diffusivity of implanted boron was observed in silicon layers that had been additionally implanted with carbon. The covalent radius of carbon (and that of boron) is smaller than the radius of the Si atom, and in the case of double doping the elastic stresses in the structures increase. However, the effect in the cases of carbon and germanium is the same. Peterström and Svensson [189] detected a decrease in the boron diffusivity in germanium-doped silicon. Berezhnov et al. [22] developed the idea that, due to the Watkins effect, all substitutional impurities with a covalent radius that differs from the lattice-atom radius serve as traps for interstitial Si atoms. This is illustrated by the curves of electrical activation of implanted boron (the dependence of the sheet concentration of the charge carriers, N_s, on the temperature of isochronal (15 min) annealing) in silicon and in silicon layers doped with germanium (Fig. 16) or carbon (Fig. 17). Emtsev and Margoryan [190] established that the stage of 'reverse annealing' for boron implanted silicon (curves *1* in Figs 16 and 17) is caused by the displacement of boron from lattice sites by interstitial Si atoms that are released in the breakup of interstitial Si–B3 complexes. There is practically no reverse-annealing stage in the curves of electric activation of boron for silicon layers doped with germanium or carbon (curves *2* in Figs 16 and 17).

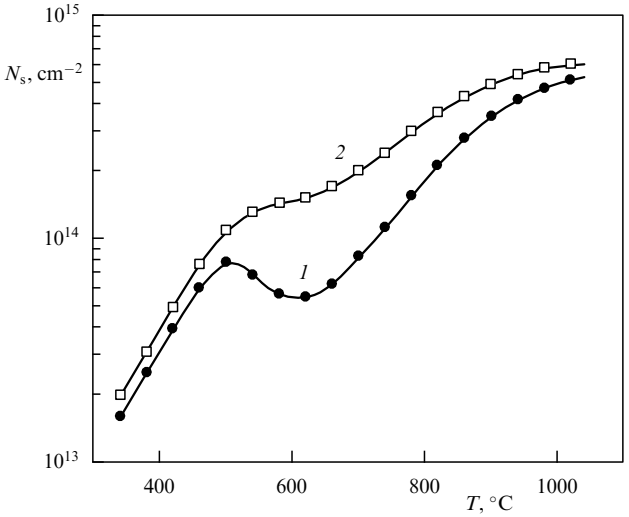

Figure 16. Electrical activation curves of implanted boron in Ge^+-doped silicon layers [178]: (*1*) check sample, B^+ ion dose is 1.3×10^{15} cm^{-2}; (*2*) Ge^+ ion dose of 1×10^{16} cm^{-2} + annealing + B^+ ion dose of 1.3×10^{15} cm^{-2}.

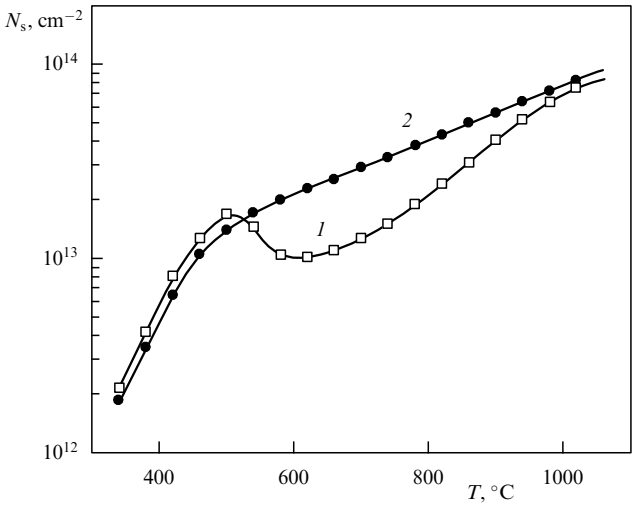

Figure 17. Electrical activation curves of implanted boron in carbon-doped silicon layers [188]: (*1*) check sample, B^+ ion dose is 1×10^{14} cm^{-2}; (*2*) C^+ ion dose of 1×10^{14} cm^{-2} + annealing + B^+ ion dose of 1×10^{14} cm^{-2}.

When the boron ion doses are large, additional introduction of radiation-induced defects does not change the boron diffusivity. In this case, however, the boron diffusivity can be reduced by predoping the silicon layers with germanium [177, 178]. This is just one more confirmation of the fact that it is the interstitial Si atoms that are responsible for the enhanced high-concentration diffusion. The advantage of germanium over carbon in this case lies in the unlimited solubility of germanium in silicon. The cross section for the displacement of germanium atoms from the silicon crystal sites is smaller than that for boron atoms [22], but the possibility of implanting germanium into a silicon layer in concentrations higher than the boron concentration makes it possible to influence the diffusion of the latter. The cross section for the displacement of carbon atoms from the crystal sites is greater than that of boron atoms, but the use of carbon is limited by its moderate solubility in silicon.

Elastic stresses are generated in ion-implanted silicon structures because of the difference in the lattice parameters of the implanted layer and substrate. The lattice parameter of the implanted layer increases due to the presence of radiation-induced defects. During the subsequent thermal treatment some radiation-induced defects are annealed, others are transformed into residual defects, while the implanted impurity is activated and is transferred to lattice sites. If the covalent radii of the atoms of the impurity and the matrix coincide or are roughly the same, as they are, for instance for Si (1.175 Å) and As (1.17 Å), no elastic stresses arise in the structures, at least within the limits of the impurity's solubility. The tetrahedral radii of boron and phosphorus are smaller than that of the Si atom. The difference in the covalent radii of boron (0.8 Å) and silicon is substantial. The misfit of the lattice parameters of the doped layer and the substrate generates a network of misfit dislocations [191]. Kalinin et al. [191] found that these dislocations absorb rodlike defects and dislocation loops. Here, double implantation of boron and germanium has proved to be useful in balancing the elastic stresses. Later, Stel'makh et al. [192] discovered that the boron-to-germanium concentration ratio should be 1 : 8. Also, Ohta et al. [193] discovered an enhancement of perfection of silicon structures ion-implanted with boron and germanium. To balance the elastic stresses in silicon ion-implanted with antimony, carbon can be implanted in addition to antimony.

6.2 Diffusion of implanted phosphorus

A characteristic feature of implanted phosphorus (just as of boron) is its anomalously high diffusivity. In lamp annealing at 900 °C, the diffusivity of phosphorus from the implanted layer exceeds the intrinsic value by a factor greater than 1000. As the annealing time increases, the diffusivity of phosphorus tends to its intrinsic value. Some researchers attribute such enhanced diffusion to the presence of excess vacancies [171, 172]. The enhancement of phosphorus diffusion in the course of oxidation of the silicon surface and, on the other hand, the slowing-down of diffusion in the production of nitride coatings [186, 193 – 195] suggest that we are dealing with stimulation of diffusion by interstitial Si atoms. Pair models were also used to describe the anomalous behavior of phosphorus diffusion, e.g., *E* centers (complexes consisting of a phosphorus atom and a vacancy) or pairs that consist of a phosphorus atom and an interstitial Si atom [196 – 198]. Burenkov et al. [199] and Ajmera et al. [200] demonstrated that the diffusivity of implanted phosphorus is reduced considerably (by a factor of 10 or more) if the layer is predoped with germanium or carbon. These results suggest that the enhanced diffusion of phosphorus is caused by the presence of silicon self-interstitials. Burenkov et al. [199] found that the diffusivity of implanted phosphorus in lamp annealing is temperature-independent: after annealing at 900, 1000, and 1050 °C the diffusion profiles were found to coincide. The effective diffusivity at such temperatures amounted to 2×10^{-12} cm^2 s^{-1}. The same value was obtained by Oehrlein et al. [201] in the case of lamp annealing at 800 °C. A close value of the diffusivity of implanted phosphorus was recorded by Negrini et al. [202] for annealing at 600 °C.

The experimentally observed temperature-independent diffusivity of implanted phosphorus upon lamp annealing can be explained if we assume that diffusion involves complexes. The enhancement of phosphorus diffusion in silicon under surface oxidation and the slowing-down of the enhanced diffusion in layers doped with Group IV elements suggest that diffusion involves complexes consisting of a phosphorus atom and an interstitial Si atom (a P*I* pair) rather than *E* centers.

The rate of pair generation is written as

$$G(x,t) = KC_{\mathrm{p}}(x,t)\, C_{\mathrm{i}}(x,t)\,, \tag{17}$$

where C_{P} is the concentration of phosphorus atoms, C_{i} is the concentration of the intrinsic interstitial Si atoms that are released as a result of the breakup of interstitial complexes, and K is the reaction rate.

At a diffusion temperature T_1, the number of complexes N is $G(x,t)\tau_1$, where τ_1 is the lifetime of a complex at this temperature. The impurity flux is

$$J_1 = D_1 \frac{\mathrm{d}N}{\mathrm{d}x} = D_1 \frac{\mathrm{d}}{\mathrm{d}x}\, G(x,t)\tau_1\,, \tag{18}$$

where D_1 is the complex diffusivity at T_1.

At a higher temperature T_2, for the impurity flux J_2 we have

$$\begin{aligned} J_2 &= D_2 \frac{\mathrm{d}}{\mathrm{d}x}\, G\tau_2 \\ &= D_1 \exp\left(\frac{E^{\mathrm{dif}}\Delta T}{kT_1T_2}\right) \frac{\mathrm{d}}{\mathrm{d}x}\, G\tau_1 \exp\left(\frac{E^{\mathrm{an}}\Delta T}{kT_1T_2}\right). \end{aligned} \tag{19}$$

The fact that the profiles for equal diffusion times at different temperatures coincide means that $J_1 = J_2$. This is possible if the diffusion activation energy of the complex, E^{dif}, is equal to the activation energy of annealing (breakup) of this complex, E^{an}. On the basis of these results, a model of this complex was proposed in Refs [88, 203]. In this model, the complex is formed when a phosphorus atom and a silicon atom find themselves at the same interstitial site. Phosphorus and silicon are not connected by a covalent chemical bond. The bond is determined by the potential relief of the crystal (Fig. 18). In this model the barrier for migration of a separate phosphorus atom is $E_{\mathrm{m}}^{\mathrm{P}}$. For a pair consisting of a phosphorus atom and an interstitial Si atom (P*I*) this barrier E_{m}^{PI} is lower, which determines the higher mobility of the P*I* pair compared to that of an isolated P atom. For this pair the annealing activation energy of the complex and the diffusion activation energy of the same complex coincide (this follows from experimental results). When the P*I* pair acquires an energy

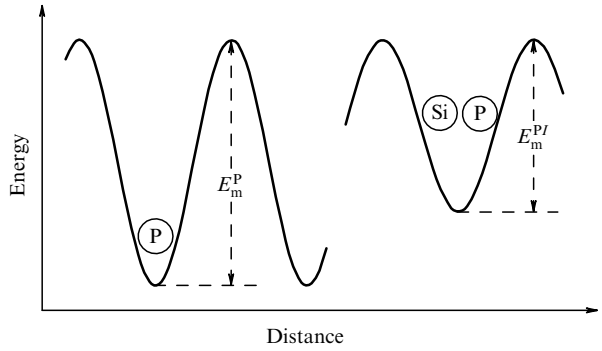

Figure 18. Energy barriers for migration of a phosphorus atom ($E_{\mathrm{m}}^{\mathrm{P}}$) and a pair consisting of a phosphorus atom and an interstitial Si atom (E_{m}^{PI}) in the silicon lattice [88].

greater than E_m^{PI}, it can jump to a neighboring interstitial position as a whole or the P and Si atoms can jump into different interstitial positions (breakup of the pair).

In view of the strong supersaturation of the implanted layer with defects (for a P^+ ion dose of 1×10^{14} cm^{-2}, the defect concentration is on the order of 10^{20} cm^{-3}, with the phosphorus concentration in the layer being on the order of 10^{19} cm^{-3}), pairs may be generated at random. However, pair formation may occur purposefully if the crystal has P atoms at lattice sites and excess Si atoms emerge. A phosphorus atom at a silicon lattice site, as well as any other substitutional atom whose covalent radius differs from that of the matrix atom, creates around itself a region of elastic strain. According to the ideas developed by Berezhnov et al. [22], when an interstitial Si atom lands inside a distorted sphere of radius R, it moves in the elastic strain field toward the source of strain (see Fig. 10). For a phosphorus atom in silicon, the radius R is about 40 Å. If two Si atoms land in such a sphere, they both move toward the P atom; one displaces the P atom to an interstitial position, the other finds itself in the same interstitial position. As a result, a PI pair is formed. In both cases, PI pairs form with an appreciable concentration as long as there is an excess concentration of interstitial Si atoms. When electrically neutral elements of Group IV (Ge and C), which serve as traps for interstitial Si atoms, are introduced into the implantation layer, the diffusivity of phosphorus is reduced.

6.3 Role of residual defects in diffusion of implanted impurities in silicon

The literature abounds with discussions concerning the role of residual defects in the diffusion of implanted impurities. Cowern et al. [204] used the TEM method to simultaneously study (a) the process of transformation of residual defects of the interstitial type {311} in implanted silicon and (b) the diffusion of boron. The researchers concluded that the time scale of the decay of {311} rodlike defects coincides with the time in which enhanced diffusion takes place. Other researchers (see Refs [205–207]) also found that the saturation time for loop growth coincided with the time in which enhanced diffusion of boron and phosphorus takes place. Cheng et al. [208] used TEM to study residual defects in silicon implanted with boron and phosphorus. The researchers came to the conclusion that, as a result of annealing at 850 °C for 5 s, all interstitial Si atoms are tied up by {311} defects. As the annealing time increases and rodlike defects decay, enhanced diffusion of implanted boron and phosphorus impurities sets in. Ajmera et al. [200] studied silicon implanted with boron and additionally with Si^+ ions and found that the number of interstitial Si atoms stored by the {311} defects was equal to the number of implanted Si^+ ions, which was about 10% of the number of stable complexes. Nevertheless, the researchers attribute the enhanced diffusion of boron to the displacement of boron atoms to the interstitial diffusion channel by interstitial Si atoms released from {311} defects. When the initial supersaturation of interstitial Si atoms in implanted silicon is strong (one atomic percent or higher), zigzag {311} defects are formed (in addition to ordinary rodlike defects). These defects are more stable under annealing and, in the opinion of the researchers, substantially increase the time of enhanced diffusion of implanted impurities [209]. Liu et al. [210] studied the enhanced diffusion of implanted boron as a function of the ion energy (5, 10, 20, and 40 keV). The ion dose amounted to 2×10^{14} cm^{-2}. They also used the TEM method to investigate the formation of {311} rodlike defects. These defects were detected only in silicon layers implanted with ions whose energy was 10 keV or higher. It was found that the residual-defect concentration increased with ion energy. For 5-keV ions, no {311} defects were formed, and the researchers state that no enhanced boron diffusion was observed. They attribute the enhanced diffusion to the presence of complexes consisting of a boron atom and an interstitial Si atom released during transformation of {311} defects. Zhang et al. [211] investigated the diffusion of implanted boron in silicon implanted with 4-keV ions to a dose of 1×10^{14} cm^{-2}. Annealing was carried out in a nitrogen atmosphere at 700–800 °C, with the annealing times ranging from 15 s to 8 h. Using the TEM method, the researchers found that no {311} defects were formed even in short annealing times. On the other hand, enhanced diffusion was observed, and was found to reach saturation in annealing times of about 15 min. These experiments irrevocably show that {311} defect formation is by no means necessary for enhanced diffusion to set in.

On the whole, all the data of such research indicate that, under thermal treatment of implanted silicon, some of the interstitial Si atoms released upon the breakup of complexes displace the impurities into the interstitial diffusion channel or form pairs with the impurity atoms, which is needed for enhanced diffusion to set in. At the same time, other interstitial Si atoms form {311} defects. As the annealing time is increased, the silicon atoms released in the transformation of residual defects sustain enhanced impurity diffusion.

7. Gettering of impurities in silicon

Impurities that belong to the transition-metal group (Fe, Co, Ni, Cu, Au, and Pt) introduce deep levels into the forbidden band and in this way strongly affect generation–recombination processes in silicon. These processes worsen the electrophysical parameters and reduce device yield. The formation of metal silicides in the electrically active regions of devices during thermal treatment also lowers quality. In the near future, silicon crystals with a metal content no higher than 2.5×10^9 cm^{-3} will be needed in the microelectronics industry [1, 2, 212]. However, the use of transition metals with their high diffusivity in the semiconductor industry, e.g., in the metallization technology, forces researchers to look for ways of purifying the active regions of crystals directly in the device fabrication process. One way of purifying crystals is to employ gettering, which means shifting metallic impurities and localizing them in the areas of the semiconductor wafer where they do no harm to the fabricated device. Both physicists who study the defect–impurity interaction in crystals, and industrial engineers contribute to the development of gettering methods. By a vivid expression of Bergholz and Gilles [213], the advances in understanding gettering are determined by the synergetic interaction of the academic studies of the defect scenarios in silicon and the wide-scale research in industry, which includes, among other things, the analysis of the statistics of producing millions of devices. The scientific basis of gettering methods being currently developed is formed by research in quasichemical reactions in solids and studies that establish the internal and external factors governing the course of these reactions, such as the type of radiation acting on the crystal, the temperature, the ionization level, the internal electric fields, and the elastic stress fields [214–216].

7.1 Intrinsic gettering

Intrinsic or internal gettering got its name in view of the use of internal resources of crystals to create trapping centers for harmful impurities. Such gettering in Czochralski-grown silicon crystals is achieved by using residual oxygen, whose concentration is about 10^{18} cm^{-3}. Instead of being an undesirable impurity, oxygen became an important agent for forming getters in the bulk of wafers in the fabrication of silicon devices. Intrinsic gettering is not directly related to ion implantation, but it is highly advisable to study this method, which has found wide application in semiconductor technology. Other methods based on ion implantation are usually comparable in efficiency with intrinsic gettering.

The formation of an internal getter presupposes the use of the following methods of heat treatment. The first heat treatment at 1150 – 1250 °C is carried out to remove oxygen from the surface layer of the wafer as a result of its diffusion into the ambient atmosphere. This process is illustrated in Fig. 19, which shows the oxygen concentration profile for a silicon wafer after annealing in an Ar atmosphere at 1200 °C for 1 h [217]. The oxygen concentration near the surface to depths of about several microns is ten times lower than in the bulk of the wafer. It is here, near the surface, that the active regions of the device are formed. The second heat treatment (650 – 800 °C) ensures nucleation of oxygen precipitates (SiO_2) in the wafer's bulk; in the surface layer, the oxygen concentration is low and no precipitates are formed. At the third stage, a higher temperature (1000 – 1100 °C) is used to ensure a more intense growth of the precipitates from the nuclei formed.

There are many papers devoted to the study of oxygen outdiffusion from silicon. The focus is on the effect that the temperature and the atmosphere used in heat treatment have on this process. Yamazaki et al. [217], Ruiz and Pollack [218], and Hu [219] detected no effect of the annealing atmosphere, including an oxidizing atmosphere [218, 219], on oxygen diffusion. Gaworzewski and Ritter [220] studied oxygen outdiffusion from silicon in the temperature range from 900 to 1230 °C with different atmospheres (H_2, N_2, Ar, and O_2). They found that the atmosphere has no effect on the oxygen diffusion profiles at depths up to 10 μm. On the other hand, Newman et al. [221] showed that when annealing was performed in the presence of oxygen at temperatures up to 500 °C, oxygen diffusion is enhanced. No such effect was observed at higher temperatures. But if the silicon samples are preheated in a hydrogen atmosphere, enhanced oxygen diffusion is observed at all annealing temperatures [222]. According to Zhong and Shimura [223], enhanced oxygen diffusion occurs even at temperatures higher than 1000 °C when annealing proceeds in a hydrogen atmosphere. A difference in the oxygen diffusivity in silicon upon annealing at 1200 °C in a hydrogen atmosphere (5.6×10^{-10} cm^2 s^{-1}) and argon (6.9×10^{-10} cm^2 s^{-1}) was reported in Ref. [215]. The authors related it to the rate of oxygen-precipitate formation. The rate of precipitate growth was found to depend on the rate at which the temperature was increased upon annealing in the presence of hydrogen and argon because of the difference in heat capacities of these gases. Izunome et al. [224] reported on the dependence of the rate of precipitate formation on the rate at which the temperature increased from 900 to 1200 °C. The formation of precipitates, in turn, lowers the rate at which oxygen diffuses from the sample.

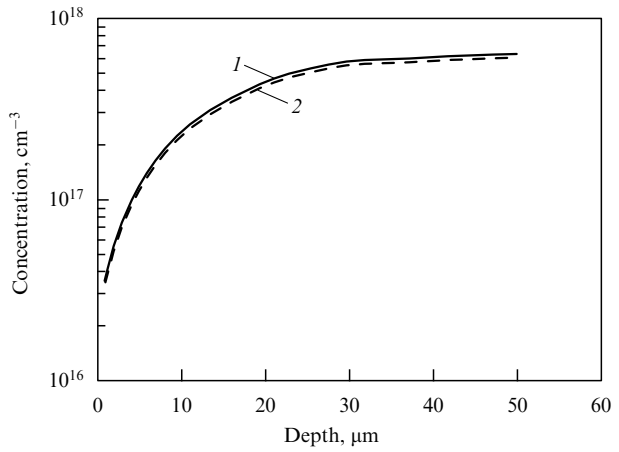

Figure 19. Oxygen concentration profile for silicon after high-temperature annealing [217]: (*1*) results of measurements by the secondary-ion mass-spectroscopy (SIMS) method; and (*2*) results of computer simulation.

Some researchers reported on enhanced diffusion of oxygen from silicon that had been heat treated at low temperatures (up to 400 °C) [225, 226]. Gösele and Tan [225] have proposed that enhanced diffusion is caused by the diffusion of quasimolecules O_2 that are in dynamic equilibrium with interstitial oxygen. A detailed study of the temperature dependence of the oxygen diffusivity at low temperatures allowed the researchers to postulate that enhanced diffusion is observed because of the formation of some kinds of rapidly diffusing centers. These centers may travel, in the course of diffusion, over large distances until they become trapped. In the opinion of the researchers, carbon atoms at lattice sites may be such traps. The nature of the rapidly diffusing centers is still unclear, but the observed behavior excludes the O_2 dimer as a possible candidate. The researchers assumed that oxygen – vacancy complexes are the rapidly diffusing centers. Some scientists attribute the enhanced outdiffusion of oxygen from silicon at low temperatures to the presence of carbon impurities in the crystals [227, 228].

The first to report about the growth of oxygen precipitates in Czochralski-grown silicon during heat treatment at 1000 °C was Kaiser [229]. The researcher also established that during heat treatment at 1350 °C the precipitates decompose and the oxygen atoms are distributed over the interstitial positions due to their higher solubility at this temperature. At that time (1957), single crystals of silicon contained a large number of dislocations, so it was difficult to determine the correct precipitation mechanism. In the same year, Lederhandler and Patel [230] found that dislocations serve as nucleation centers for oxygen precipitates. Two decades later, Hu [231] showed that in dislocation-free silicon precipitation may occur homogeneously in the form of discrete particles; here, oxygen – vacancy complexes serve as nucleation centers for the precipitates. Further research revealed that the density of the precipitates depends on the initial concentration of oxygen, the concentration of other impurities and defects, and the heat-treatment procedures. The nucleation and growth of precipitates are determined by the following mechanisms: (1) homogeneous nucleation due to oxygen supersaturation; (2) heterogeneous nucleation on structural defects, which may have existed or could form and grow during thermal treatment; and (3) further growth of precipitates if their nuclei arose while the crystal was being grown [231 – 233].

The research conducted by Wada et al. [234] showed that precipitate growth is determined by the oxygen diffusion rate. Ham [235] found the interstitial oxygen concentration (from the 9-μm IR absorption line), the precipitate density (from the etch pits), and the precipitate size (from the data on small-angle low-energy neutron scattering) during heat treatment. The results made it possible to conclude that the precipitation process can be described by Ham's theory [235], according to which the precipitate density N is determined by the equation

$$N = \frac{3}{4\pi}\left(\frac{C_P}{C_O - C_S}\right)^{1/2}(3D\tau_0)^{-3/2}, \tag{20}$$

where C_S is the equilibrium solubility of oxygen after annealing, C_P is the oxygen concentration in the SiO_2 precipitates (4.5×10^{22} cm^{-3}), C_O is the initial oxygen concentration, D is the oxygen diffusivity, and τ_0 is the time constant in the exponential dependence of the interstitial oxygen concentration on the precipitation time.

As a result of their research, Rozgonyi et al. [236] arrived at the following conclusions: the higher the initial oxygen concentration in silicon, the greater the number of nucleation centers that form as a result of low-temperature (750 °C) treatment; for the same initial oxygen concentration, the nucleation center density increases with the time of low-temperature annealing; and the higher the nucleation center density, the greater the precipitation rate in high-temperature annealing.

The kinetic model of oxygen precipitation was developed in Refs [237–239]. The evolution of the precipitate density is represented by rate equations for precipitates of size n (the number of oxygen atoms in it):

$$\frac{\partial f(n,x,t)}{\partial t} = J(n,x,t) - J(n+1,x,t), \qquad n \geqslant 2, \tag{21}$$

$$J(n,x,t) = g(n-1,x,t)\,f(n-1,x,t) - d(n,x,t)\,f(n,x,t), \tag{22}$$

where $f(n,x,t)$ is the concentration of precipitates containing n oxygen atoms, and $g(n,x,t)$ and $d(n,x,t)$ are the precipitate growth and dissolution rates, respectively. Precipitates may be as large as several hundred nanometers, so that the number of rate equations becomes unmanageably large. Hence, Eqns (21) and (22) are transformed into the differential Fokker–Plank equation:

$$\frac{\partial f(n,x,t)}{\partial t} = -\frac{\partial J(n,x,t)}{\partial n}, \tag{23}$$

$$J(n,x,t) = -B\frac{\partial f(n,x,t)}{\partial n} + A f(n,x,t), \tag{24}$$

$$A = \frac{g(n,x,t) + d(n,x,t)}{2}, \qquad B = g(n,x,t) - d(n,x,t) - \frac{\partial A}{\partial n}. \tag{25}$$

Since the differential equation (23) is invalid for small precipitates, the model we are discussing here incorporates the rate equations (21) and (22) for small precipitates ($n < 20$) and the differential equation (23) for large precipitates. It is assumed that the precipitates are immobile. In addition, for separate oxygen atoms we have the equation

$$\frac{\partial C_O}{\partial t} = \frac{\partial^2 C_O}{\partial x^2} - \frac{\partial}{\partial t}\sum_{n>2} f(n,x,t)n, \tag{26}$$

where $C_O = f(1,x,t)$ is the oxygen atom concentration. The first term on the right-hand side of Eqn (26) describes the diffusion of oxygen atoms, and the second term reflects the change in the amount of precipitated oxygen.

The growth rate for a spherical precipitate containing n oxygen atoms can be written as follows [240]:

$$g(n,x,t) = 4\pi r^2 \delta C_O^{if} v \exp\left(-\frac{\Delta G_{n\to n+1}}{kT}\right), \tag{27}$$

where r is the precipitate radius, δ is the thickness of the precipitate–matrix interface (it is assumed to be equal to the elementary hopping length of an oxygen ion, ~ 2 nm), C_O^{if} is the oxygen atom concentration at the precipitate–matrix interface, and v is the oxygen atom hopping rate in diffusion. According to Vineyard [241],

$$v = \frac{6D_{Oc}}{g\delta^2}, \tag{28}$$

where g is the number of equivalent diffusion paths ($g = 36$), and D_{Oc} is the pre-exponential factor in the oxygen diffusivity D_O [242]. According to Turnbull and Fisher [243], the energy barrier is specified as follows:

$$\Delta G_{n\to n+1} = G_{ac} + \frac{1}{2}\frac{\partial G_n}{\partial n}, \tag{29}$$

where G_{ac} is the free activation energy; and G_n is the free Gibbs energy of a precipitate containing n oxygen atoms, which is the sum of the bulk and surface energies,

$$G_n = -nkT\ln\frac{C_O}{C_O^{eq}} + 4\pi r^2\gamma, \tag{30}$$

with k being the Boltzmann constant, T the temperature, C_O^{eq} the equilibrium oxygen concentration, and γ the surface energy density.

The rate of precipitate dissolution, $d(n,x,t)$, can be obtained from the growth equation [244]

$$\frac{dn}{dt} = g(n,x,t) - d(n,x,t) = K_r(C_O^{if} - C_O^{if,eq}), \tag{31}$$

$$d(n,x,t) = K_r C_O^{if,eq}, \qquad K_r = 4\pi r^2 \delta v \exp\left(-\frac{\Delta G_{n\to n+1}}{kT}\right), \tag{32}$$

where $C_O^{if,eq}$ is the equilibrium oxygen concentration at the precipitate–matrix interface calculated on the assumption that $dG_n/dn = 0$ and $C_O = C_O^{if,eq}$.

An alternative form of the growth law $\partial n/\partial t$ can be obtained for the steady state by solving the diffusion equation in spherical coordinates:

$$\frac{\partial n}{\partial t} = K_d(C_O - C_O^{if}), \qquad K_d = \frac{\partial n}{\partial r}\frac{\Omega}{2}\frac{D_O}{r}, \tag{33}$$

where Ω is the molecular volume of SiO_2 [245]. Using equations (31)–(33), we can write C_O^{if} in the following form:

$$C_O^{if} = \frac{K_r C_O^{if,eq} + K_d C_O}{K_r + K_d}. \tag{34}$$

Senkader and Hobler [239] conducted the necessary experiments and did the calculations required by this model. They found that there was good agreement between the

experimental and theoretical results concerning the dependence of the passage of interstitial oxygen into precipitates on the initial oxygen concentration and the annealing regimes, the oxygen distribution over the depth of the wafer, and the evolution of the precipitate size and density.

The oxygen precipitates that form in silicon manifest themselves in experiments. Koizuka and Yamada-Kaneta [246] used deep-level transient spectroscopy (DLTS) and found that oxygen precipitation in silicon causes the appearance of deep levels in the forbidden band: $E_v + 0.30$ eV and $E_c - 0.25$ eV. These levels are related to EPR centers in identical samples [247]. The discovered centers are similar to the P_{b0} and P_{b1} centers observed in the thermally oxidized silicon structures [248, 249]. These centers are attributed to dangling bonds at the silicon substrate – oxidized layer interface. Hence, Koizuka and Yamada-Kaneta [247] concluded that the deep levels $E_v + 0.30$ eV and $E_c - 0.25$ eV are P_b centers generated at the silicon – oxygen precipitate interface. Oxygen precipitates also manifest themselves in IR absorption, and 1218- and 1183-cm^{-1} absorption bands are related to planar oxygen precipitates [250], while 1124-cm^{-1} bands are related to spheroidal oxygen precipitates [251]. The initial oxygen concentration determines the shape and size of the forming precipitates. Borghesi et al. [252] found that as the initial oxygen concentration in silicon increases, the flat precipitates grow to a certain critical size. If the initial oxygen concentration exceeds 7×10^{17} cm^{-3}, the spheroidal precipitates grow continuously as the initial oxygen concentration increases, while the flat precipitates, after reaching a certain size, transform into volume precipitates.

The question of how carbon participates in oxygen precipitation has been widely discussed in the literature. There are several viewpoints here. According to Kishino et al. [253, 254], the presence of carbon accelerates oxygen precipitation. Tang et al. [255] concluded that the presence of carbon in silicon suppresses oxygen precipitation. On the other hand, the results of Tan et al. [256] suggest that carbon does not affect oxygen precipitation in silicon. Shimura [257] assumed that in silicon with high carbon content the carbon atoms at lattice sites are centers of heterogeneous precipitate nucleation. As the number of oxygen precipitates increases, the concentration of carbon in the lattice decreases. This was found to be true at annealing temperatures not exceeding 800 – 850 °C. If the temperature was higher, the increase in the number of oxygen precipitates was not accompanied by a decrease in carbon concentration. In Shimura's opinion [257], in this case the carbon atoms act as catalysts, changing the surface energy of the precipitates. According to Liu et al. [258], the effect of carbon on oxygen precipitation is determined by the thermal history of the crystal. If the crystals were not preannealed or were annealed at low temperatures, such as 450 or 650 °C, carbon actively participated in oxygen precipitation. At the same time, if the crystals were actively preannealed at 1200 °C, carbon had practically no effect on precipitation. In the opinion of Liu et al. [258], carbon affects precipitate growth as long as the precipitates are small, but it does not affect the further growth of large precipitates. Leroncille [259] believes that the forming complexes of the C – O type are nucleation centers for oxygen precipitation. According to Shimura and Hockett's data [260], the presence of nitrogen atoms also affects the nucleation of oxygen precipitates in silicon. Aihara et al. [261] assume that the effect of nitrogen on the precipitation process is indirect; i.e., it reveals itself by acting on the point defect concentration; this could also be true of carbon. The displacement of these impurities from lattice sites by interstitial Si atoms by the Watkins mechanism may have an effect on the balance of point defect concentrations.

The growth of oxygen precipitates is accompanied by the formation of interstitial-type stacking faults and dislocation loops. Elastic stresses at the precipitate – matrix interface also lead to the formation of dislocations [262]. It is known that dislocations are decorated by impurities, and so it was initially assumed that it is precisely the trapping of metallic impurities by dislocations that are the cause of the gettering effect on precipitates [263 – 265]. The trapping of impurities by structural defects is determined by the binding energy E, the temperature T, and the impurity concentration C. The probability P for an impurity atom to occupy place on a structural defect is given by the following formula:

$$P = \frac{1}{1 + (1/C)\exp(-E/kT)} . \qquad (35)$$

In addition to these parameters, which are determined by the type of a defect and an impurity, the rate of crystal cooling has an effect on the precipitation process. The precipitation of iron on dislocation loops and long dislocations is observed if the iron concentration is no lower than 10^{15} cm^{-3} when the crystal is slowly cooled from high temperatures (1100 °C [266]) to room temperature. Iron atoms are evenly distributed along a dislocation and do not coalesce into particles of an appreciable size. Copper precipitation on dislocations can be detected by the TEM method if the initial copper concentration in the crystal is higher than 6×10^{16} cm^{-3}. Copper precipitates form on dislocations both in the case of slow cooling and in the case of rapid cooling (1600 K s^{-1}). Oxygen precipitates are shaped like isolated cylinders located along a dislocation line. If the initial oxygen concentration is high and annealing continues for a long time, the cylinders merge and form one continuous cylinder on a dislocation line.

As a result of their studies of the kinetics of iron gettering by oxygen precipitates, Gilles et al. [267] came to the conclusion that it is the centers that are located directly on precipitates rather than on dislocations that show the highest efficiency of gettering. It is assumed that the dangling bonds at the precipitate – silicon crystal interface are the gettering centers. The deposition of transition metals directly on oxygen precipitates was recorded by Ourmazd and Schröter [264], who used the TEM method. Comparing the results of depositing iron on dislocations created through plastic deformation of silicon grown by the floating-zone method with those of gettering iron onto oxygen precipitates in Czochralski-grown silicon, Tan et al. [56] came to the conclusion that, for the efficiency of gettering to be the same, the dislocation density must be very high, 2×10^9 cm^{-2}.

7.2 Gettering by damage layers

The first reports about gettering of metallic impurities onto damage layers were Refs [268, 269]. Buck et al. [269] studied the gettering of Fe, Co, Ni, Cu, and Au onto damage layers produced by implanting 100-keV Si^+ ions to a dose of 10^{16} cm^{-2}. 1000-Å thick metal layers were deposited on the back side of the wafer by the sputtering technique. This was followed by annealing at 900 °C for 30 or 300 min. Rutherford backscattering of He ions was used to observe the redistribution of the metals over the wafer. It was found that copper and nickel are most effectively gettered onto the

residual defects of the damage layer; Fe, Co, and Au are gettered less effectively. In Refs [269–272], the efficiency of gettering of transition metals by layers produced through ion implantation and phosphorus diffusion is compared. The factors that influence the gettering capacity of diffusion layers are still unclear. This property could result from the formation of complexes consisting of a metal atom and a phosphorus atom. The interstitial-type stacking faults and dislocation loops may also exhibit the gettering property in the case of phosphorus diffusion. Goetzberger and Shockley [270] found that after annealing at 1000 °C the efficiency of gettering by a diffusion layer proved to be higher than that by defects created through ion implantation of silicon. Here, the Cu and Au atoms in diffusion layers are located at lattice sites, while in ion-implanted damage layers they are in interstitial positions. Buck et al. [269] used the RBS method to study the gettering of gold by defect layers produced through implantation of Ar, O, P, Si, and As. The efficiency of such gettering is compared with that of gettering by phosphorus-diffusion layers. At temperatures up to 1000 °C, the gettering by layers produced through implantation with Ar^+ ions was found to be more effective than that by diffusion layers; at 1150 °C, the efficiencies are the same; and at 1000 °C, the efficiency of gettering by damage layers was found to be determined by the type of ion in the following sequence: Ar > O > P > Si > As > B. In all the cases, residual defects (rodlike defects and dislocation loops) serve as gettering centers. In the opinion of the researches, the gettering efficiencies in this sequence of ions is determined by the number of residual defects.

Wong et al. [273] found that the efficiency of gettering of Au and Cu by layers produced through C^+ ion implantation is higher (by a factor of 10) than that by layers produced through implantation of O, Ni, BF_2, Ne, and Ar ions. As the C^+ ion dose was increased from 10^{15} to 10^{16} cm^{-2}, the amount of gettered Au was found to increase linearly with the implantation dose. Additional injection of oxygen into these layers does not influence the efficiency of the gettering of metals. This proves, in the opinion of the researchers, that the efficiency of gettering should be related directly to carbon rather than to the growth of oxygen precipitates stimulated by carbon.

Benton et al. [274] studied the gettering of Fe by damage layers produced by B^+ ion implantation. The efficiency of gettering by these layers proved to be much higher than that of gettering by layers created by implantation of other ions, including carbon ions. The higher gettering efficiency is related to the formation of complexes consisting of iron and boron. At high doses of B^+ ions implanted in silicon, B_3Si inclusions are formed during heat treatment [266]. With boron-ion doses amounting to $(2.5-5) \times 10^{16}$ cm^{-2} and ion energies of 50 and 300 keV, the size of the amorphous B_3Si inclusions that form after annealing at 600–1000 °C is about 10 nm. They effectively getter the impurities of metals such as Fe, Co, Cu, and Au. The metal atom–boron silicide binding energies have been determined. For the above impurities, they are in the range of 1.2 to 2.5 eV. Both in the gettering rate at 600–1000 °C and in the residual impurity concentration this method has proved to be more effective than gettering by SiO_2 precipitates.

The use of high-energy (megaelectronvolts) ion implantation makes it possible to place the gettering layer on the planar side of the wafer, close to the active regions of the device, which ensures effective gettering at lower temperatures and shorter durations of annealing. This method is suitable very well for the technology of the modern semiconductor industry and ensures a substantial improvement of the device parameters [275–277]. Kuroi et al. [278] studied the gettering of Cu and Fe by damage layers created by implanting high-energy Si^+ (2.4 MeV) and B^+ (1.2 MeV) ions with doses amounting to 1×10^{15} cm^{-2}. Layers fabricated by implantation of Si^+ ions are more effective getters, due to the large number of residual defects. TEM studies have shown that after annealing at 800 °C the main residual defects are rodlike defects, after heat treatment at 900 °C they are rodlike defects and dislocation loops, and after annealing at 1000 °C they are primarily dislocation loops. In all the cases, copper atoms are gettered more effectively than iron atoms. Borland and Koelsch [276] found that damage layers getter not only metallic impurities but also oxygen atoms.

In addition to being gettered on damage layers within the projected range R_p, impurities are gettered at depths on the order of $R_p/2$ [279–282]. While residual defects in the layer near R_p are well-detected by the TEM method, this method cannot be used to bring out the layers at a depth on the order of $R_p/2$. It is believed that at such depths the layers contain vacancy clusters that cannot be visualized by the TEM method [279, 283]. Benton et al. [274] found that in silicon implanted with highly energetic Si^+ ions, the gettering of iron by a layer at $R_p/2$ is stronger than by a layer at R_p. In Czochralski-grown silicon, the efficiency of Fe gettering is reduced due to the trapping of oxygen atoms by the layer located at $R_p/2$. The redistribution of Fe and O atoms over the wafer was detected in these experiments by the SIMS method. The weak temperature dependence of the solubility of Cu and Ni impurities in silicon [282] made it possible to determine the contributions of the damage layers at R_p and $R_p/2$ into decoration at different temperatures. Here, the damage layers were fabricated by implanting 2.3-MeV Si^+ ions to a dose of 1×10^{15} cm^{-2}. As a result of annealing at 900 °C for 1 h, the copper is located primarily in the layer at R_p; after an additional annealing at 700 °C for 1 h, copper is located primarily in the layer at $R_p/2$. If the samples are then again annealed at 1000 °C, copper again is gettered by the layer at R_p. During such a successive redistribution of copper atoms over the layers, the total concentration of the decorating impurity remains unchanged. This research has made it possible to determine the binding energies of Cu and Ni atoms with the defects located in the damage layers at R_p and $R_p/2$.

Kögler et al. [280] investigated the gettering of metallic impurities by the $R_p/2$ layer that forms after high-energy implantation and subsequent annealing at 700 and 900 °C. The residual defects were studied by the TEM method. According to these researchers, the residual defects in the $R_p/2$ region are of an interstitial nature rather than of a vacancy nature, contrary to the assumption made by Venezia et al. [279] and Brown et al. [283]. However, in their latest paper on the subject, Kögler et al. [284] have changed their opinion in favor of the vacancy nature of defects in the $R_p/2$ layer. They were able, in their opinion, by additionally implanting Si^+ ions into the $R_p/2$ layer to compensate for the excess vacancies and thus lower the gettering capability of that layer.

Gueorguiev et al. [285] studied the gettering of copper by layers created by implanting silicon with 3.5-MeV Si^+ or P^+ ions to doses 5×10^{14} and 1×10^{15} cm^{-2}. The researchers found that, in addition to the gettering layer near R_p, there is a

deeper gettering layer with a higher gettering capability. They believe that small clusters of intrinsic interstitial atoms that cannot be resolved in an electron microscope serve as gettering centers.

Kögler et al. [286] investigated the spatial redistribution of gettered copper in silicon with a buried amorphous layer. The damage layer was created by implanting 4-MeV Ge^+ ions to a dose of 5×10^{15} cm^{-2}. On the opposite side of the silicon wafer, 45-keV copper ions were implanted to a dose of 5×10^{13} cm^{-2}. After annealing at 500 °C for 1 h, all of the copper was found to move to the inner (deeper) amorphous – crystalline silicon interface. The researchers believe that the amorphous layer serves as a barrier for the diffusion of copper atoms. After annealing at 650 °C and crystallization of the amorphous layer the copper is located at both boundaries of the former amorphous layer. Here, more copper is at the upper interface. After annealing at 1000 °C, copper remains at the deeper amorphous layer – crystal interface, while from the surface interface it travels to the region where the amorphous layer was earlier. Parallel studies by the TEM method allowed the researchers to conclude that copper mostly decorates small dislocation loops of the interstitial type and, to a much lesser degree, line dislocations.

To electrically activate the implanted impurities and anneal radiation-induced defects on the active side of the wafer, Troitski et al. [287] carried out additional high-intensity implantation on the reverse side of the wafer. In addition to the effect of impurity activation, the residual defects that formed on the reverse side showed themselves to be effective getters for metallic impurities in silicon.

7.3 Microcavities as getters in implanted silicon

Recent years have seen the development of a gettering method based on the fabrication of layers containing microcavities (micropores) inside silicon wafers [288 – 293]. These microcavities are created by implanting silicon with ions of hydrogen or helium (to doses ranging from 10^{16} to 10^{17} cm^{-2}) and then by thermally treating the samples (800 – 1000 °C). The metal atoms getter on the dangling bonds on the inner walls of these micropores. It is still unclear how these micropores nucleate. What is known is that implantation generates vacancy complexes. The largest of these complexes, which appear directly as a result of irradiation of silicon with reactor neutrons or ions, are tetravacancies [294], but the prevailing, in concentration, vacancy defects are divacancies. Subsequent heat treatment of the irradiated silicon restructures the radiation-induced defects, with the result that pentavacancy complexes may form, and so may other polyvacancy complexes that have to be identified [295, 296]. Calculations have shown that the stable complexes in silicon are those consisting of six vacancies (V_6) and of ten vacancies (V_{10}) [297]. These vacancy defects can serve as traps for hydrogen atoms and form complexes of the V_2H_6, V_6H_{12}, or $V_{10}H_{16}$ type. The Si – H vibrations in these complexes manifest themselves in a number of bands (1883, 1926, 1957, and 2213 cm^{-1}) in the Raman scattering spectra of implanted and hydrogenated silicon [297]. As the dose of H^+ ions is increased, the complexes become larger and then form gas-filled microcavities resembling spheres or planar inclusions (platelets).

As the samples are heated to 400 °C, the atomic hydrogen in the microcavities forms H_2 molecules. The gas pressure in the cavities may be very high, on the order of 1 GPa [297, 298]. The hydrogen molecules that form in the process manifests themselves in Raman scattering spectra at a frequency of 4158 cm^{-1}, provided that there are H_2 molecules in the micropores. Initially this vibrational band was attributed to hydrogen molecules in interstitial positions [299], but the calculations done in Refs [300 – 302] showed that in a tetrahedral interstice of silicon the vibrational frequency of the H_2 molecule will be strongly shifted relative to its eigenvalue. Comparison of the calculated values with the experimental data led to the conclusion that an H_2 molecule in a tetrahedral interstice corresponds to a vibration with a frequency equal to 3618 cm^{-1} [303 – 305].

While studying the Raman spectra of silicon irradiated by Si^+ ions and treated in hydrogen plasma at different substrate temperatures (60 – 400 °C), among the well-known vibrational bands of hydrogen molecules Kitajima et al. [306] discovered a new band at 3822 cm^{-1}. This band was related to the vibrations in H_2 molecules incorporated in polyvacancy complexes. By comparing the calculated frequencies of Si – H and H – H vibrations and the experimental data on the Raman scattering spectra, Kitajima et al. [307] concluded that the 3822-cm^{-1} band is caused by vibrations in an H_2 molecule incorporated in a divacancy.

At temperatures higher than 400 °C, hydrogen abandons the silicon crystal, leaving the microcavities empty. After annealing at 550 °C, only one-half of the implanted hydrogen remains in the cavities; at 750 °C this amount reduces to less than 1% [308, 309]. According to the data of Kitajima et al. [307], the activation energy for diffusion of an H_2 molecule in silicon is 0.95 eV, while Markevich et al. [310] arrived at a value of 0.78 eV. The diffusion barrier is influenced by the position of the Fermi level in the crystal. Under laser illumination, the H_2 molecules in silicon become mobile at cryogenic temperatures [311]. There is also an alternative model of diffusion of hydrogen through the dissociation of the molecule followed by diffusion of the atoms. However, the dissociation energy of the molecule amounts to 1.74 eV [312], which is much higher than the activation energy for diffusion of the H_2 molecule as a whole.

Apparently, irradiation and vacancy generation are not really necessary for the formation of gas – vacancy complexes followed by microcavity growth. The limited solubility of hydrogen and helium in silicon and their segregation into complexes are the reasons why microcavities filled with gas are formed in silicon. Leitch et al. [313] found that in hydrogenated silicon at the hydrogen plasma temperature of 150 °C the H_2 molecules occupy tetrahedral interstices, and a band at 3601 cm^{-1} is detected in the Raman spectra. At higher plasma temperatures (> 150 °C), a vibrational band at 4157 cm^{-1} was observed in the spectra, which suggests that microcavities filled with hydrogen were being formed. Kitajima et al. [307] studied the depth distribution of molecular hydrogen for hydrogenated crystalline silicon and silicon preimplanted with 200-keV Si^+ ions. The researchers found that the hydrogen molecules in the microcavities (a Raman scattering line at 4160 cm^{-1}) are largely located in the nondamaged part of the crystal.

The threshold nature of microcavity formation suggests that the segregation process is responsible for it. The data of Raineri et al. [314] on the formation, during heat treatment, of cavities in silicon implanted with He^+ ions imply that the volume concentration of helium atoms must be no lower than 3.5×10^{20} cm^{-3}. For a helium ion dose of 1×10^{15} cm^{-2} (the ion energy is 40 keV), the concentration of helium at the distribution maximum amounts to 4×10^{19} cm^{-3}, and no

cavities appear during annealing [297]. If the helium dose is much higher than the critical value of 5×10^{16} cm^{-2}, microcavities are formed directly during implantation without additional heat treatment [297]. The size of the cavities is moderate (1.1–4.5 nm). After heat treatment (800 °C for 10 min), the cavities become larger, with sizes ranging from 3 to 17 nm. The threshold effect is not related to the concentration of radiation-induced defects. When light ions (H^+ or He^+) are implanted to a dose of 10^{15} cm^{-2}, the radiation-induced defect concentration reaches saturation due to annihilation of the newly formed vacancies and interstitial atoms with the stable defects introduced earlier [315]. Akiyama et al. [297] observed in silicon implanted with He^+ ions to a dose of 1×10^{16} cm^{-2} and annealed at 800 °C a planetary-like system of microcavities (Fig. 20). A large cavity is at the center of this system (about 57 nm on average), which is surrounded by smaller cavities in one plane (Fig. 20b). This plane is parallel to the sample surface. Figure 20c shows that the cavities are surrounded by elastic stress fields.

At present there are two models of microcavity coalescence [290, 291, 309]. It is assumed that up to 1000 °C the mechanism of Ostwald ripening operates. According to this mechanism, small cavities release vacancies and He atoms, which move to the larger cavities. Above 1000 °C the small cavities, on the whole, become mobile and coalescence into larger cavities. This mechanism is known as the migration–coalescence mechanism.

Griffioen et al. [288] were the first to study the rate at which helium is released by the cavities as functions of helium concentration and heat treatment regimes. Then, Myers et al. [316] showed that microcavities freed from helium are effective traps for metallic Cu and Au impurities. This work has stimulated the development of this gettering technology used in the production of VLSI circuits [293, 310, 314, 317]. The results of the research suggest that chemisorption to the dangling bonds on the inner walls of the microcavities is responsible for the gettering of metallic impurities.

The studies of gettering of transition metals by microcavities at different temperatures have shown that the process is determined by the diffusion rate of the impurity atoms. Zhang et al. [318] observed gettering of copper in cavities created by implanting H^+ ions immediately after annealing at 500 °C, but the annealing time amounted to several hours. As the temperature of heat treatment increases, the gettering efficiency grows. This is due not only to the increase in the diffusion rate but also to the decomposition of precipitates of metal silicides [319, 320].

Zhang et al. [320] compared the efficiency of gettering on cavities created by H^+ and He^+ ion implantation. The researchers came to the conclusion that copper is better gettered on microcavities created by He^+ ion implantation, since the residual hydrogen competes with metals in the formation of bonds with the microcavity walls. On the other hand, Job et al. [321] found that the oxygen in silicon is gettered more effectively on microcavities created by implantation of hydrogen rather than by helium. If the heat treatment is carried out in a hydrogen atmosphere, the effect is stronger than if it is carried out in a nitrogen atmosphere. The explanation is that hydrogen enhances the diffusion of oxygen.

Kinomura et al. [322] investigated gettering of platinum and silver on microcavities. The getter layer was formed by implantation of 70-keV H^+ ions to a dose of 3×10^{16} cm^{-2} and subsequent annealing at 850 °C for 1 h. Then, 70-keV Pt^+ and Ag^+ ions were implanted on the same side of the wafer. Then, the wafer was again subjected to heat treatment at 850 °C for 1 h. It was found that for a 1×10^{14} cm^{-2} dose of Pt^+ ions and a 3×10^{14} cm^{-2} dose of Ag^+ ions, all the impurities move to microcavities. When ion doses are 1×10^{15} cm^{-2}, 50% of silver and only 6% of platinum are gettered on the microcavities. The reason is the formation of platinum silicides and the escape of silver to the surface.

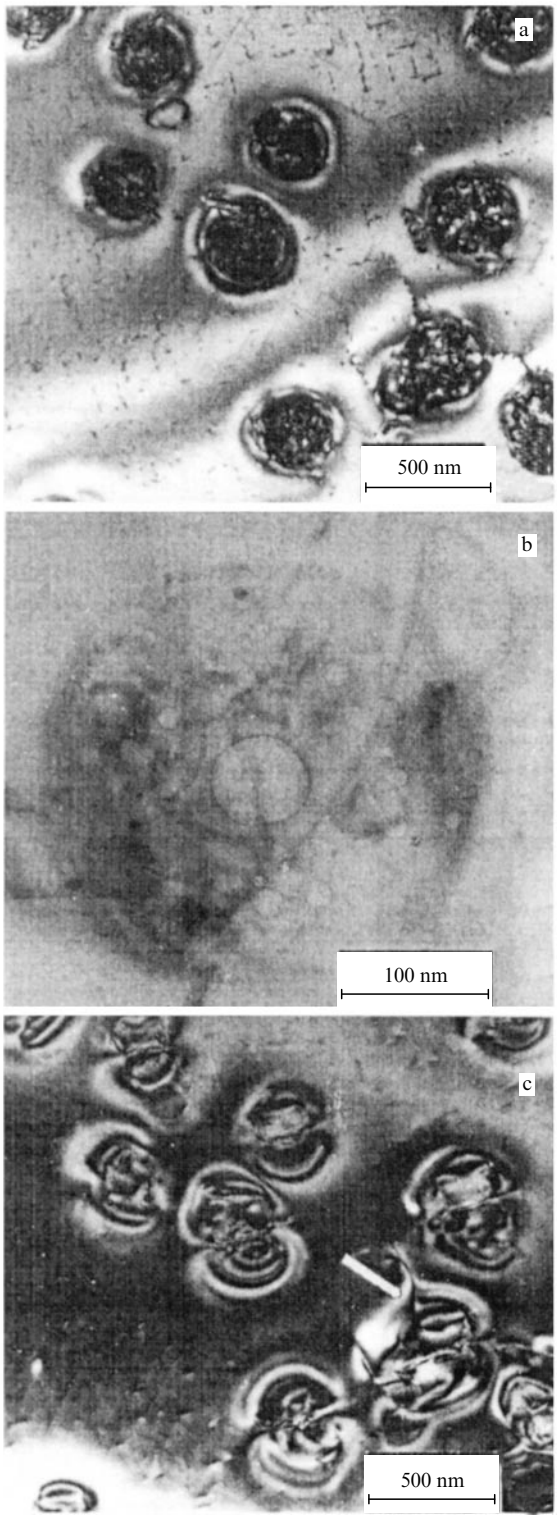

Figure 20. TEM micrographs of silicon with microcavities [297].

Under similar conditions, gold implanted to a dose of 1×10^{15} cm^{-2} is completely gettered on microcavities [323].

Detailed studies of gettering of Ni have been carried out by Mohadjeri et al. [324]. The doses of Ni^+ ions and the substrate temperatures were varied during implantation. The researchers found that the gettering efficiency is smaller if the layer becomes amorphous. Recrystallization of the layer triggers the formation of nickel silicide $NiSi_2$; of all silicides, the value of the lattice parameter of $NiSi_2$ is closest to that of crystalline silicon: the difference in lattice parameters is about 0.4% [325]. This silicide crystallizes epitaxially on the silicon surface. However, research done at different temperatures (650, 800, and 1000 °C) has shown that when the Ni^+ ion dose is 1×10^{15} cm^{-2}, all nickel may find itself in microcavities created by implantation of 100-keV H^+ ions to a dose of 3×10^{16} cm^{-2}. When the dose of Cu^+ ions is large (3×10^{15} cm^{-2}) and heat treatment is carried out at 750 °C, a polycrystalline layer is formed. About 80% of copper goes to microcavities and the remaining 20% stays in the polycrystalline layer on grain boundaries. No silicide phase is formed in this case [290]. Myers et al. [316, 326] found that Cu and Ni are tied up stronger in microcavities than in metal silicides and on oxygen precipitates SiO_2.

Research done by Godey et al. [290], Myers et al. [292], and Wong-Leung et al. [327] demonstrated that in addition to chemisorption, transition metals trapped in microcavities can form three-dimensional precipitates of metal silicides. This happens when all the bonds on the walls of the cavities are tied up by impurity atoms, i.e., a continuous monolayer of metal is formed. The removal of metals from crystals by precipitation is of interest only when their concentrations are high, i.e., higher than the solubility limit of the particular element. The special importance of gettering of metallic impurities on cavities lies in the possibility of cleaning the crystal from all impurities even at small concentrations (below the solubility limit) by chemisorption.

Myers et al. [293, 328] quantitatively studied the gettering of transition metals (Cu, Au, Fe, and Co) on microcavities in silicon formed by implantation of He^+ ions and subsequent thermal treatment. The researchers determined the binding energies of the metal atoms with the cavity walls (with respect to their state in a solid solution) and the binding energies in the metal silicides. First, the silicide layer was formed, and then the impurity transport onto the created layer of microcavities was recorded. The reaction strength with which an impurity interacts either with a cavity wall [cav] or with a silicide precipitate [sil] is determined by the change in the free energy, ΔG, when one metal atom is transferred from the bound state to the solid solution. The concentration of the dissolved metal in equilibrium with chemisorption on the cavity wall is given by the formula

$$C_{\text{cav}} = \frac{\theta}{1-\theta} \exp\left(-\frac{\Delta G_{\text{cav}}}{kT}\right), \tag{36}$$

where C_{cav} is expressed in atomic fractions, and θ is the fraction of occupied traps on the cavity wall.

The equation for the equilibrium between the dissolved impurities and the impurities that have precipitated into the metal silicide phase has the form

$$C_{\text{sil}} = \exp\left(-\frac{\Delta G_{\text{sil}}}{kT}\right). \tag{37}$$

When $\theta \ll 1$, i.e., when the cavities are far from being filled, the gettering energy for cavities in equilibrium with the silicide phase can be found from the equilibrium condition $C_{\text{cav}} = C_{\text{sil}}$. Combining Eqns (36) and (37), we obtain

$$\frac{\theta}{1-\theta} = \exp\left(\frac{\Delta G_{\text{cav}} - \Delta G_{\text{sil}}}{kT}\right). \tag{38}$$

By measuring in the layer of microcavities the amount of gettered metal replenished from the distant silicide layer, we can find the binding energy ΔG_{cav}, provided that ΔG_{sil} is known from independent experiments.

Lee and Corbett [294] and Petersen et al. [328] also carried out experiments in which they studied the transfer of the impurity used in gettering from one microcavity layer to another microcavity layer that is an exact copy of the first. Measuring the impurity flux Φ from one layer to the other as long as $\theta_1 \neq \theta_2$, the researchers directly found the binding energy ΔG_{cav}. The diffusion flux Φ is specified as follows:

$$\Phi \approx \frac{\Delta C_{\text{S}} D N_{\text{Si}}}{\Delta x}, \tag{39}$$

where D is the diffusivity of the metal, N_{Si} is the atomic silicon density, Δx is the distance between the microcavity layers, and ΔC_{S} is the difference in the concentrations of the dissolved impurity in equilibrium with one layer and with two layers. For the case of two microcavity layers, Eqn (38) becomes

$$\Delta C_{\text{S}} \approx \left(\frac{\theta_1}{1-\theta_1} - \frac{\theta_2}{1-\theta_2}\right) \exp\left(-\frac{\Delta G_{\text{cav}}}{kT}\right). \tag{40}$$

Determining, in these experiments, the binding energy of a metal atom on the cavity wall, ΔG_{cav}, we can use Eqn (38) and the results of experiments in the redistribution of the metal between the microcavity layer and the silicide layer to find ΔG_{sil}. Petersen et al. [328] assume that in these experiments they were able to determine ΔG_{sil} for Cu and Au more exactly than it had been done earlier. The researchers found that Cu and Au are more likely to form bonds on the cavity surface ($\Delta G_{\text{cav}} > \Delta G_{\text{sil}}$), while Co and Fe are more likely to form precipitates of metal silicides in the bulk phase ($\Delta G_{\text{cav}} < \Delta G_{\text{sil}}$). However, in the case of Co and Fe, when their concentrations are lower than the silicide precipitation threshold, effective gettering also proceeds according to the chemisorption mechanism. The concentrations of these impurities in the crystal can be reduced by several orders of magnitude. Getter layers may be on the active side of the wafer and on the opposite side. This type of gettering fits very well into the technology of microelectronics.

The possibility of wafer cleaving along a layer of microporous silicon forms the basis of the 'Smart-Cut' technology of fabricating silicon-on-insulator structures [329]. Popov et al. [330] used the 'Dele-Cut' method (a variety of the Smart-Cut method) to fabricate silicon-on-insulator structures with record thin films of silicon (3 nm). These structures are characterized by extreme planeness of interfaces and a low concentration of surface states on them.

8. Conclusion

The study of quasichemical reactions in solids and of factors that affect these reactions (temperature, ionization level, internal electric fields, and elastic stress fields) forms the scientific basis of the science of semiconductor materials. The level of understanding of the physics of the defect–impurity interaction allows us to control the properties of

implanted silicon. Using specially implanted impurities or defects, we can fight impurities and defects. Most enlightening here is the suppression of formation of residual defects (dislocations) by using the multistep method of implantation or by introducing electrically neutral substitutional impurities (carbon). This makes it possible to lower the density of dislocation loops in ion-implanted layers by several orders of magnitude and thus radically improve the electrophysical parameters of discrete devices and integrated circuits. Special introduction of impurities belonging to Group IV (C and Ge) ensures a significant reduction (by a factor of 10 or more) of the diffusivity of boron and phosphorus implanted in silicon, which is important for submicron technology.

The creation of radiation-induced defects by ion implantation makes it possible to form getter layers in silicon wafers. Such layers can be used to rid wafers of residual impurities, primarily rapidly diffusing transition-metal elements, and of intrinsic defects. Here, layers of microporous silicon created by implantation of hydrogen or helium ions are most promising, both in terms of effectiveness and technology.

Despite the significant advances, the topic of defect impurity interaction is far from being exhausted. The most important factor in the advances in the field of defect engineering in silicon is the close interaction of academic science and industrial research.

The authors are grateful to N N Gerasimenko and P V Zhukovskiĭ for useful discussions involving some of the aspects of the present review.

References

1. Mozer A P *Solid State Phenom.* **69–70** 1 (1999)
2. Mil'vidskiĭ M G *Izv. Vyssh. Ucheb. Zaved. Mater. Elektron. Tekh.* (1) 1 (2000)
3. Kumakhov M A, Komarov F F *Energeticheskie Poteri i Probegi Ionov v Tverdykh Telakh* (Energy Loss and Ion Ranges in Solids) (Minsk: Izd. BGU, 1979) [Translated into English (New York: Gordon and Breach Sci. Publ., 1981)]
4. Burenkov A F et al. *Tablitsy Parametrov Prostranstvennogo Raspredeleniya Ionno-Implantirovannykh Primeseĭ* (Tables of Ion Implantation Spatial Distributions) (Minsk: Izd. BGU, 1980) [Translated into English (New York: Gordon and Breach Sci. Publ., 1986)]
5. Gibbons J F *Proc. IEEE* **60** 1062 (1972) [Translated into Russian *TIIER* **60** (9) 53 (1972)]
6. Lenchenko V M, Akilov Yu Z *Fiz. Tekh. Poluprovodn.* **5** 397 (1971)
7. Akilov Yu Z, Lenchenko V M *Fiz. Tekh. Poluprovodn.* **8** 30 (1974)
8. Gerasimenko N N et al. *Fiz. Tekh. Poluprovodn.* **6** 1978 (1972)
9. Gerasimenko N N et al. *Fiz. Tekh. Poluprovodn.* **7** 2297 (1973)
10. Watkins G D *Mater. Sci. Forum* **143–147** (2) 5 (1993)
11. Stein H J *Appl. Phys. Lett.* **15** 61 (1969)
12. Barnes C E *IEEE Trans. Nucl. Sci.* **NS-16** 28 (1969)
13. Vavilov V S, Chelyadinskiĭ A R *Usp. Fiz. Nauk* **165** 347 (1995) [*Phys. Usp.* **38** 333 (1995)]
14. Corbett J W, Watkins G D *Phys. Rev. Lett.* **7** 314 (1961)
15. Watkins G D, in *Lattice Defects in Semiconductors: Invited and Contributed Papers from the Intern. Conf., Freiburg, Switzerland, 22–25 July 1974* (Inst. of Phys. Conf. Ser. No. 23) (London: Institute of Physics, 1975) p. 1
16. Watkins G D, in *Radiation Damage and Defects in Semiconductors: Proc. of the Intern. Conf., Reading, England, July 19–21, 1972* (Inst. of Phys. Conf. Ser. No. 16) (London: Institute of Physics, 1973) p. 228
17. Watkins G D *J. Phys. Soc. Jpn.* **18** (Suppl. 2) 22 (1963)
18. McKeighen R E, Koehler J S *Phys. Rev. B* **4** 462 (1971)
19. Gwozdz P S, Koehler J S *Phys. Rev. B* **6** 4571 (1972)
20. Bourgoin J C, Corbett J W *Phys. Lett. A* **38** 135 (1972)
21. Weiser K *Phys. Rev.* **126** 1427 (1962)
22. Berezhnov N I et al. *Nucl. Instrum. Meth. B* **73** 357 (1993)
23. Watkins G D, in *Radiation Effects in Semiconductors* (Ed. F L Vook) (New York: Plenum Press, 1968) p. 67
24. Wada T et al. *Bull. Daido Inst. Technol.* **33** 107 (1997)
25. Mukashev B N, Abdullin K A, Gorelkinskii Yu V *Phys. Status Solidi A* **168** 73 (1998)
26. Gerasimenko N N, Dvurechenskiĭ A V, Smirnov L S *Fiz. Tekh. Poluprovodn.* **5** 1700 (1971)
27. Beezhold W, Brower K L *IEEE Trans. Nucl. Sci.* **NS-19** 209 (1973)
28. De Wit J C, Ammerlaan C A, Watkins G D, in *Ion Implantation in Semiconductors: Proc. of the 2nd Intern. Conf., Garmisch-Partenkirchen, Germany, 1971* (Eds I Ruge, J Graul) (Berlin: Springer-Verlag, 1971) p. 39
29. Stein H J, Vook F L, Borders J A *Appl. Phys. Lett.* **14** 328 (1969)
30. Brower K L, Beezhold W *J. Appl. Phys.* **43** 3499 (1972)
31. Lee Y-H, Gerasimenko N N, Corbett J W *Phys. Rev. B* **14** 4506 (1976)
32. Brower K L *Phys. Rev. B* **14** 872 (1976)
33. Lee Y H, Kim Y M, Corbett J W *Radiat. Eff.* **15** 77 (1972)
34. Corbett J W, Karins J P, Tan T Y *Nucl. Instrum. Methods* **182/183** 457 (1981)
35. Berezhnov N I, Stelmakh V F, Chelyadinskii A R *Phys. Status Solidi A* **78** 121 (1983)
36. Jadan M, Berezhnov N I, Chelyadinskii A R *Phys. Status Solidi B* **189** K1 (1995)
37. Chelyadinskiĭ A R, Varichenko V S, Zaĭtsev A M *Fiz. Tverd. Tela* **40** 1627 (1998) [*Phys. Solid State* **40** 1478 (1998)]
38. Jung W, Newell G S *Phys. Rev.* **132** 648 (1963)
39. Botvin V A et al. *Fiz. Tekh. Poluprovodn.* **6** 1683 (1972) [*Sov. Phys. Semicond.* **6** 1453 (1973)]
40. Araika O J et al. *Nucl. Instrum. Meth. B* **73** 503 (1993)
41. Stel'makh V F, Tkachev V D, Chelyadinskiĭ A R *Fiz. Tverd. Tela* **20** 2196 (1978) [*Sov. Phys. Solid State* **20** 1267 (1978)]
42. Yoon M et al. *Appl. Phys. Lett.* **75** 2791 (1999)
43. Fedina L et al. *Phys. Status Solidi A* **171** 147 (1999)
44. Fedina L I, Gutakovskiĭ A K, Aseev A L *Izv. Vyssh. Ucheb. Zaved. Mater. Elektron. Tekh.* (3) 19 (2000)
45. Liefting J R, Custer J S, Saris F W *Mater. Sci. Eng. B* **25** 60 (1994)
46. Li J, Jones K S *Appl. Phys. Lett.* **73** 3748 (1998)
47. Tan T Y *Mater. Res. Soc. Symp. Proc.* **2** 163 (1981)
48. Lee Y H *Appl. Phys. Lett.* **73** 1119 (1998)
49. Tan T Y, Foel H *Bull. Am. Phys. Soc.* **25** 372 (1980)
50. Aseev A L et al. *Fiz. Tekh. Poluprovodn.* **13** 764 (1979)
51. Schreutelkamp R J et al. *Mater. Sci. Rep.* **6** 275 (1991)
52. Brown R A et al. *Nucl. Instrum. Meth. B* **127/128** 55 (1997)
53. Sechan K, Washburn J *Radiat. Eff.* **14** 267 (1972)
54. Wu W-K, Washburn J *J. Appl. Phys.* **48** 3742 (1977)
55. Jones K S, Prussin S, Weber E R *Appl. Phys. A* **45** 1 (1988)
56. Bicknell R W *Proc. R. Soc. London Ser. A* **311** 75 (1969)
57. Sechan K, Washburn J *Radiat. Eff.* **26** 31 (1975)
58. Tamura M et al. *Nucl. Instrum. Meth. B* **21** 438 (1987)
59. Simpson T W, Mitchell I V *Nucl. Insrum. Meth. B* **127/128** 94 (1997)
60. Tamura M, Suzuki T *Nucl. Instrum. Meth. B* **39** 318 (1989)
61. Davidson S M, Brooker G R *Radiat. Eff.* **6** 33 (1970)
62. Lambert J A, Dobson P S *Philos. Mag. A* **44** 1043 (1981)
63. Cembali F et al. *Radiat. Eff.* **36** 111 (1978)
64. Jasper C, Hoover A, Jones K S *Appl. Phys. Lett.* **75** 2629 (1999)
65. Narajan J, Fletcher J *Mater. Res. Soc. Symp. Proc.* **2** 191 (1981)
66. Mader S, in *Ion Implantation: Science and Technology* (Ed. J F Ziegler) (Orlando: Academic Press, 1984) p. 84
67. Kalinin V V, Aseev A L, Gerasimenko N N *Fiz. Tekh. Poluprovodn.* **13** 28 (1979)
68. Benton J L et al. *J. Appl. Phys.* **82** 120 (1997)
69. Tan T Y et al. *Mater. Res. Soc. Symp. Proc.* **2** 179 (1981)
70. Krakow W, Tan T Y, Foell H *Mater. Res. Soc. Symp. Proc.* **2** 185 (1981)
71. Lampin E, Senez V *Nucl. Instrum. Meth. B* **147** 13 (1999)
72. Bonafos C, Mathiot D, Claverie A *J. Appl. Phys.* **83** 3008 (1998)
73. Kim J et al. *Phys. Rev. B* **55** 16186 (1997)
74. Arai N, Takeda S, Kohyama M *Phys. Rev. Lett.* **78** 4265 (1997)
75. Claverie A et al. *Nucl. Instrum. Meth. B* **147** 1 (1999)
76. Cowern N E B et al. *Phys. Rev. Lett.* **82** 4460 (1999)
77. Pan G Z, Tu K N, Prussin S *Appl. Phys. Lett.* **71** 659 (1997)
78. Eaglesham D J et al. *Appl. Phys. Lett.* **65** 2305 (1994)

79. Gerasimenko N N, in *Trudy 2-go Sovetsko-Amerikanskogo Seminara po Ionnoĭ Implantatsii, Pushchino, 1979* (Proc. 2nd Soviet–American Seminar on Ion Implantation) (Ed. L S Smirnov) (Novosibirsk: Izd. NGU, 1979) p. 351
80. Ostwald W *Z. Phys. Chem.* **34** 495 (1900)
81. Burton B, Speight M V *Philos. Mag. A* **53** 385 (1985)
82. Hu S M *Mater. Res. Soc. Symp. Proc.* **2** 333 (1980)
83. Dunham S T *Appl. Phys. Lett.* **63** 464 (1993)
84. Huang R Y S, Dutton R W *J. Appl. Phys.* **74** 5821 (1993)
85. Meekison C D *Philos. Mag. A* **69** 379 (1994)
86. Seibt M *Solid State Phenom.* **32–33** 463 (1993)
87. Hu S M *Mater. Sci. Eng. R* **13** 105 (1994)
88. Chelyadinskiĭ A R, Burenkov V A *Fiz. Tverd. Tela* **40** 1995 (1998) [*Phys. Solid State* **40** 1806 (1998)]
89. Russell K C *Adv. Colloid Interface Sci.* **13** 205 (1980)
90. Chason E et al. *J. Appl. Phys.* **81** 6513 (1997)
91. Moller K, Jones K S, Law M E *Appl. Phys. Lett.* **72** 2547 (1998)
92. Raman R et al. *Appl. Phys. Lett.* **74** 1591 (1999)
93. Fatima S et al. *Appl. Phys. Lett.* **74** 1141 (1999)
94. Crowder B L, Title R S *Radiat. Eff.* **6** 63 (1970)
95. Chelyadinskii A R, Jadan M, Taher Haki, in *Proc. of the Intern. Conf. Ion Implantation of Science and Technology, Naleczow, Poland, 22–24 Jan., 1997* (Ed. D Maczka) (Lublin: Technical Univ. of Lublin, 1997) p. 114
96. Zhevno A N, Sidorik V V, Tkachev V D *Dokl. Akad. Nauk Bel. SSR* **20** 409 (1976)
97. Coffa S, Libertino S, Spinella C *Appl. Phys. Lett.* **76** 321 (2000)
98. Coffa S et al. *Appl. Phys. Lett.* **73** 1571 (1998)
99. Gerasimenko N N, Mordkovich V N *Poverkhnost* (6) 5 (1987)
100. Legotin D L, Bubnovskaya O V, Tyapunina N A *Vestn. Mosk. Univ. Ser. 3: Fiz., Astron.* (1) 58 (1996)
101. Fladda G et al. *Appl. Phys. Lett.* **16** 313 (1970)
102. Mayer J W et al. *Can. J. Phys.* **46** 663 (1968)
103. Lilak A D et al. *Appl. Phys. Lett.* **74** 2038 (1999)
104. Nelson R S, in *Radiation Damage and Defects in Semiconductors: Proc. of the Intern. Conf., Reading, England, July 19–21, 1972* (Inst. of Phys. Conf. Ser. No. 16) (London: Institute of Physics, 1973) p. 140
105. Xia Z et al. *Vacuum* **46** 1071 (1995)
106. Liefting R, PhD Thesis Degree (Enschede: Univ. of Twente, 1992)
107. Acco S, Saris F W, Custer J S *Mater. Sci. Eng. B* **34** 168 (1995)
108. Merli P G, Zignani F *Radiat. Eff. Lett.* **50** 115 (1980)
109. Cerofolini G F et al. *J. Appl. Phys.* **56** 2981 (1984)
110. Chen L J et al. *J. Appl. Phys.* **52** 3304 (1981)
111. Bruel M et al. *Nucl. Instrum. Methods* **189** 135 (1981)
112. Tolstykh V P, Khit'ko V I, Shiryaev S Yu *Poverkhnost* (5) 90 (1986)
113. Komarov F F et al. *Radiat. Eff. Lett.* **85** 243 (1985)
114. Andreev V S, Efimov S B, Komarov F F *Pis'ma Zh. Tekh. Fiz.* **11** 1110 (1985) [*Sov. Tech. Phys. Lett.* **11** 460 (1985)]
115. Komarov F F et al. *Radiat. Eff.* **90** 307 (1985)
116. Holland O W et al. *Radiat. Eff.* **90** 127 (1985)
117. Elliman R G et al. *Nucl. Insrum. Meth. B* **19/20** 435 (1987)
118. Leiberich A, Mayer D M, Knoell R V *Nucl. Instrum. Meth. B* **19/20** 457 (1987)
119. Berti M et al. *Nucl. Instrum. Meth. B* **19/20** 475 (1987)
120. Komarov F F, Novikov A P, Tolstykh V P, in *Materialy 16-go Vsesoyuzn. Soveshch. po Fizike Vzaimodeĭstviya Zaryazhennykh Chastits s Kristallami, Moskva, 1987* (Proc. 16th All-Union Workshop in Physics of Interaction of Charged Particles and Crystals, Moscow, 1987) (Moscow: Izd. MGU, 1987) p. 126
121. Holland O W, Narayan J *Appl. Phys. Lett.* **44** 758 (1984)
122. Gadili E et al. *Jpn. J. Appl. Phys. Pt. 1* **24** 14 (1985)
123. Komarov F F et al. *Fiz. Tekh. Poluprovodn.* **20** 1726 (1986) [*Sov. Phys. Semicond.* **20** 1081 (1986)]
124. Olson G L et al. *Mater. Res. Soc. Symp. Proc.* **23** 375 (1984)
125. Galloni R et al. *Nucl. Instrum. Meth. B* **19/20** 446 (1987)
126. Holland O W, Narayan J *Mater. Res. Soc. Symp. Proc.* **27** 235 (1984)
127. Cembali G F, Merli P G, Zignani F *Appl. Phys. Lett.* **38** 808 (1981)
128. Cembali G et al. *Appl. Phys. Lett.* **40** 62 (1982)
129. Dietrich H B, Corazzi R J, Tseng W F *Mater. Res. Soc. Symp. Proc.* **27** 241 (1984)
130. Rupprecht H *J. Vac. Sci. Technol.* **15** 1669 (1978)
131. Westendorp J F M et al. *Nucl. Instrum. Meth. B* **37/38** 357 (1989)
132. Kakoschke R et al. *IEEE Trans. Electron Dev.* **ED-37** 1052 (1990)
133. Kaim R E *Solid State Technol.* **33** 103 (1990)
134. Gerasimenko N N "Sposob ionnogo vnedreniya v kristallicheskie podlozhki" ("A method for implanting ions in crystalline substrates"), Author's Certificate USSR No. 906304 (filed 14.10.81)
135. Liefting J R et al. *Mater. Res. Soc. Symp. Proc.* **235** 173 (1992)
136. Liefting J R et al. *Appl. Phys. Lett.* **63** 1134 (1993)
137. Wong H et al. *Appl. Phys. Lett.* **52** 1023 (1988)
138. Liefting J R, Custer J S, Saris F W *Mater. Res. Soc. Symp. Proc.* **235** 179 (1992)
139. Stolk P A et al. *J. Appl. Phys.* **81** 6031 (1997)
140. Libertino S et al. *Appl. Phys. Lett.* **71** 389 (1997)
141. Watkins G D, Brower K L *Phys. Rev. Lett.* **36** 1329 (1976)
142. Tamura M, Ando T, Ohyu K *Nucl. Instrum. Meth. B* **59/60** 572 (1991)
143. Strane J W et al. *J. Appl. Phys.* **79** 637 (1996)
144. Kobayashi N et al. *Nucl. Instrum. Meth. B* **127/128** 350 (1997)
145. Tsukamoto K et al. *Nucl. Instrum. Meth. B* **59/60** 584 (1991)
146. Serre C et al. *J. Appl. Phys.* **77** 2978 (1995)
147. Vlasenko L S et al. *Fiz. Tekh. Poluprovodn.* **33** 1164 (1999) [*Semicond.* **33** 1059 (1999)]
148. Werner P et al. *Appl. Phys. Lett.* **70** 252 (1997)
149. Claverie A et al. *Nucl. Instrum. Meth. B* **127/128** 22 (1997)
150. Simpson T W, Goldberg R D, Mitchell I V *Appl. Phys. Lett.* **67** 2857 (1995)
151. Berezhnov N I, Suprun-Belevich Yu P, Chelyadinskiĭ A R *Izv. Vyssh. Uchebn. Zaved. Fiz.* (4) 55 (1991) [*Sov. Phys. J.* **34** 325 (1991)]
152. Rzhanov A V, Gerasimenko N N, Vasil'ev S V *Pis'ma Zh. Tekh. Fiz.* **7** 1221 (1981) [*Sov. Tech. Phys. Lett.* **7** 521 (1981)]
153. Gay H C, Griot D "Thermal annealing by microwave assisted focused beam", Motorola Patent No. R 9016040 (filed 20.12.90)
154. Gay H-C, Gibert P, Lin-Kwang J *J. Appl. Phys.* **88** 3968 (2000)
155. Zhao Q-T, Wang Z-L *Nucl. Instrum. Meth. B* **108** 81 (1996)
156. Lu W X et al. *Appl. Phys. Lett.* **55** 1838 (1989)
157. Borkovskaya O Yu et al. *Fiz. Tekh. Poluprovodn.* **17** 1349 (1983) [*Sov. Phys. Semicond.* **17** 856 (1983)]
158. Nicholas K H et al. *Appl. Phys. Lett.* **26** 320 (1975)
159. Bohm H-J et al. *IEEE Trans. Electron Dev.* **ED-35** 1616 (1988)
160. Takahashi M, Konaka S, Kajiyama K *J. Appl. Phys.* **54** 6041 (1983)
161. Bull C et al. *Solid State Electron.* **22** 95 (1979)
162. Ikeda T et al. *Jpn. J. Appl. Phys.* **14** 311 (1975)
163. Tamura M, Yoshihiro N, Ikeda T *Appl. Phys. Lett.* **27** 427 (1975)
164. Prussin S *J. Appl. Phys.* **45** 1635 (1974)
165. Ashburn P et al. *Solid State Electron.* **20** 731 (1977)
166. Liefting R et al. *IEEE Trans. Electron Dev.* **ED-41** 50 (1994)
167. Wijburg R C et al. *IEEE Trans. Electron Dev.* **ED-38** 111 (1991)
168. Sze S M *Semiconductor Devices, Physics and Technology* (New York: Wiley, 1985)
169. Wong H, Cheung N W, Wong S S *Nucl. Instrum. Meth. B* **37/38** 970 (1989)
170. Gibbons J F *Appl. Phys. Lett.* **23** 49 (1972)
171. Aleksandrov O V, Kozlovskii V V, Popov V V *Phys. Status Solidi A* **110** 61 (1986)
172. Gerasimenko N N et al. *Fiz. Tekh. Poluprovodn.* **9** 2117 (1975)
173. Werner H W et al. *Appl. Phys.* **2** 262 (1973)
174. Gorban' A N, Gorodokhin V A *Izv. Vyssh. Uchebn. Zaved. Fiz.* (9) 56 (1988)
175. Stel'makh V F et al. *Fiz. Tekh. Poluprovodn.* **19** 739 (1985) [*Sov. Phys. Semicond.* **19** 455 (1985)]
176. Stelmakh V F et al. *Phys. Status Solidi A* **89** 45 (1985)
177. Stel'makh V F, Suprun-Belevich Yu R, Chelyadinskiĭ A R *Izv. Vyssh. Uchebn. Zaved. Fiz.* (9) 114 (1987)
178. Stelmakh V F, Suprun-Belevich Yu R, Chelyadinskii A R *Phys. Status Solidi A* **112** 381 (1989)
179. Chelyadinskii A R, Taher Haki *Phys. Status Solidi A* **142** 331 (1994)
180. Stelmakh V F, Suprun-Belevich Yu R, Chelyadinskii A R *Phys. Res.* **8** 288 (1988)
181. Hu S M *Phys. Rev.* **180** 773 (1969)
182. Servidori M et al. *J. Appl. Phys.* **65** 98 (1989)
183. Servidori M et al. *Nucl. Instrum. Meth. B* **39** 347 (1989)
184. Ryssel H, Ruge I *Ionenimplantation* (Stuttgart: Teubner, 1978) [Translated into English: *Ion Implantation* (Chichester: Wiley, 1986); translated into Russian (Moscow: Nauka, 1983)]

185. Gerasimenko N N, Zherebtsov A S, Kamnev A B *Mikroelektronika* **4** 611 (1975)
186. Scheid E, Chenevier P *Phys. Status Solidi A* **93** 523 (1986)
187. Gossmann H J et al. *Appl. Phys. Lett.* **63** 639 (1993)
188. Jadan M, Chelyadinskii A R, in *X Intern. Conf. Ion Implantation Technology, Catania, Italia, June 13–17, 1994*, Abstracts (Ed. R Jones) (Amsterdam: North-Holland, 1994) p. 3.85
189. Peterström S, Svensson B G *J. Appl. Phys.* **71** 1215 (1992)
190. Emtsev V V, Margoryan M A *Pis'ma Zh. Tekh. Fiz.* **10** 1063 (1984) [*Sov. Tech. Phys. Lett.* **10** 449 (1984)]
191. Kalinin V V, Gerasimenko N N, Stenin S I *Fiz. Tverd. Tela* **18** 2803 (1976)
192. Stel'makh V F, Suprun-Belevich Yu R, Chelyadinskiĭ A R *Poverkhnost': Fiz., Khim., Mekh.* (10) 123 (1989)
193. Ohta K, Sakano J, Furukawa S *Nucl. Instrum. Meth. B* **59/60** 1113 (1991)
194. Fahey P et al. *Appl. Phys. Lett.* **46** 784 (1985)
195. Mathiot D, Pfister J C *J. Appl. Phys.* **55** 3518 (1984)
196. Schwettmann F N, Kendal D L *Appl. Phys. Lett.* **19** 218 (1971)
197. Yoshida M *J. Appl. Phys.* **48** 2169 (1977)
198. Fair B, Tsai C C *J. Electrochem. Soc.* **124** 1107 (1977)
199. Burenkov V A, Jadan M, Chelyadinskii A R, in *Proc. of the Intern. Conf. Ion Implantation of Science and Technology, Naleczow, Poland, 22–24 Jan., 1997* (Ed. D Maczka) (Lublin: Technical Univ. of Lublin, 1997) p. 108
200. Ajmera A C, Rozgonyi G A, Fair R B *Appl. Phys. Lett.* **52** 813 (1988)
201. Oehrlein G S, Cohen S A, Sedgwick T O *Appl. Phys. Lett.* **45** 417 (1984)
202. Negrini P et al. *Philos. Mag. A* **61** 553 (1990)
203. Chelyadinskii A R, Taher Haki, Suprun-Belevich Yu R, in *Fall Meeting MRS, Boston, 1993* (Ed. M Stovola) (Boston: Academic Press, 1993) p. J.28
204. Cowern N E B et al. *Appl. Phys. Lett.* **65** 2981 (1994)
205. Xu J et al. *J. Appl. Phys.* **81** 107 (1997)
206. Gencer A H, Dunham S T *J. Appl. Phys.* **81** 631 (1997)
207. Bonafos C et al. *J. Appl. Phys.* **82** 2855 (1997)
208. Cheng J Y et al. *J. Appl. Phys.* **80** 2105 (1996)
209. Agarwal A et al. *Appl. Phys. Lett.* **70** 3332 (1997)
210. Liu J et al. *J. Appl. Phys.* **81** 1656 (1997)
211. Zhang L H et al. *Appl. Phys. Lett.* **67** 2025 (1995)
212. Rozgoni G A et al. *J. Cryst. Growth* **85** 300 (1987)
213. Bergholz W, Gilles D *Phys. Status Solidi B* **222** 5 (2000)
214. Mil'vidskiĭ M G, Osvenskiĭ V B *Strukturnye Defekty v Monokristallakh Poluprovodnikov* (Structure Defects in Semiconductor Single Crystals) (Moscow: Metallurgiya, 1984) p. 210
215. Smirnov L S (Ed.) *Fizicheskie Protsessy v Obluchennykh Poluprovodnikakh* (Physical Processes in Irradiated Semiconductors) (Novosibirsk: Nauka, 1977)
216. Bolotov V V et al. *Voprosy Radiatsionnoĭ Tekhnologii Poluprovodnikov* (A Survey of Semiconductor Radiation Techniques) (Ed. L S Smirnov) (Novosibirsk: Nauka, 1980) [Translated into English (Moscow: Mir Publ., 1983)]
217. Yamazaki H et al. *J. Appl. Phys.* **87** 4194 (2000)
218. Ruiz H J, Pollack G P *J. Electrochem. Soc.* **125** 128 (1978)
219. Hu S M *Appl. Phys. Lett.* **36** 561 (1980)
220. Gaworzewski P, Ritter H *Phys. Status Solidi A* **67** 511 (1981)
221. Newman R C et al. *J. Appl. Phys.* **70** 3061 (1991)
222. McQuaid S A et al. *J. Appl. Phys.* **77** 1427 (1995)
223. Zhong L, Shimura F *J. Appl. Phys.* **73** 707 (1993)
224. Izunome K et al. *Appl. Phys. Lett.* **68** 49 (1996)
225. Gösele U, Tan T Y *Appl. Phys. A* **28** 79 (1982)
226. McQuaid S A et al. *J. Appl. Phys.* **86** 1878 (1999)
227. Shimura F, Higuchi T, Hockett R S *Appl. Phys. Lett.* **53** 69 (1988)
228. Wijaranakula W *J. Appl. Phys.* **68** 6538 (1990)
229. Kaiser W *Phys. Rev.* **105** 1751 (1957)
230. Lederhandler S, Patel J R *Phys. Rev.* **108** 239 (1957)
231. Hu S M *J. Appl. Phys.* **52** 3974 (1981)
232. Newman R C *J. Phys.: Condens. Matter* **12** R335 (2000)
233. Voronkov V V, Mil'vidskiĭ M G, Grinshteĭn P M *Kristallografiya* **34** 199 (1989) [*Sov. Phys. Crystallogr.* **31** 115 (1989)]
234. Wada K, Inoue N, Kohra K *J. Cryst. Growth* **49** 749 (1980)
235. Ham F S *J. Phys. Chem. Solids* **6** 335 (1958)
236. Rozgonyi G A et al. *Appl. Phys. Lett.* **29** 531 (1976)
237. Senkader S, Esfandyari J, Hobler G *J. Appl. Phys.* **78** 6469 (1995)
238. Esfandyari J et al. *J. Electrochem. Soc.* **143** 995 (1996)
239. Senkader S, Hobler G, in *Early Stages of Oxygen Precipitation in Silicon* (NATO ASI Ser., Ser. 3, Vol. 17, Ed. R Jones) (Dordrecht: Kluwer Acad. Publ., 1996) p. 447
240. Christian J W *The Theory of Transformations in Metals and Alloys* Pt. 1 (Oxford: Pergamon Press, 1975)
241. Vineyard G H *J. Phys. Chem. Solids* **3** 121 (1957)
242. Mikkelsen J *Mater. Res. Soc. Symp. Proc.* **59** 1 (1986)
243. Turnbull D, Fisher J C *J. Chem. Phys.* **17** 71 (1949)
244. Burke J *The Kinetics of Phase Transformations in Metals* (Oxford: Pergamon Press, 1965)
245. Tiller W A, Oh S *J. Appl. Phys.* **64** 375 (1988)
246. Koizuka M, Yamada-Kaneta H *J. Appl. Phys.* **84** 4255 (1998)
247. Koizuka M, Yamada-Kaneta H *J. Appl. Phys.* **88** 1784 (2000)
248. Caplan P J et al. *J. Appl. Phys.* **50** 5847 (1979)
249. Poindexter E H, Caplan P J *Prog. Surf. Sci.* **14** 201 (1983)
250. Hu S M *J. Appl. Phys.* **51** 5945 (1980)
251. Sassella A et al. *Appl. Phys. Lett.* **75** 1131 (1999)
252. Borghesi A et al. *Mater. Sci. Eng. B* **73** 145 (2000)
253. Kishino S et al. *J. Appl. Phys.* **50** 8240 (1979)
254. Kishino S, Matsushita Y, Kanamori M *Jpn. J. Appl. Phys. Pt. 1* **21** 1 (1982)
255. Tang S S, Shen Y Y, Li Y Z *Chinese J. Semicond.* **7** 489 (1986)
256. Tan T Y, Gardner E E, Tice W K *Appl. Phys. Lett.* **30** 175 (1977)
257. Shimura F *J. Appl. Phys.* **59** 3251 (1986)
258. Liu P et al. *J. Appl. Phys.* **87** 3669 (2000)
259. Leroncille J *Phys. Status Solidi A* **74** 159 (1982)
260. Shimura F, Hockett R S *Appl. Phys. Lett.* **48** 224 (1986)
261. Aihara K et al. *J. Appl. Phys.* **88** 3705 (2000)
262. Tan T Y, Tice W K *Philos. Mag.* **34** 615 (1976)
263. Tice W K, Tan T Y *Appl. Phys. Lett.* **28** 564 (1976)
264. Ourmazd A, Schröter W *Appl. Phys. Lett.* **45** 781 (1984)
265. Colas E G, Weber E R *Appl. Phys. Lett.* **48** 1371 (1986)
266. Sumino K *Mater. Sci. Eng. B* **72** 67 (2000)
267. Gilles D, Weber E R, Hahn S K *Phys. Rev. Lett.* **64** 196 (1990)
268. Masters B J, Fairfield J M, Crowder B L, in *Ion Implantation* (Ed. F H Eisen, L T Chadderton) (London: Gordon and Breach Sci. Publ., 1971) p. 81
269. Buck T M, Pickar K A, Poate J M *Appl. Phys. Lett.* **21** 485 (1972)
270. Goetzberger A, Shockley W *J. Appl. Phys.* **31** 1821 (1960)
271. Huntley F A, Willoughby A F W *J. Electrochem. Soc.* **120** 914 (1973)
272. Seidel T E, Meek R L, Cullis A G *J. Appl. Phys.* **46** 600 (1975)
273. Wong H, Cheung N W, Chu P K *Appl. Phys. Lett.* **52** 889 (1988)
274. Benton J L et al. *J. Electrochem. Soc.* **143** 1406 (1996)
275. Lambert J L, Reese M *Solid State Electron.* **11** 1055 (1968)
276. Borland J O, Koelsch R *Solid State Technol.* **36** 28 (1993)
277. Wang Z L et al. *J. Appl. Phys.* **71** 3780 (1992)
278. Kuroi T et al. *Jpn. J. Appl. Phys. Pt. 1* **32** 303 (1993)
279. Venezia V C et al. *Appl. Phys. Lett.* **73** 2980 (1998)
280. Kögler R et al. *Appl. Phys. Lett.* **75** 1279 (1999)
281. Brown R A et al. *Mater. Res. Soc. Symp. Proc.* **438** 155 (1997)
282. Koveshnikov S, Kononchuk O *Appl. Phys. Lett.* **73** 2340 (1998)
283. Brown R A et al. *J. Appl. Phys.* **84** 2459 (1998)
284. Kögler R et al. *Nucl. Instrum. Meth. B* **186** 298 (2002)
285. Gueorguiev Y M et al. *Appl. Phys. Lett.* **75** 3467 (1999)
286. Kögler R et al. *Nucl. Instrum. Meth. B* **148** 334 (1999)
287. Troitski V Yu, Gerasimenko N N, Smirnov A V, in *Ion Implantation 2000: Proc. of the Intern. Conf., Alpach, Austria, 17–22 Sept. 2000* (Eds H Ryssel et al.) (New York: IEEE, 2000) p. 334
288. Griffioen C C et al. *Nucl. Instrum. Meth. B* **27** 417 (1987)
289. Wong-Leung J et al. *Appl. Phys. Lett.* **66** 1231 (1995)
290. Godey S et al. *J. Appl. Phys.* **87** 2158 (2000)
291. Delamare R et al. *Nucl. Instrum. Meth. B* **186** 324 (2002)
292. Myers S M, Follstaedt D M, Bishop D M *Mater. Sci. Forum* **143–147** 1635 (1994)
293. Myers S M, Follstaedt D M *J. Appl. Phys.* **79** 1337 (1996)
294. Lee Y-H, Corbett J W *Phys. Rev. B* **9** 4351 (1974)
295. Ramdas A K, Fan H Y *J. Phys. Soc. Jpn.* **18** 34 (1963)
296. Daly D F, Pickar K A *Appl. Phys. Lett.* **15** 267 (1969)
297. Akiyama T et al. *Jpn. J. Appl. Phys. Pt. 2* **38** L1363 (1999)
298. Fichtner P F P et al. *Appl. Phys. Lett.* **70** 732 (1997)
299. Muto S, Takeda S, Hirata M *Philos. Mag. A* **72** 1057 (1995)

300. Murakami K et al. *Phys. Rev. Lett.* **77** 3161 (1996)
301. Okamoto Y, Saito M, Oshiyama A *Phys. Rev. B* **56** R10016 (1997)
302. Van de Walle C G *Phys. Rev. Lett.* **80** 2177 (1998)
303. Hourahine B et al. *Phys. Rev. B* **57** R12666 (1998)
304. Leitch A W R, Alex V, Weber J *Phys. Rev. Lett.* **81** 421 (1998)
305. Pritchard R E et al. *Phys. Rev. B* **56** 13118 (1997)
306. Kitajima M et al. *Jpn. J. Appl. Phys. Pt. 2* **38** L691 (1999)
307. Kitajima M et al. *Mater. Sci. Eng. B* **58** 13 (1999)
308. Cerofolini G F et al. *Phys. Rev. B* **46** 2061 (1992)
309. Myers S M et al. *Phys. Rev. B* **47** 13380 (1993)
310. Markevich V P, Suezawa M, Murin L I *Mater. Sci. Eng. B* **58** 26 (1999)
311. Hourahine B et al. *Mater. Sci. Eng. B* **58** 24 (1999)
312. Van de Walle C G *Phys. Rev. B* **49** 4579 (1994)
313. Leitch A W R, Weber J, Alex V *Mater. Sci. Eng. B* **58** 6 (1999)
314. Raineri V et al. *J. Appl. Phys.* **78** 3727 (1995)
315. Matthews M D, Ashby S J *Philos. Mag.* **27** 1313 (1973)
316. Myers S M, Bishop D M, Follstaedt D M *Mater. Res. Soc. Symp. Proc.* **283** 549 (1993)
317. Skorupa W et al. *Appl. Phys. Lett.* **67** 2992 (1995)
318. Zhang M et al. *Appl. Phys. Lett.* **72** 830 (1998)
319. Zhang M et al. *Nucl. Instrum. Meth. B* **134** 360 (1998)
320. Zhang M et al. *J. Appl. Phys.* **85** 94 (1999)
321. Job R et al. *Appl. Phys. A* **72** 325 (2001)
322. Kinomura A et al. *Nucl. Instrum. Meth. B* **127/128** 297 (1997)
323. Wong-Leung J, Nygren E, Williams J S *Nucl. Instrum. Meth. B* **106** 424 (1995)
324. Mohadjeri B, Williams J S, Wong-Leung J *Appl. Phys. Lett.* **66** 1889 (1995)
325. Ishiwara H, Saitoh S, Hikosaka K *Jpn. J. Appl. Phys.* **20** 843 (1981)
326. Myers S M, Bishop D M, Follstaedt D M *Mater. Res. Soc. Symp. Proc.* **316** 33 (1994)
327. Wong-Leung J et al. *Nucl. Instrum. Meth. B* **96** 253 (1995)
328. Petersen G A, Myers S M, Follstaedt D M *Nucl. Instrum. Meth. B* **127/128** 301 (1997)
329. Saint-Jacques R G *Nucl. Instrum. Methods* **209/210** 333 (1983)
330. Popov V P et al. *Mikroelektronika* **31** 274 (2002) [*Russ. Microelectron.* **31** 232 (2002)]